NASA/TM–2013-217999

An Approximate Solution and Master Curves for Buckling of Symmetrically Laminated Composite Cylinders

Michael P. Nemeth
Langley Research Center, Hampton, Virginia

May 2013

NASA STI Program . . . in Profile

Since its founding, NASA has been dedicated to the advancement of aeronautics and space science. The NASA scientific and technical information (STI) program plays a key part in helping NASA maintain this important role.

The NASA STI program operates under the auspices of the Agency Chief Information Officer. It collects, organizes, provides for archiving, and disseminates NASA's STI. The NASA STI program provides access to the NASA Aeronautics and Space Database and its public interface, the NASA Technical Report Server, thus providing one of the largest collections of aeronautical and space science STI in the world. Results are published in both non-NASA channels and by NASA in the NASA STI Report Series, which includes the following report types:

- TECHNICAL PUBLICATION. Reports of completed research or a major significant phase of research that present the results of NASA Programs and include extensive data or theoretical analysis. Includes compilations of significant scientific and technical data and information deemed to be of continuing reference value. NASA counterpart of peer-reviewed formal professional papers, but having less stringent limitations on manuscript length and extent of graphic presentations.

- TECHNICAL MEMORANDUM. Scientific and technical findings that are preliminary or of specialized interest, e.g., quick release reports, working papers, and bibliographies that contain minimal annotation. Does not contain extensive analysis.

- CONTRACTOR REPORT. Scientific and technical findings by NASA-sponsored contractors and grantees.

- CONFERENCE PUBLICATION. Collected papers from scientific and technical conferences, symposia, seminars, or other meetings sponsored or co-sponsored by NASA.

- SPECIAL PUBLICATION. Scientific, technical, or historical information from NASA programs, projects, and missions, often concerned with subjects having substantial public interest.

- TECHNICAL TRANSLATION. English-language translations of foreign scientific and technical material pertinent to NASA's mission.

Specialized services also include organizing and publishing research results, distributing specialized research announcements and feeds, providing information desk and personal search support, and enabling data exchange services.

For more information about the NASA STI program, see the following:

- Access the NASA STI program home page at *http://www.sti.nasa.gov*

- E-mail your question to help@sti.nasa.gov

- Fax your question to the NASA STI Information Desk at 443-757-5803

- Phone the NASA STI Information Desk at 443-757-5802

- Write to:
  STI Information Desk
  NASA Center for AeroSpace Information
  7115 Standard Drive
  Hanover, MD 21076-1320

NASA/TM–2013-217999

An Approximate Solution and Master Curves for Buckling of Symmetrically Laminated Composite Cylinders

Michael P. Nemeth
Langley Research Center, Hampton, Virginia

National Aeronautics and
Space Administration

Langley Research Center
Hampton, Virginia 23681-2199

May 2013

Available from:

NASA Center for AeroSpace Information
7115 Standard Drive
Hanover, MD 21076-1320
443-757-5802

Summary

Nondimensional linear-bifurcation buckling equations for balanced, symmetrically laminated cylinders with negligible shell-wall anisotropies and subjected to uniform axial compression loads are presented. These equations are solved exactly for the practical case of simply supported ends. Nondimensional quantities are used to characterize the buckling behavior that consist of a stiffness-weighted length-to-radius parameter, a stiffness-weighted shell-thinness parameter, a shell-wall nonhomogeneity parameter, two orthotropy parameters, and a nondimensional buckling load. Ranges for the nondimensional parameters are established that encompass a wide range of laminated-wall constructions and numerous generic plots of nondimensional buckling load versus a stiffness-weighted length-to-radius ratio are presented for various combinations of the other parameters. These plots are expected to include many practical cases of interest to designers. Additionally, these plots show how the parameter values affect the distribution and size of the festoons forming each response curve and how they affect the attenuation of each response curve to the corresponding solution for an infinitely long cylinder.

To aid in preliminary design studies, approximate formulas for the nondimensional buckling load are derived, and validated against the corresponding exact solution, that give the attenuated buckling response of an infinitely long cylinder in terms of the nondimensional parameters presented herein. A relatively small number of "master curves" are identified that give a nondimensional measure of the buckling load of an infinitely long cylinder as a function of the orthotropy and wall inhomogeneity parameters. These curves reduce greatly the complexity of the design-variable space as compared to representations that use dimensional quantities as design variables. As a result of their inherent simplicity, these "master curves" are anticipated to be useful in the ongoing development of buckling-design technology.

Symbols

$\mathcal{A}, \mathcal{B}$	nondimensional modal amplitudes defined by equations (13)-(15)
$A_{11}, A_{12}, A_{22}, A_{66}$	orthotropic-cylinder membrane stiffnesses, lb/in.
c_x	nondimensional coefficient defined by equations (44)
$D_{11}, D_{12}, D_{22}, D_{66}$	orthotropic-cylinder bending stiffnesses, in-lb
$D_m( ), D_c( ), D_b( )$	nondimensional linear differential operators defined by equations (3)-(5)
E, G	Young's modulus of elasticity and shear modulus of an isotropic material, respectively, psi
$\bar{E}$	reference value of Young's modulus of elasticity (see equation (44a)), psi

E_L, E_T, G_{LT}	lamina moduli (see Table 1), psi
h	cylinder thickness (see figure 1), in.
$\mathtt{I}$	nondimensional wall nonhomogeneity measure defined by equation (19)
L	cylinder length (see figure 1), in.
$m \in \{1, 2, 3, ...\}$	number of axial half waves in buckle pattern (see equation (13))
m_{cr}	value of m at buckling
$n \in \{0, 1, 2, 3, ...\}$	number of circumferential waves in buckle pattern (see equation (13) and figure 2)
n_{cr}	value of n at buckling
N, N_{cr}	circumferential wave number defined by equation (20c) and value of N at buckling, respectively
N_x, N_x^{cr}	compressive axial prebuckling stress resultant and corresponding value at buckling, respectively
$\tilde{p}$, $\tilde{p}_{cr}$	nondimensional loading parameter defined by equation (12) and corresponding value at buckling, respectively
R	cylinder radius (see figure 1), in.
x, y	cylinder coordinate system (see figure 1), in.
X, X_{cr}	quantity defined by equation (28) and value at buckling, respectively
α_b, α_m	nondimensional stiffness-weighted length-to-radius ratios defined by equations (8) and (6), respectively
β	nondimensional orthotropy parameter defined by equation (9)
δF	nondimensional buckling-stress function (see equations (1) and (2))
δW	nondimensional radial-displacement field at buckling (see equations (1) and (2))
$\eta = \frac{y}{R}$	nondimensional cylinder circumferential coordinate
θ	lamina fiber angle (see figure 1), degrees

λ, λ_{cr}	stiffness-weighted axial-buckle aspect ratio defined by equation (23) and value at buckling, respectively
Λ, Λ_{cr}	nondimensional stiffness-weighted axial half-wave length of a buckle pattern defined by equation (18) and value at buckling, respectively
μ	nondimensional orthotropy parameter defined by equations (7)
ν_m	laminate membrane Poisson's ratio defined by equation (10)
ν_{LT}	lamina major Poisson's ratio (see Table 1)
$\xi = \frac{x}{L}$	nondimensional cylinder axial coordinate
ρ	stiffness-weighted radius-to-thickness ratio defined by equation (11)
$\sigma_x^{cr} = \frac{N_x^{cr}}{h}$	value of the uniform axial stress at buckling, psi

Introduction

As evidenced by recent studies, efforts to develop shell-buckling design technology for laminated-composite cylinders are still underway.[1, 2] Despite these and other efforts, the technology still has not reached the level of maturity needed to obtain the full weight-saving potential of shell structures, especially those made of laminated-composite materials. The major impediment is a lack of validated analysis and design methods. As a result, NASA SP 8007,[3] developed in the late 1960s, is still the primary resource used by American industry for the design of buckling-resistant cylindrical shells. The procedure used in NASA SP 8007 has become a paradigm that accounts for the effects of initial geometric imperfections and edge support conditions by applying empirical "knockdown" factors to relatively simple classical linear-bifurcation buckling solutions. Although this class of solutions are very approximate, they generally provide insight into how variations in design parameters affect performance. Thus, it is useful to have relatively simple approximate analyses and formulas for predicting response trends that can be used as part of a building-block design process.

Recent examples of design-technology development for buckling of laminated-composite cylinders have been presented in references 1 and 2. Specifically, baseline design formulas are presented for balanced, symmetrically laminated cylinders with walls that are effectively homogeneous and specially orthotropic. This approach was motivated by existing designs in which the allowable range of structural dimensions are such that the laminate is composed of a relatively large number of plies that are distributed uniformly through the thickness. Thus, it follows that modelling a cylinder wall as a homogeneous and specially orthotropic material is not a serious limitation in a preliminary design process, for a significant number of practical applications. Moreover, this approach is a logical first step in a building-block approach for more

general, laminate constructions with plies at the outer faces that are substantially different from those near the mid-plane. Most importantly, this approach yields significant simplification of the buckling equations and facilitates the development of simple design formulas in terms of useful nondimensional parameters, as evidenced by the results presented in references 1 and 2. Of particular importance are the "master curves" presented in these references that represent the behavior of a wide range of practical laminate constructions in a very concise manner. Specifically, the "master curves" presented in references 1 and 2 are plots of normalized buckling stress versus normalized buckling strain that are presented as a function of laminate composition. By including strain in these plots, both structural stiffness and load-capacity requirements can be considered in the design process. Moreover, curves such as these permit common behavior trends to be identified for a wide variety of laminated-cylinder configurations. The formulas and results presented in references 1 and 2 represent a significant first-approximation advancement in design technology for compression-loaded laminated-composite cylinders.

The objective of the present study is to extend work presented in references 1 and 2 to include the cylinder-wall heterogeneity that cannot be neglected in a buckling analysis without introducing significant errors. Herein, cylinder-wall heterogeneity refers to laminate constructions in which there exists a significant through-the-thickness variation of the layer properties or orientations. Of particular interest herein are symmetric laminates with plies at the outer faces that are substantially different from those near the mid-plane. For convenience, this class of heterogeneous laminates are referred to herein as "sandwich-like" laminates. Use of the term "sandwich-like" herein is intended to connote the arrangement of plies and does not imply the existence of significant transverse shearing flexibility commonly associated with sandwich plates. To accomplish this objective, a set of nondimensional linear-bifurcation buckling equations and parameters are presented for balanced, symmetrically laminated cylinders subjected to uniform axial compression loads and in a membrane-stress prebuckling state. Anisotropy of the shell wall is presumed to be negligible. Then, a linear bifurcation buckling analysis is presented for the classical simply supported boundary conditions that are typically used in the preliminary design of cylinders. Next, approximate formulas for the buckling loads of infinitely long cylinders are derived. Results that establish the range of the nondimensional parameters appearing in the buckling analysis and simplified formulas are then presented. With the parameter ranges established, plots of nondimensional buckling load versus a stiffness-weighted length-to-radius ratio are presented for various combinations of the remaining parameters governing the behavior and for a very broad range of laminate constructions. Finally, relatively fewer "master curves" are presented for infinitely long cylinders that give a nondimensional measure of buckling as a function of the orthotropy parameters and the wall inhomogeneity measure. In addition, approximate formulas for the critical stresses are given that utilize the information in these curves. Thus, these "master curves" are anticipated to be useful in the ongoing development of buckling-design technology.

Bifurcation-Buckling Equations

To accomplish the objective of the present study, it is convenient to use the nondimensional parameters and equations presented in reference 4. When specialized to right circular cylindrical shells, such as that shown in figure 1, these equations correspond to Donnell-type, linear-

bifurcation buckling equations for symmetric laminates. In particular, the compatibility equation is given by

$$D_m(\delta F) = \sqrt{12}\, D_c(\delta W) \tag{1}$$

and the transverse equilibrium equation is given by

$$D_b(\delta W) + \sqrt{12}\, D_c(\delta F) = -\tilde{p}\pi^2 \frac{\partial^2 \delta W}{\partial \xi^2} \tag{2}$$

where $D_m(\,)$, $D_b(\,)$, and $D_c(\,)$ are nondimensional linear differential operators. The symbol δW denotes the nondimensional radial-displacement buckling mode and δF denotes the corresponding stress function. For symmetric laminates with negligible coupling between inplane stretching and shearing deformations, and between pure bending and twisting deformations, these operators are given by

$$D_m(\delta F) = \frac{1}{\alpha_m^2} \frac{\partial^4 \delta F}{\partial \xi^4} + 2\mu \frac{\partial^4 \delta F}{\partial \xi^2 \partial \eta^2} + \alpha_m^2 \frac{\partial^4 \delta F}{\partial \eta^4} \tag{3}$$

$$D_c(\delta W) = \rho \frac{\partial^2 \delta W}{\partial \xi^2} \tag{4}$$

$$D_b(\delta W) = \frac{1}{\alpha_b^2} \frac{\partial^4 \delta W}{\partial \xi^4} + 2\beta \frac{\partial^4 \delta W}{\partial \xi^2 \partial \eta^2} + \alpha_b^2 \frac{\partial^4 \delta W}{\partial \eta^4} \tag{5}$$

The nondimensional coordinates in these equations are defined as $\xi = \frac{x}{L}$ and $\eta = \frac{y}{R}$, where x is the axial coordinate, y is the circumferential arc-length coordinate, L is the cylinder length, R is the cylinder radius, $0 \le \xi \le 1$, and $0 \le \eta \le 2\pi$. The nondimensional parameters appearing in these equations are given by

$$\alpha_m = \frac{L}{R}\left(\frac{A_{22}}{A_{11}}\right)^{\frac{1}{4}} \tag{6}$$

$$\mu = \frac{A_{11}A_{22} - A_{12}^2 - 2A_{12}A_{66}}{2A_{66}\sqrt{A_{11}A_{22}}} \tag{7}$$

$$\alpha_b = \frac{L}{R}\left(\frac{D_{22}}{D_{11}}\right)^{\frac{1}{4}} \tag{8}$$

$$\beta = \frac{D_{12} + 2D_{66}}{\sqrt{D_{11}D_{22}}} \tag{9}$$

$$\nu_m = \frac{A_{12}}{\sqrt{A_{11}A_{22}}} \tag{10}$$

$$\rho = \frac{R}{h}\sqrt{1-\nu_m^2}\left[\frac{A_{11}A_{22}\,h^4}{144D_{11}D_{22}}\right]^{\frac{1}{4}} \tag{11}$$

where A_{11}, A_{12}, A_{22}, A_{66}, D_{11}, D_{12}, D_{22}, and D_{66} are the stiffnesses of classical laminated-shell theory (see reference 5), and the corresponding stiffnesses A_{16}, A_{26}, D_{16}, and D_{26} are presumed negligible. The parameter defined by equation (11) is a stiffness-weighted shell-wall thinness metric. The quantity $\tilde{p}$ is the nondimensional loading parameter defined by

$$\tilde{p} = \frac{N_x R^2}{\pi^2\sqrt{D_{11}D_{22}}} \tag{12}$$

where N_x is the magnitude of the uniform compressive axial stress resultant, that is presumed to exist prior to buckling, in classical linear bifurcation analyses for cylinders.

Buckling Analysis

For the purpose of preliminary design, cylinders with simply supported edges that restrict circumferential displacements are often used because they faciliate a simple analytical solution. These boundary conditions are usually referred to as the classical boundary conditions for simply supported shells and are denoted as "S2" boundary conditions in the recent book by Jones (see p. 477).[6] The nondimensional buckling modes for these boundary conditions are given by

$$\delta W = \mathscr{A}\sin(m\pi\xi)\cos(n\eta) \tag{13}$$

where $0 \le \xi \le 1$, $0 \le \eta \le 2\pi$, $m \in \{1, 2, 3, ...\}$ is the number of axial half-waves, $n \in \{0, 1, 2, ...\}$ is the number of full circumferential waves (see figure 2), and $\mathscr{A}$ is the indeterminate modal amplitude. A typical buckling mode is shown in figure 3a that exhibits one full axial wave and four full circumferential waves. The corresponding contour plot of the radial displacement is shown in figure 3b. Buckling modes with $n = 0$ and $n \neq 0$ are referred to herein as axisymmetric and asymmetric modes, respectively.

Substituting equation (13) into equation (1) indicates that the stress function can be represented by

$$\delta F = \mathscr{B}\sin(m\pi\xi)\cos(n\eta) \tag{14}$$

where $\mathscr{B}$ is related to the amplitude $\mathscr{A}$. Specifically, substituting equations (13) and (14) into equation (1) yields

$$\mathscr{E} = -\left[\frac{2\sqrt{3}\,\rho\, m^2\pi^2}{n^4\alpha_m^2 + 2\mu n^2 m^2\pi^2 + \dfrac{m^4\pi^4}{\alpha_m^2}}\right]\mathscr{A} \tag{15}$$

Substituting equation (15) into equation (14) and the result into equation (2), along with equation (13), and setting the coefficient of the trigonometric functions equal to zero yields the following equation for the eigenvalues $\tilde{p} = \tilde{p}(m, n)$

$$\tilde{p}\pi^2 = \frac{n^4\alpha_b^2}{m^2\pi^2} + 2\beta n^2 + \frac{\pi^2 m^2}{\alpha_b^2} + \frac{12\rho^2}{\dfrac{n^4\alpha_m^2}{m^2\pi^2} + 2\mu n^2 + \dfrac{m^2\pi^2}{\alpha_m^2}} \tag{16}$$

For a given set of material properties and cylinder dimensions, the nondimensional parameters appearing in equation (15) are fixed values. The nondimensional buckling load, $\tilde{p}_{cr}$, is then given by the smallest value of $\tilde{p}$ that is found for $m \in \{1, 2, 3, ...\}$ and $n \in \{0, 1, 2, ...\}$. The corresponding wave numbers are denoted by m_{cr} and n_{cr}.

Approximate Buckling Formulas

To obtain simple, approximate buckling formulas, similar to that given in reference 1, equation (16) is differentiated as if $\tilde{p} = \tilde{p}(m, n)$ is a continuous function and m and n are real variables. Although not strictly correct, this approach gives useful results for certain ranges of the nondimensional parameters appearing in equation (16). To obtain a minimum set,

$$d\tilde{p} = \frac{\partial\tilde{p}}{\partial m}\,dm + \frac{\partial\tilde{p}}{\partial n}\,dn = 0 \tag{17}$$

is enforced. In general, the partial derivatives appearing in equation (17) are very complicated functions of the variables m and n. To remedy this situation, it is convenient to introduce a nondimensional axial half-wave length Λ of a buckle pattern defined by

$$\Lambda = \left(\frac{L}{\pi m R}\right)^2\left(\frac{A_{22}}{A_{11}}\right)^{\frac{1}{2}} \tag{18}$$

and a positive-valued wall nonhomogeneity measure given by the following ratio of extensional and bending stiffnesses

$$\mathtt{I} = \left(\frac{A_{11}D_{22}}{D_{11}A_{22}}\right)^{\frac{1}{2}} \tag{19}$$

For a homogeneous wall, $\mathtt{I} = 1$. Because m is the number of axial half waves in a given bifurcation eigenvector, it follows that the quantity L/m is the axial half-wave length of the eigenvector. Substituting equations (18) and (19) into equations (6) and (8) yields

$$\left(\frac{\alpha_m}{\pi m}\right)^2 = \Lambda \tag{20a}$$

$$\left(\frac{\alpha_b}{\pi m}\right)^2 = \Lambda \mathtt{I} \tag{20b}$$

As the cylinder length increases to infinity, Λ behaves like a continuous variable and minimization of $\tilde{p}$ by differentiation with respect to Λ represents solutions for an infinitely long cylinder that buckles into a local shell mode and not into an overall column mode. Likewise, it is convenient to introduce

$$N = n^2 \tag{20c}$$

By using equations (20), equation (16) becomes

$$\tilde{p}\pi^2 = N^2 \Lambda \mathtt{I} + 2\beta N + \frac{1}{\Lambda \mathtt{I}} + \frac{12\rho^2}{\Lambda N^2 + 2\mu N + \frac{1}{\Lambda}} \tag{21}$$

Now, it is observed that application of the chain rule of differentiation to equation (17) reveals that minimization of $\tilde{p}$ with respect to Λ and N is equivalent to minimization with respect to m and n, respectively. Enforcing $\frac{\partial \tilde{p}}{\partial \Lambda} = 0$ and simplifying gives

$$\left(\mathtt{I} N^2 - \frac{1}{\mathtt{I}\Lambda^2}\right)\left[\frac{1}{\Lambda} + 2\mu N + \Lambda N^2\right]^2 - 12\rho^2\left[N^2 - \frac{1}{\Lambda^2}\right] = 0 \tag{22}$$

Likewise, enforcing $\frac{\partial \tilde{p}}{\partial N} = 0$ gives

$$\left(\beta + \mathtt{I}\Lambda N\right)\left[\frac{1}{\Lambda} + 2\mu N + \Lambda N^2\right]^2 - 12\rho^2\left(\mu + \Lambda N\right) = 0 \tag{23}$$

for values of $N > 0$, which yields

$$\left[\frac{1}{\Lambda} + 2\mu N + \Lambda N^2\right]^2 = 12\rho^2 \frac{\mu + \Lambda N}{\beta + \mathtt{I}\Lambda N} \tag{24}$$

Substituting equation (24) into equation (22) gives

$$\left[\mathbf{I}^2\Lambda^2N^2 - 1\right]\left(\mu + \Lambda N\right) - \mathbf{I}\left(\beta + \mathbf{I}\Lambda N\right)\left[\Lambda^2N^2 - 1\right] = 0 \tag{25a}$$

for values of $N > 0$. For the case of $N = 0$, minimization of equation (21) with respect to nonzero values of Λ is given by equation (22), which reduces to

$$-\frac{1}{\mathbf{I}\Lambda^2} + 12\rho^2 = 0 \tag{25b}$$

Here, it is important to note that values of Λ and N that satisfy equations (24) and (25), denoted by Λ_{cr} and N_{cr}, respectively, yield the critical value of $\tilde{p}$, denoted by $\tilde{p}_{cr}$, when substituted into equation (21).

Solutions that minimize the right-hand side of equation (21) are obtained by examining the cases of $N = 0$ and $N > 0$ separately. For the case of $N = 0$, equation (25b) yields

$$\Lambda_{cr} = \frac{1}{2\sqrt{3\mathbf{I}}\,\rho} \tag{26}$$

Substituting equation (26) for Λ and $N = 0$ into equation (21) gives the result

$$\tilde{p}_{cr} = \frac{4\sqrt{3}\,\rho}{\pi^2\sqrt{\mathbf{I}}} \tag{27}$$

where it is implied that $N_{cr} = 0$. This solution corresponds to short-wave-length, axisymmetric buckle patterns.

Solutions of equations (24) and (25a) for $N > 0$ are found in the present study by defining a positive-valued quantity X given by

$$X = \mathbf{I}\Lambda N \tag{28}$$

so that equation (25a) becomes

$$\left(\beta - \mathbf{I}\mu\right)X^2 + \left(1 - \mathbf{I}^2\right)X + \mathbf{I}\left(\mu - \mathbf{I}\beta\right) = 0 \tag{29}$$

equation (24) becomes

$$\left[\frac{\mathbf{I}}{X} + 2\mu + \frac{X}{\mathbf{I}}\right]^2N^2 = \frac{12\rho^2}{\mathbf{I}}\,\frac{\mathbf{I}\mu + X}{\beta + X} \tag{30}$$

and equation (21) becomes

$$\tilde{p}\pi^2 = \left(X + 2\beta + \frac{1}{X}\right)N + \frac{12\rho^2}{\left(\frac{X}{\mathtt{I}} + 2\mu + \frac{\mathtt{I}}{X}\right)N} \tag{31}$$

This transformation allows N to be expressed in terms of the nondimensional parameters and the new variable X. In particular, equation (30) is solved for N to get

$$N = 2\rho X\sqrt{3\mathtt{I}}\ \sqrt{\frac{\mathtt{I}\mu + X}{\beta + X}}\left[\mathtt{I}^2 + 2\mu\mathtt{I}X + X^2\right]^{-1} \tag{32}$$

Equation (32) is now used to eliminate N from equation (31), which yields $\tilde{p}$ a function of X; that is, equation (31) becomes

$$\tilde{p} = \frac{2\sqrt{3\mathtt{I}}\rho}{\pi^2}\sqrt{\frac{\mathtt{I}\mu + X}{\beta + X}}\left[\frac{X^2 + 2\beta X + 1}{X^2 + 2\mu\mathtt{I}X + \mathtt{I}^2} + \frac{\beta + X}{\mathtt{I}\mu + X}\right] \tag{33}$$

The critical values of $\tilde{p}$ are obtained by substituting the positive-valued solutions to equation (29), denoted by $X = X_{cr}$, into equation (33). In particular, the solutions to equation (29) are given by

$$X_{cr} = \frac{\mathtt{I}^2 - 1}{2(\beta - \mathtt{I}\mu)}\left[1 \pm \sqrt{1 + \frac{4\mathtt{I}(\beta - \mathtt{I}\mu)(\mathtt{I}\beta - \mu)}{(\mathtt{I}^2 - 1)^2}}\right] \tag{34a}$$

for $\beta - \mathtt{I}\mu \neq 0$ and $\mathtt{I} \neq 1$. The corresponding values of $\tilde{p}_{cr}$ and N_{cr} are given by

$$\tilde{p}_{cr} = \frac{2\sqrt{3\mathtt{I}}\rho}{\pi^2}\sqrt{\frac{\mathtt{I}\mu + X_{cr}}{\beta + X_{cr}}}\left[\frac{X_{cr}^2 + 2\beta X_{cr} + 1}{X_{cr}^2 + 2\mu\mathtt{I}X_{cr} + \mathtt{I}^2} + \frac{\beta + X_{cr}}{\mathtt{I}\mu + X_{cr}}\right] \tag{34b}$$

$$N_{cr} = 2\rho X_{cr}\sqrt{3\mathtt{I}\left(\frac{\mathtt{I}\mu + X_{cr}}{\beta + X_{cr}}\right)}\left[X_{cr}^2 + 2\mu\mathtt{I}X_{cr} + \mathtt{I}^2\right]^{-1} \tag{34c}$$

Additionally, equation (28) yields

$$\Lambda_{cr} = \frac{X_{cr}}{\mathtt{I}N_{cr}} \tag{34d}$$

These results correspond to short-wave-length, non-axisymmetric buckle patterns. It is important to note that as $X_{cr} + \mathtt{I}\mu \rightarrow 0$, $\tilde{p}_{cr} \rightarrow \infty$.

For, the case of $N > 0$ and $\mathtt{I} = 1$ and either $\beta - \mathtt{I}\mu \neq 0$ or $\beta - \mathtt{I}\mu = 0$, the solution to equation (29) is given by $X_{cr} = 1$ and equation (34b) reduces to

$$\tilde{p}_{cr} = \frac{4\sqrt{3}\rho}{\pi^2} \sqrt{\frac{1+\beta}{1+\mu}} \tag{35a}$$

which is identical to the corresponding result presented in reference 1. Additionally, equation (34c) reduces to

$$N_{cr} = \frac{\sqrt{3}\,\rho}{\sqrt{(1+\beta)(1+\mu)}} \tag{35b}$$

and equation (34d) becomes

$$\Lambda_{cr} = \frac{\sqrt{(1+\beta)(1+\mu)}}{\sqrt{3}\,\rho} \tag{35c}$$

For this case, $\tilde{p}_{cr} \rightarrow \infty$ as $\mu \rightarrow -1$ and the corresponding axisymmetric buckling solution given by equations (26) and (27) govern the response. For cases with $\beta - \mathtt{I}\mu = 0$ and $\mathtt{I} \neq 1$, equation (29) reduces to $X = -\beta$, which yields physically inadmissible solutions for positive values of β, since $X > 0$ by definition. In addition, equations (34b)-(34d) become singular. Solutions for this case are obtained by re-examining equations (21)-(23). First, equation (23) yields

$$\left[\mathtt{I}\left(\frac{1}{\Lambda} + 2\mu N + \Lambda N^2\right)^2 - 12\rho^2\right](\mu + \Lambda N) = 0 \tag{36}$$

which is satisfied by selecting

$$\left(\frac{1}{\Lambda} + 2\mu N + \Lambda N^2\right)^2 = \frac{12\rho^2}{\mathtt{I}} \tag{37}$$

Substituting equation (37) into equation (22) gives

$$\left(\mathtt{I} - \frac{1}{\mathtt{I}}\right)\frac{1}{\Lambda^2} = 0 \tag{38}$$

Enforcing $\mathtt{I} \neq 1$ requires Λ^{-1} to go to zero, which means that the buckle patterns have axial half waves that are on the order of the cylinder length. Next, substituting $\Lambda^{-1} = 0$ back into equation (37) gives

$$2\mu N + \Lambda N^2 = \pm 2 \sqrt{\frac{3}{\mathtt{I}}}\, \rho \tag{39}$$

For this equation, and equation (21), it is presumed that $N \rightarrow 0$ such that $N^2\Lambda$ and $N\Lambda$ are finite valued. As a result, equation (21) with $\beta = \mathtt{I}\mu$ yields the result

$$\tilde{p}_{cr} = \frac{4\sqrt{3\mathtt{I}}\,\rho}{\pi^2} \tag{40}$$

The results producing equation (40) indicate that long-wave-length buckle patterns exist. In addition, it is important to note that the analysis presented by equation (22)-(35) is not valid for very long cylinders that exhibit buckle patterns with axial half waves that are on the order of the cylinder length. For the general case of long-wave-length buckle patterns, the parameter Λ is presumed to approach infinity and the parameter N is presumed to approach zero such that $N^2\Lambda$ and $N\Lambda$ remain finite. Applying these presumptions to equation (21) gives

$$\tilde{p}\pi^2 = N^2\Lambda\mathtt{I} + \frac{12\rho^2}{N^2\Lambda} \tag{41}$$

Minimization of this equation with respect to $N^2\Lambda$ gives

$$\tilde{p}_{cr} = \frac{4\sqrt{3\mathtt{I}}\,\rho}{\pi^2} \tag{42}$$

which is identical to equation (40), with no restrictions on the values of $\mathtt{I}$, β, or μ. For this case, the buckle pattern is axisymmetric; that is, $N_{cr} = 0$. Note that the $\sqrt{\mathtt{I}}$ appears in the numerator of equation (42) and in the denomenator of equation (27) for the short-wavelength axisymmetic buckle pattern.

Results and Discussion

In the present section, results that indicate the possible ranges of the nondimensional parameters and coefficients defined by equations (6)-(11) and (19) are presented first. Based on these ranges, generic buckling results obtained by minimization of equation (16) with respect to m and n are presented entirely in terms of the nondimensional parameters defined herein. These generic results are based on very wide parameter ranges and, as a result, encompass a wide range of geometries and laminate constructions and also illustrate a wide spectrum of behavioral trends.

Next, “master curves” for infinitely long cylinders are presented. In particular, two nearly identical sets of results are presented that were obtained by minimization of equation (16) with respect to m and n for extremely long cylinders and by using the approximate formulas derived herein.

Parameter and Coefficient Ranges

The nondimensional parameters and coefficients defined herein have been presented for a wide variety of balanced, symmetric laminates in reference 7 for the nine material systems given in Table 1. Two laminate families of particular interest that are discussed in this reference are the $[(\pm 45/0/90)_p]_S$ and $[(0/90/\pm 45)_p]_S$ quasi-isotropic laminates, and the $[(+\theta/-\theta)_p]_S$ and $[(-\theta/+\theta)_p]_S$ angle-ply laminates. The results presented in reference 7 for the $[(+\theta/-\theta)_p]_S$ and the $[(-\theta/+\theta)_p]_S$ angle-ply laminates indicate the following ranges:

$$0.279 \le \beta \le 2.76$$

$$-0.788 \le \mu \le 5.43$$

$$0.341 \le (A_{22}/A_{11})^{1/4} \le 2.93$$

$$\mathtt{I} = 1$$

$$0.446 \le \sqrt{1 - \nu_m^2}\left[\frac{A_{11}A_{22}\,h^4}{144 D_{11}D_{22}}\right]^{\frac{1}{4}} \le 0.999$$

for the nine material systems, regardless of the value of the stacking sequence index p. Likewise, the results for the $[(\pm 45/0/90)_p]_S$ quasi-isotropic laminates indicate:

$$1.03 \le \beta \le 2.22$$

$$0.926 \le (D_{22}/D_{11})^{1/4} \le 1.00$$

$$0.958 \le \sqrt{1 - \nu_m^2}\left[\frac{A_{11}A_{22}\,h^4}{144 D_{11}D_{22}}\right]^{\frac{1}{4}} \le 1.09$$

for the nine material systems and for p = 1,2, ..., 8. Moreover, for the $[(0/90/\pm 45)_p]_S$ quasi-isotropic laminates the results indicate:

$$0.266 \le \beta \le 0.968$$

$$0.862 \le (D_{22}/D_{11})^{1/4} \le 1.00$$

$$0.875 \le \sqrt{1-\nu_m^2}\left[\frac{A_{11}A_{22}\,h^4}{144D_{11}D_{22}}\right]^{\frac{1}{4}} \le 0.956$$

for the nine material systems and p = 1,2, ..., 8. For both families of quasi-isotropic laminates, $(A_{22}/A_{11})^{1/4} = 1$ and $\mu = 1$, regardless of the lamina material system and the number of plies. Thus, it follows that the heterogeneity parameter has the range $0.862 \le \mathtt{I} \le 1.00$ for both families of quasi-isotropic laminates, regardless of the lamina material system and the number of plies.

Two other laminate families considered herein are the $[(\pm 45/0_2)_p]_S$ axially stiff laminates and the $[(\pm 45/90_2)_p]_S$ circumferentially stiff laminates with integer values for the index p = 1, 2, ..., 8. Results obtained in the present study for the $[(\pm 45/0_2)_p]_S$ laminates yielded:

$$1.04 \le \beta \le 2.24$$

$$0.531 \le \mu \le 0.987$$

$$1.01 \le \mathtt{I} \le 1.72$$

$$0.687 \le (A_{22}/A_{11})^{1/4} \le 0.941$$

$$0.901 \le \sqrt{1-\nu_m^2}\left[\frac{A_{11}A_{22}\,h^4}{144D_{11}D_{22}}\right]^{\frac{1}{4}} \le 0.988$$

for the nine material systems and p = 1,2, ..., 8. For the $[(\pm 45/90_2)_p]_S$ laminates, the same ranges for β, μ, and $\sqrt{1-\nu_m^2}\left[\frac{A_{11}A_{22}\,h^4}{144D_{11}D_{22}}\right]^{\frac{1}{4}}$ were obtained. In contrast, the ranges $0.582 \le \mathtt{I} \le 0.989$, $1.06 \le (A_{22}/A_{11})^{1/4} \le 1.45$ were obtained for the nine material systems and p = 1, 2, ..., 8.

Sandwich-like laminates with pairs of 0-deg and 90-deg plies lumped between pairs of angle plies were also considered in the present study. In particular, results were obtained in the present study for $[(+\theta/-\theta)_2/(0/90)_4]_S$ laminates that revealed:

$$0.083 \le \beta \le 1.58$$

$$1.22 \le \mu \le 16.89$$

$$0.543 \le \mathtt{I} \le 1.50$$

$$0.845 \le (A_{22}/A_{11})^{1/4} \le 1.18$$

$$0.988 \le \sqrt{1 - \nu_m^2}\left[\frac{A_{11}A_{22}h^4}{144D_{11}D_{22}}\right]^{\frac{1}{4}} \le 1.18$$

for the nine material systems and for $0 \le \theta \le 90$ deg. Results were also obtained in the present study for 24-ply $[90_p/0_q]_S$ laminates that indicate:

$$0.065 \le \beta \le 0.697$$

$$1.71 \le \mu \le 17.85$$

$$1.04 \le \mathtt{I} \le 3.42$$

$$0.568 \le (A_{22}/A_{11})^{1/4} \le 1.76$$

$$.829 \le \sqrt{1 - \nu_m^2}\left[\frac{A_{11}A_{22}h^4}{144D_{11}D_{22}}\right]^{\frac{1}{4}} \le 1.69$$

for the nine material systems and for $p = 1, 2, ..., 11$. Similarly, results for 24-ply $[0_p/90_q]_S$ laminates that exhibit the same ranges for β, μ, $(A_{22}/A_{11})^{1/4}$, and $\sqrt{1 - \nu_m^2}\left[\frac{A_{11}A_{22}h^4}{144D_{11}D_{22}}\right]^{\frac{1}{4}}$ were obtained. In contrast, the range of the heterogeneity parameter given by $0.292 \le \mathtt{I} \le 0.962$ was obtained for the nine material systems and for $p = 1, 2, ..., 11$.

Generic Buckling Results

The nondimensional buckling loads obtained by minimization of equation (16) with respect to m and n are shown in figures 4-75 as a function of the stiffness-weighted length-to-radius ratio α_m defined by equation (6). Six curves are shown in each figure that correspond to values of the orthotropy parameter $\mu = -1, 0, 1, 5, 10$ and 20. Figures 4-75 are also composed of three groups of related curves. In particular, figures 4-27 correspond to results for the stiffness-weighted thinness ratio $\rho = 25$, figures 28-51 correspond to results for $\rho = 100$, and figures 52-75 correspond to results for $\rho = 1000$. Within each of these three groups, 24 curves are presented for combinations of the values of the orthotropy parameter $\beta = 0, 1, 2$, and 3 and for values of the nonhomogeneity parameter $\mathtt{I} = 0.25, 0.5, 1, 1.5, 2$, and 4. In computing these results, equations (6), (8), and (19) were used to obtain $\alpha_b = \sqrt{\mathtt{I}}\alpha_m$.

The results in figures 4-75 generally show a series of festoon curves in which the amplitudes of the festoons attenuate to a negligible magnitude as the stiffness-weighted length-to-radius ratio α_m increases. Likewise, the nondimensional buckling loads forming a given curve attenuate to the constant value associated with the corresponding infinitely long cylinder that buckles into a local

shell mode, not an overall column mode. The results in figures 4-75 also generally show that the festoons making up the curves become less prominent as β decreases, as μ increases, or as $\mathtt{I}$ increases for each group of curves corresponding to a given value of ρ. Additionally, the festoons become generally less pronounced for a group of curves as the value of ρ increases.

"Master Curves"

As evidenced by the parameter ranges presented herein, the numerous results appearing in figures 4-75 are applicable to a very broad range of symmetrically laminated cylinders. However, it is desirable to reduce these results into a compact form suitable for preliminary design that captures the essential trends and that provides adequate estimates of the buckling resistance. This reduction was performed in the present study by observing that each festoon curve appearing in figures 4-75 has a useful, practical lower bound that is given by the buckling load of the corresponding infinitely long cylinder. These lower-bound buckling loads were obtained in the present study for selected values of β, μ, ρ, and $\mathtt{I}$ by minimizing equation (16) with respect to m and n for relatively large values of α_m. Moreover, the curves in figures 4-75 with the pronounced festoons required significantly larger values of α_m than the curves that exhibit rapid attenuation of the buckling load with increasing values of α_m. This process typically involves minimization over a very large set of values for m and n. As a result, the determination of a buckling load following this process involves a large number of computations.

The approximate buckling loads for infinitely long cylinders that are given herein by the smallest positive value of $\tilde{p}_{cr}$ obtained from equations (27), (34b), and (42) require significantly fewer computations than the minimization of equation (16). To demonstrate the accuracy of these approximate buckling loads, several attempts were made during the present study to find a concise means of comparison applicable to the wide range of values for β, μ, ρ, and $\mathtt{I}$ appearing in figures 4-75. The comparisons presented in figures 76-79 were found to be adequate. An important step in arriving at the form of these figures was found when parametric studies revealed that plots of $\tilde{p}_{cr}$ versus μ have the same shape for a fixed value of β and any value of ρ. In addition, it was found that identical sets of curves were produced for a given values of $\mathtt{I}$ and its reciprocal. Moreover, equation (35a) revealed that $\dfrac{\pi^2 \tilde{p}_{cr}}{4\sqrt{3}\,\rho} = 1$ for an isotropic material. These facts led to the use of $\dfrac{\pi^2 \tilde{p}_{cr}}{4\sqrt{3}\,\rho}$ as the ordinate in figures 76-79.

Four pairs of red and blue curves are shown in each of figures 76-79. Each pair corresponds to a given value of the orthotropy parameter β. The blue curves correspond to buckling loads obtained by minimizing equation (16) with respect to m and n for $\alpha_m = 100$. The red curves correspond to the smallest positive value $\tilde{p}_{cr}$ obtained from equation (27) for short-wave-length, axisymmetric buckle patterns, from equation (34b) for short-wave-length, non-axisymmetric buckle patterns, and from equation (42) for long-wave-length, axisymmetric buckle patterns. All

of the curves shown in these figures were computed for a value of $\rho = 100$. In solving equation (34b), it was found that equation (34a) exhibited only one positive-valued root.

Inspection of the results used to obtain figures 76-79 indicated differences in buckling loads for each pair of curves that are less than 3%. Similar results were obtained for values of $\rho = 1000$ and 25 which exhibited differences in buckling loads for each corresponding pair of curves that are less than 3% and 8%, respectively. Overall, the differences in each pair of corresponding buckling loads obtained from the two solution methods are insignificant compared to the inherrent variability in the material properties. It is important to observe that the results in figures 76-79 are applicable to an enormous number of laminate constructions. Moreover, the compact form of figures 76-79 make the design space easier to navigate and interpret.

The results presented in figures 76-79 show that the nondimensional buckling load $\frac{\pi^2 \tilde{p}_{cr}}{4\sqrt{3}\,\rho}$ decreases as the orthotropy parameters β or μ decrease. Moreover, the effect of decreasing μ on the nondimensional buckling load is reduced as the nonhomogeneity parameter I becomes greater or less than a value equal to one. The further I departs from $I = 1$, the more the nondimensional buckling loads are reduced.

Approximate Formulas for Critical Stresses

The results presented in figures 76-79 are also useful for estimating the critical stress in a cylinder incipient to buckling. Specifically, approximate formulas for the critical stress of a geometrically perfect cylinder, σ_x^{cr}, are obtained by using $\sigma_x^{cr} = \frac{N_x^{cr}}{h}$ with equation (12) to get

$$\sigma_x^{cr} = \frac{\tilde{p}_{cr}\pi^2}{R^2 h}\sqrt{D_{11}D_{22}} \tag{43}$$

An insightful, alternate form of equation (43) is obtained by using equation (11) to get

$$\sigma_x^{cr} = c_x \frac{\bar{E}h}{R} \tag{44a}$$

where

$$c_x \equiv \sqrt{\frac{1-\nu_m^2}{3}}\left[\frac{144\, A_{11}A_{22}D_{11}D_{22}}{\bar{E}^4 h^8}\right]^{\frac{1}{4}}\left(\frac{\pi^2 \tilde{p}_{cr}}{4\sqrt{3}\,\rho}\right) \tag{44b}$$

and the term in parentheses is the ordinate used in figures 76-79. The symbol $\bar{E}$ denotes a convenient reference modulus of elasticity and is included in equations (44) to provide some freedom in the way one may want to represent the critical stress for a given problem. For example, consider an isotropic material with a modulus E and Poisson's ratio ν. For this material, $\frac{\pi^2 \tilde{p}_{cr}}{4\sqrt{3}\,\rho} = 1$ and using $\bar{E} = E$ in equations (44) yields the well-known formula

$$\sigma_x^{cr} = \frac{1}{\sqrt{3\left(1-\nu^2\right)}} \frac{Eh}{R} \approx 0.6 \frac{Eh}{R} \tag{45}$$

that is often used in the design of isotropic cylinders. For a given class of laminated cylinders, picking the reference modulus to be the effective axial modulus of a specific laminate configuration in the class may yield a desired physical interpretation of equation (44a) that is useful in the design of these cylinders.

Concluding Remarks

A set of nondimensional linear-bifurcation buckling equations for balanced, symmetrically laminated cylinders subjected to uniform axial compression loads have been presented that are based on Donnell's equations. These equations presume negligible shell-wall anisotropies and have been solved exactly for the practical case of simply supported ends. Nondimensional quantities have been used to characterize the buckling behavior that consist of a stiffness-weighted length-to-radius parameter, a stiffness-weighted shell-thinness parameter, a shell-wall nonhomogeneity parameter, two parameters that quantify membrane and bending orthotropies, and a nondimensional buckling load. Results that establish the range of the nondimensional parameters appearing in the buckling analysis have also been presented that encompass a wide range of laminated-wall constructions. Numerous generic plots of nondimensional buckling load versus a stiffness-weighted length-to-radius ratio are presented for various combinations of the remaining parameters governing the behavior. These plots span the established ranges of the nondimensional parameters and are expected to include many practical cases of interest to designers. Additionally, these plots show how the parameter values affect the distribution and size of the festoons forming each response curve and how they affect the attenuation of each response curve to the corresponding solution for an infinitely long cylinder.

To aid in preliminary design studies, approximate formulas for the nondimensional buckling load have been derived. These formulas give the attenuated buckling response of an infinitely long cylinder in terms of the previously described nondimensional parameters and have been validated against the corresponding exact solution. An important finding of the present study is that a relatively small number of "master curves" have been identified that give a nondimensional measure of the buckling load of an infinitely long cylinder as a function of the orthotropy and wall inhomogeneity parameters. In particular, these curves reduce greatly the complexity of the design-variable space as compared to representations that use dimensional quantities as design variables. Approximate formulas for the critical stresses have also been given that utilize the

information in these curves. As a result of their inherent simplicity, these "master curves" are anticipated to be useful in the ongoing development of buckling-design technology.

References

1. Nemeth, M. P. and Mikulas, M. M., Jr.: *Simple Formulas and Results for Buckling-Resistance and Stiffness Design of Compression-Loaded Laminated-Composite Cylinders*. NASA/TP-2009-215778, August 2009.

2. Mikulas, M. M., Jr.; Nemeth, M. P.; Oremont, L.; and Jegley, D. C.: Effect of Boundary Conditions on the Axial Compression Buckling of Homogeneous Orthotropic Composite Cylinders in the Long Column Range. *Proceedings of the AIAA/ASME/ASCE/AHS/ASC 52nd Structures, Structural Dynamics, and Materials Conference,* 2011, AIAA paper 2011-2126.

3. Anon.: *Buckling of Thin-Walled Circular Cylinders*. NASA Space Vehicle Design Criteria, NASA SP-8007, September 1965, revised August 1968.

4. Nemeth, M. P.: *Nondimensional Parameters and Equations for Buckling of Symmetrically Laminated Thin Elastic Shallow Shells*. NASA TM 104060, 1991.

5. Jones, R. M.: *Mechanics of Composite Materials*. Second ed., Taylor & Francis, 1999.

6. Jones, R. M.: *Buckling of Bars, Plates, and Shells*. Bull Ridge Publishing, 2006.

7. Nemeth, M. P.: *Nondimensional Parameters and Equations for Nonlinear and Bifurcation Analyses of Thin Anistropic Quasi-Shallow Shells*. NASA/TP-2010-216726, 2010.

Table 1. Lamina Properties

Lamina property*	Material Systems								
	Boron-Al	S-glass-epoxy	Kevlar 49-epoxy	IM7/ 5260	AS4/ 3502	AS4/ 3501-6	Boron-epoxy	IM7/ PETI-5	P-100/ 3502
E_L, Msi	33	7.5	11.02	22.1	18.5	20.01	29.58	20.35	53.5
E_T, Msi	21	1.7	0.8	1.457	1.64	1.30	2.68	1.16	0.73
ν_{LT}	0.23	0.25	0.34	0.258	0.30	0.30	0.23	0.29	0.31
G_{LT}, Msi	7.0	0.80	0.33	0.860	0.87	1.03	0.81	0.61	0.76

* The symbols L and T denote the longitudinal fiber and transverse matrix directions of a specially orthotropic lamina, respectively.

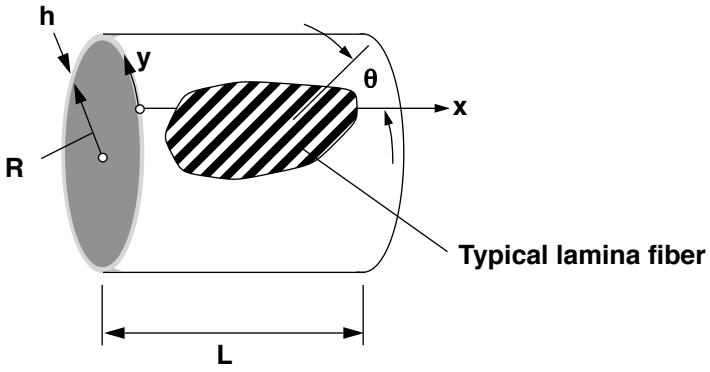

Figure 1. Cylinder geometry, surface coordinate system, and lamina fiber orientation.

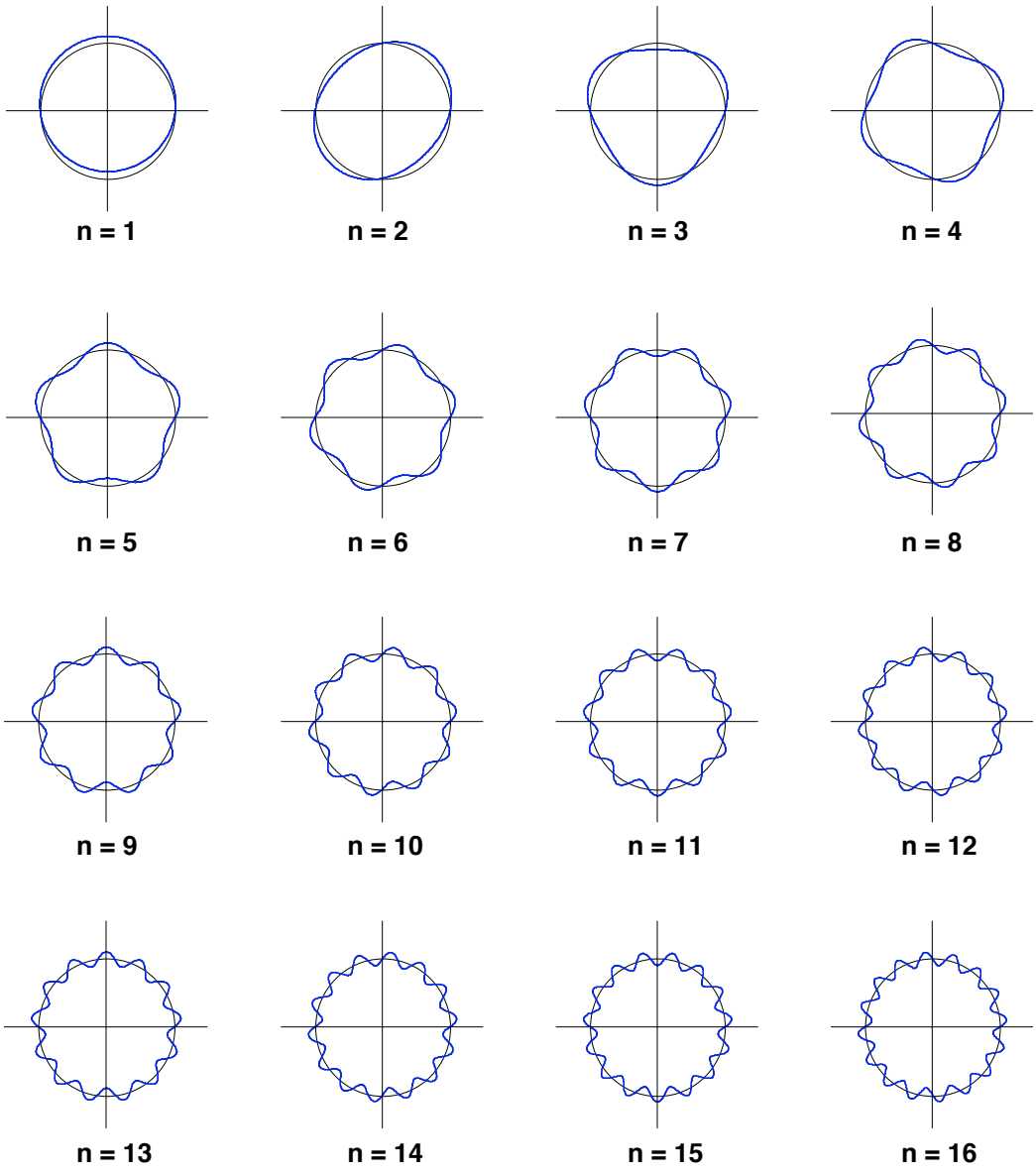

Figure 2. Circumferential waveforms used in equation (12).

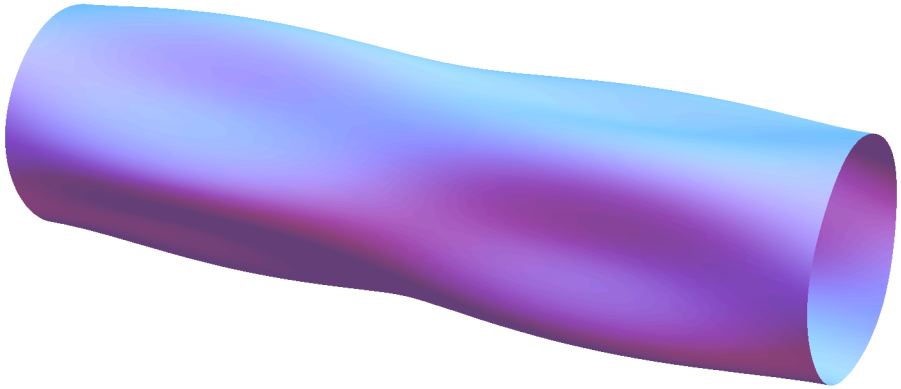

(a) Three-dimensional rendering of a buckling mode

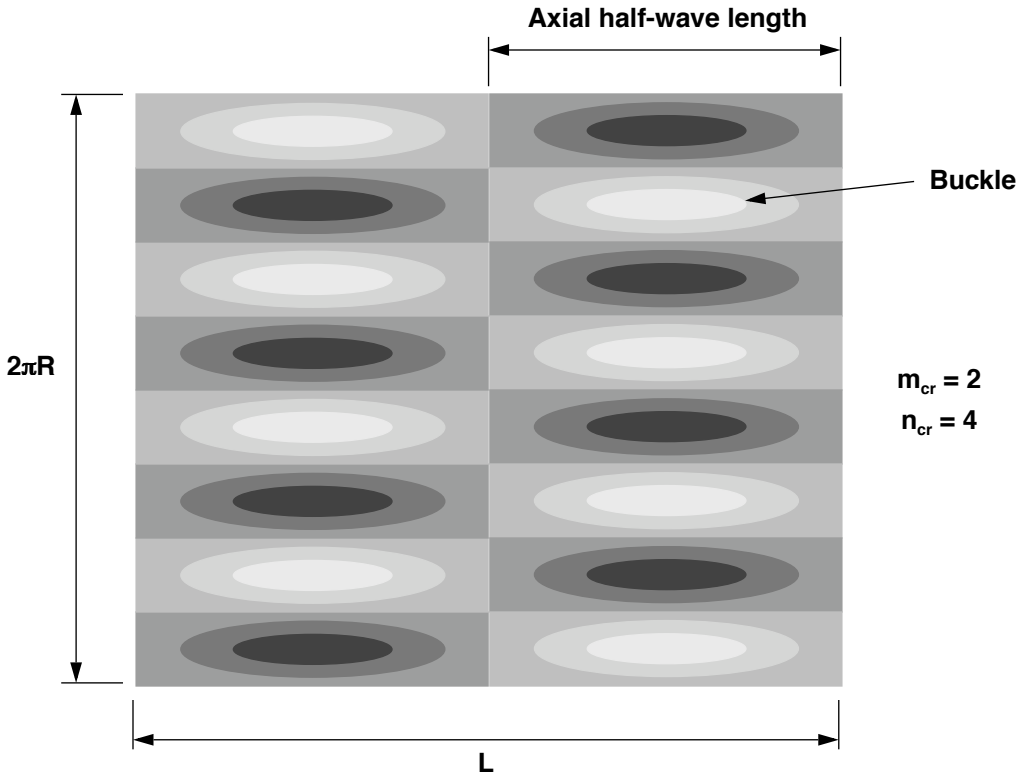

(b) Contour plot of the radial displacement

Figure 3. Typical buckle pattern of a compression-loaded cylinder.

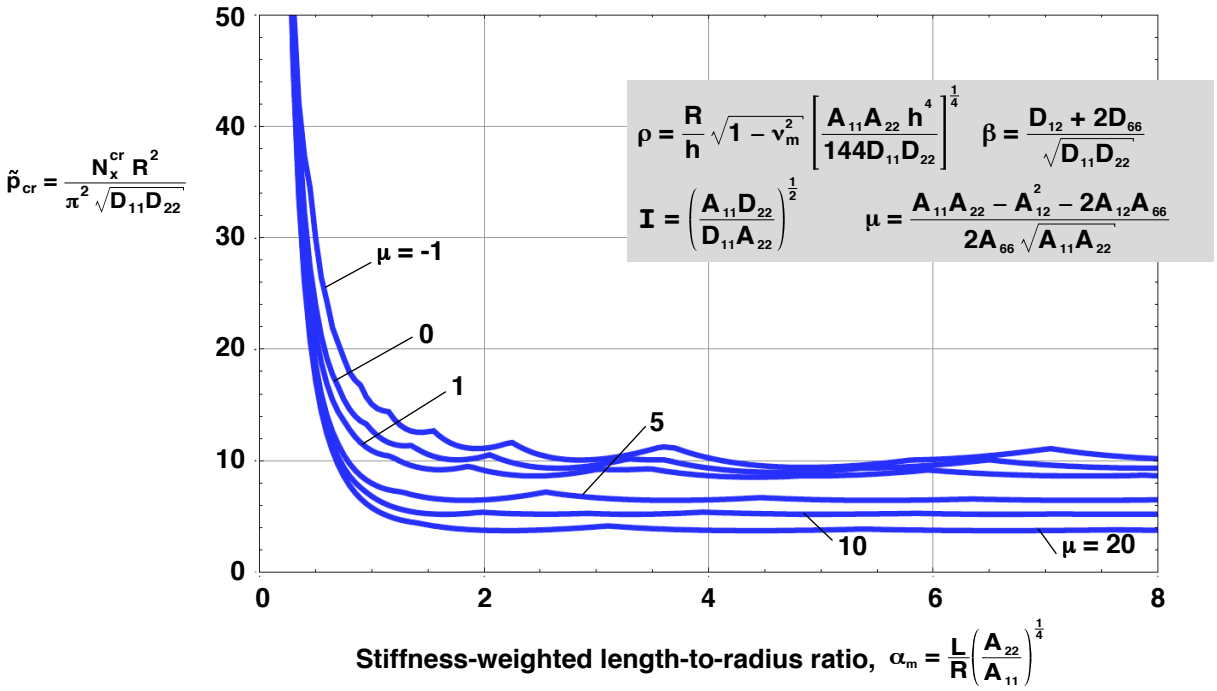

Figure 4. Effects of parameters α_m and μ on nondimensional buckling loads on cylinders with $\beta = 0$, $\gamma = 0.25$, and $\rho = 25$.

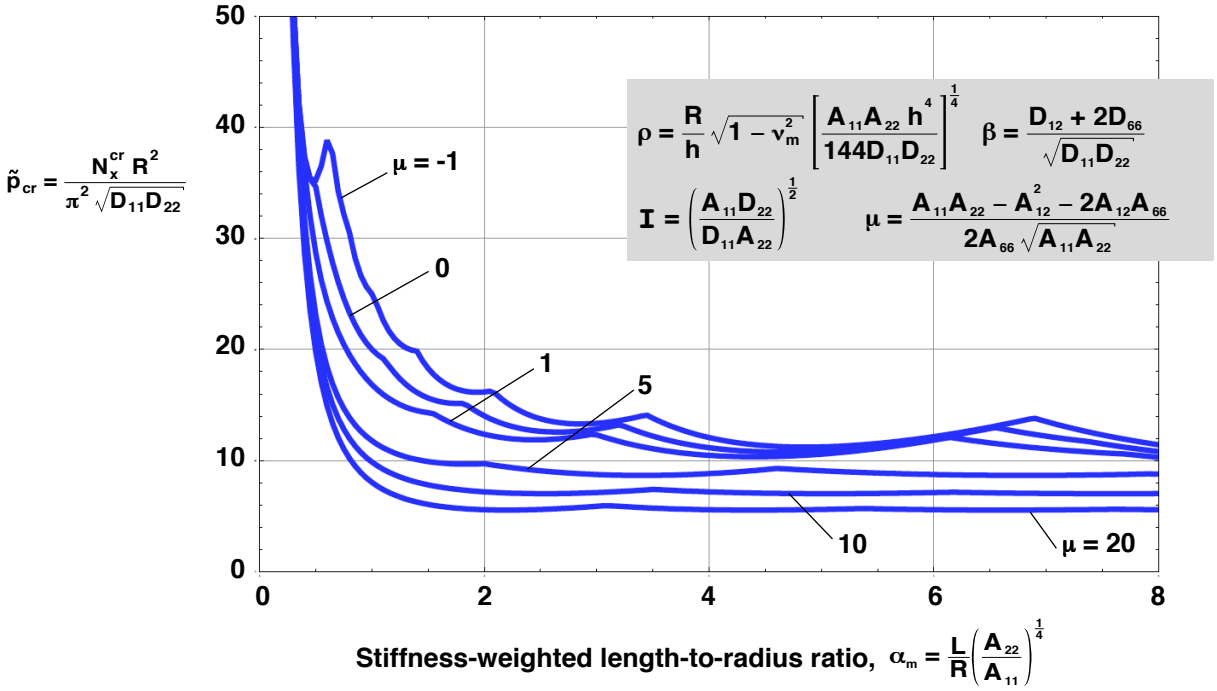

Figure 5. Effects of parameters α_m and μ on nondimensional buckling loads on cylinders with $\beta = 1$, $\gamma = 0.25$, and $\rho = 25$.

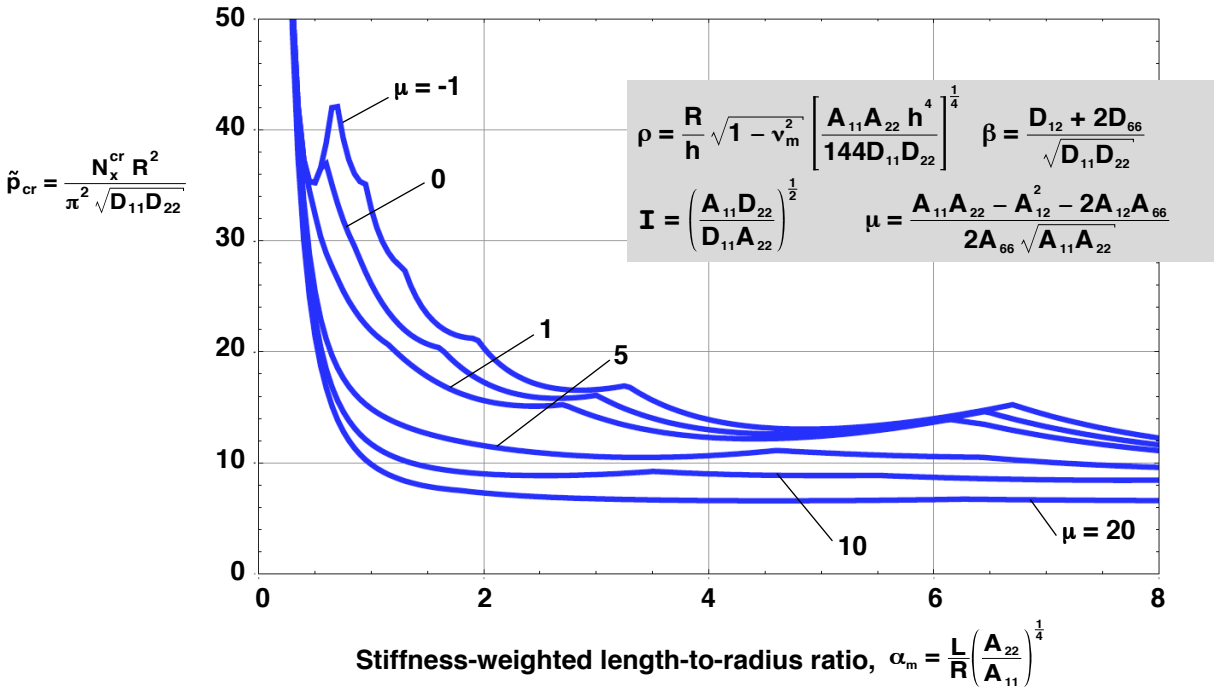

Figure 6. Effects of parameters α_m and μ on nondimensional buckling loads on cylinders with $\beta = 2$, $\gamma = 0.25$, and $\rho = 25$.

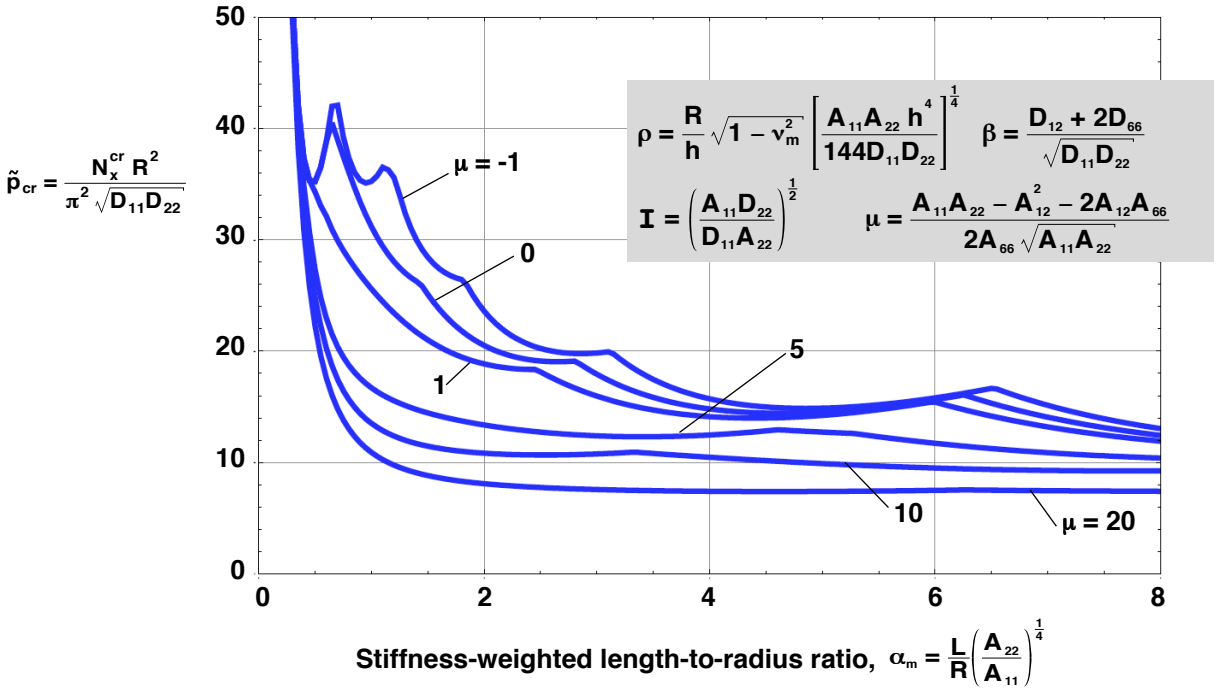

Figure 7. Effects of parameters α_m and μ on nondimensional buckling loads on cylinders with $\beta = 3$, $\gamma = 0.25$, and $\rho = 25$.

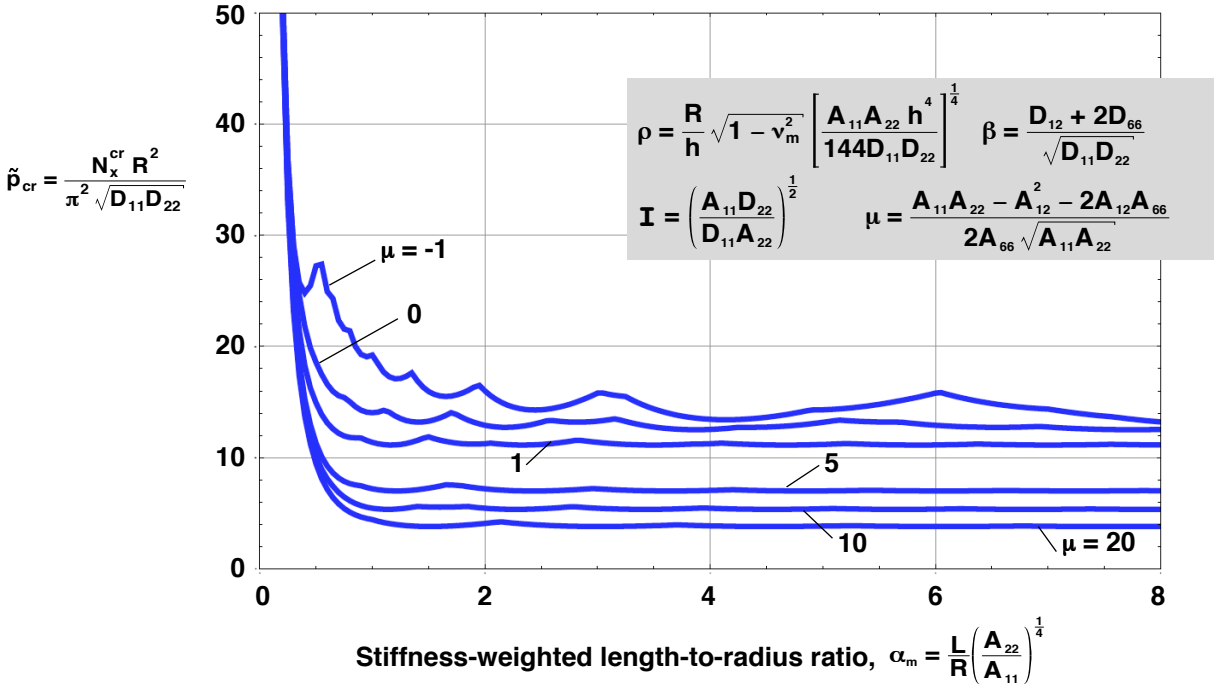

Figure 8. Effects of parameters α_m and μ on nondimensional buckling loads on cylinders with $\beta = 0$, $\gamma = 0.5$, and $\rho = 25$.

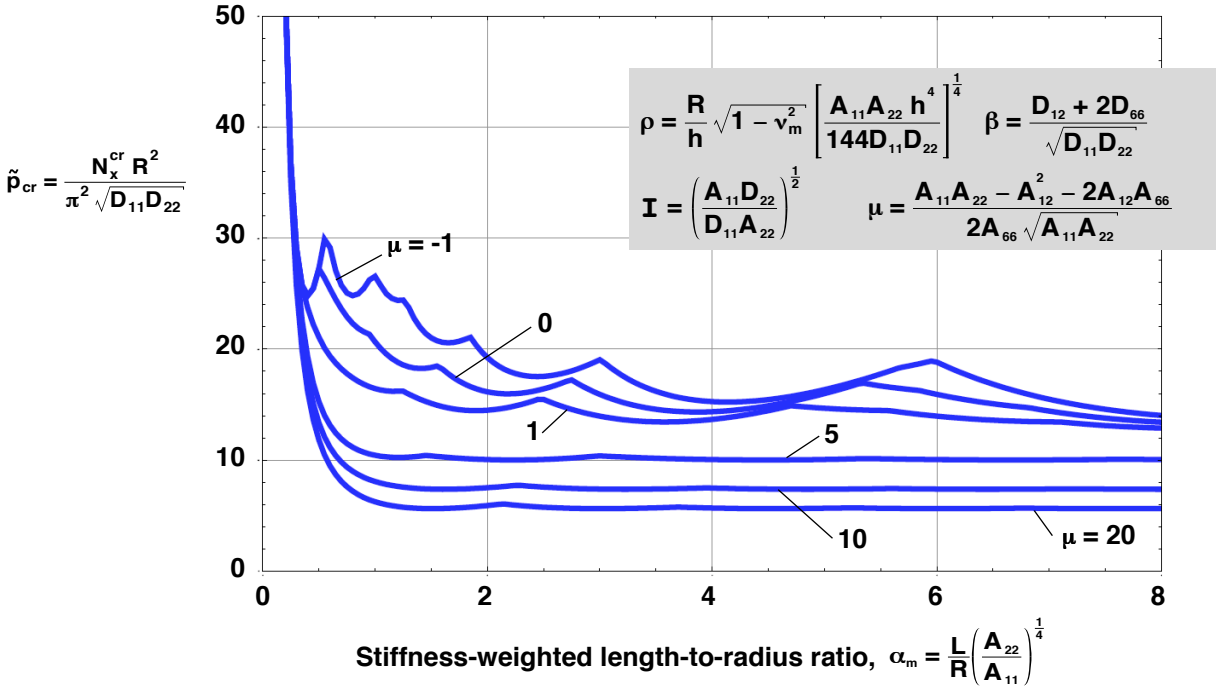

Figure 9. Effects of parameters α_m and μ on nondimensional buckling loads on cylinders with $\beta = 1$, $\gamma = 0.5$, and $\rho = 25$.

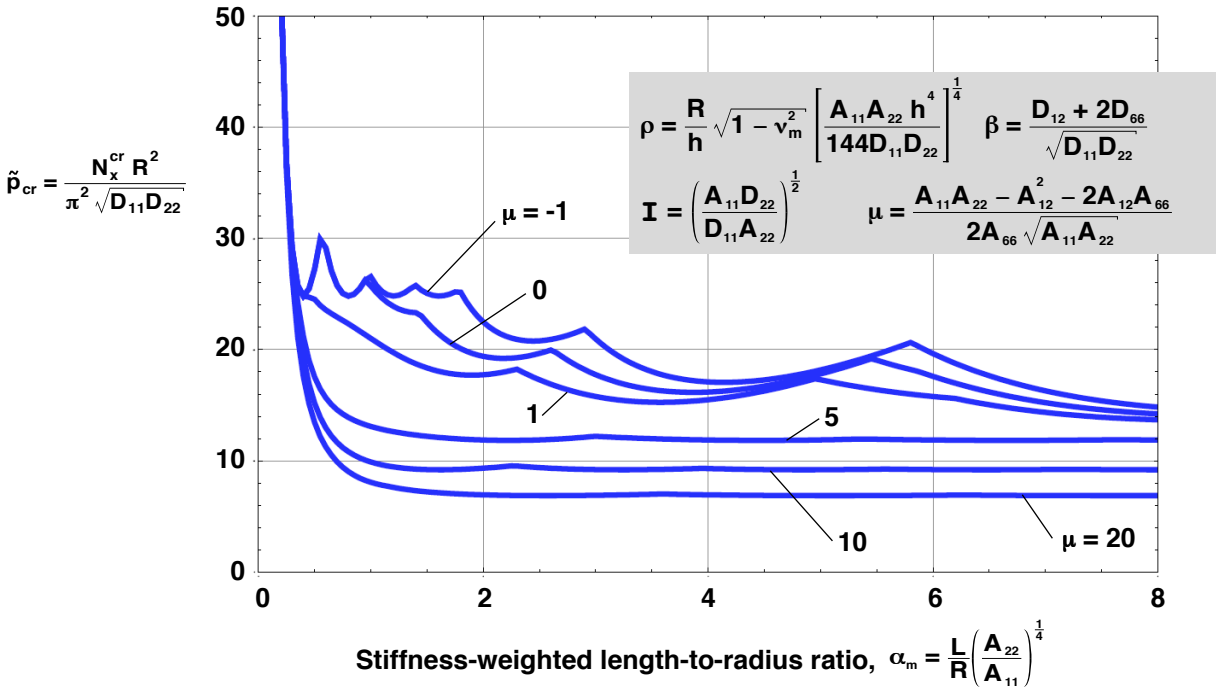

Figure 10. Effects of parameters α_m and μ on nondimensional buckling loads on cylinders with $\beta = 2$, $\gamma = 0.5$, and $\rho = 25$.

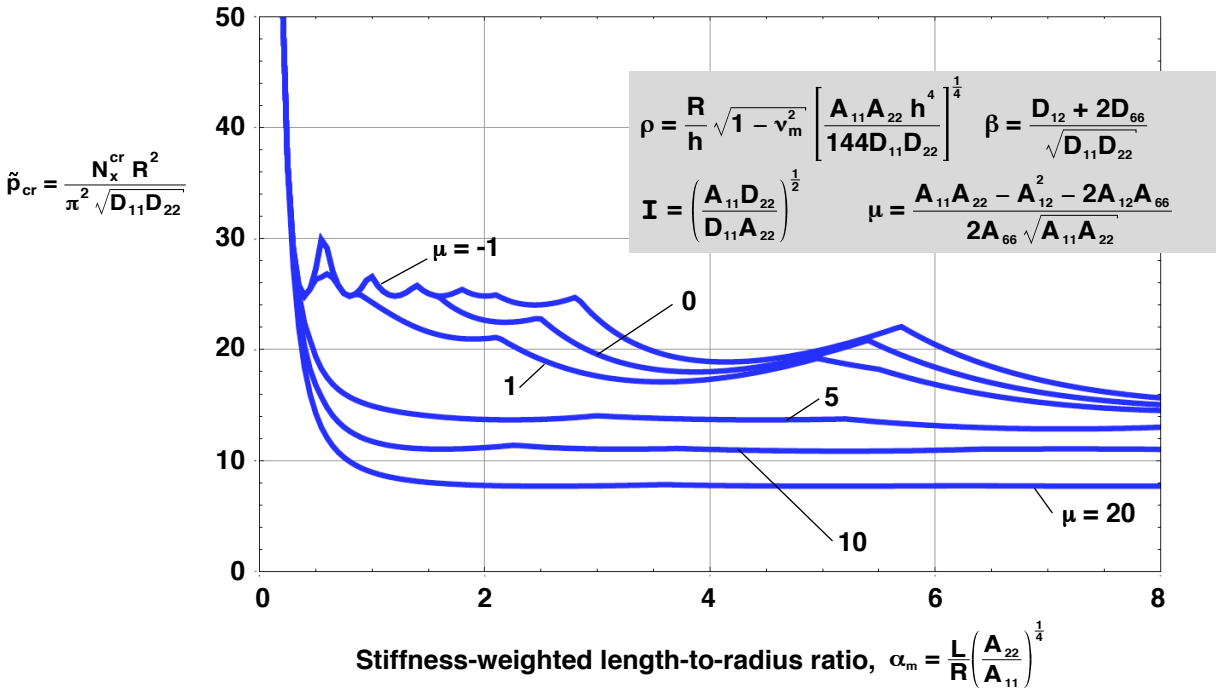

Figure 11. Effects of parameters α_m and μ on nondimensional buckling loads on cylinders with $\beta = 3$, $\gamma = 0.5$, and $\rho = 25$.

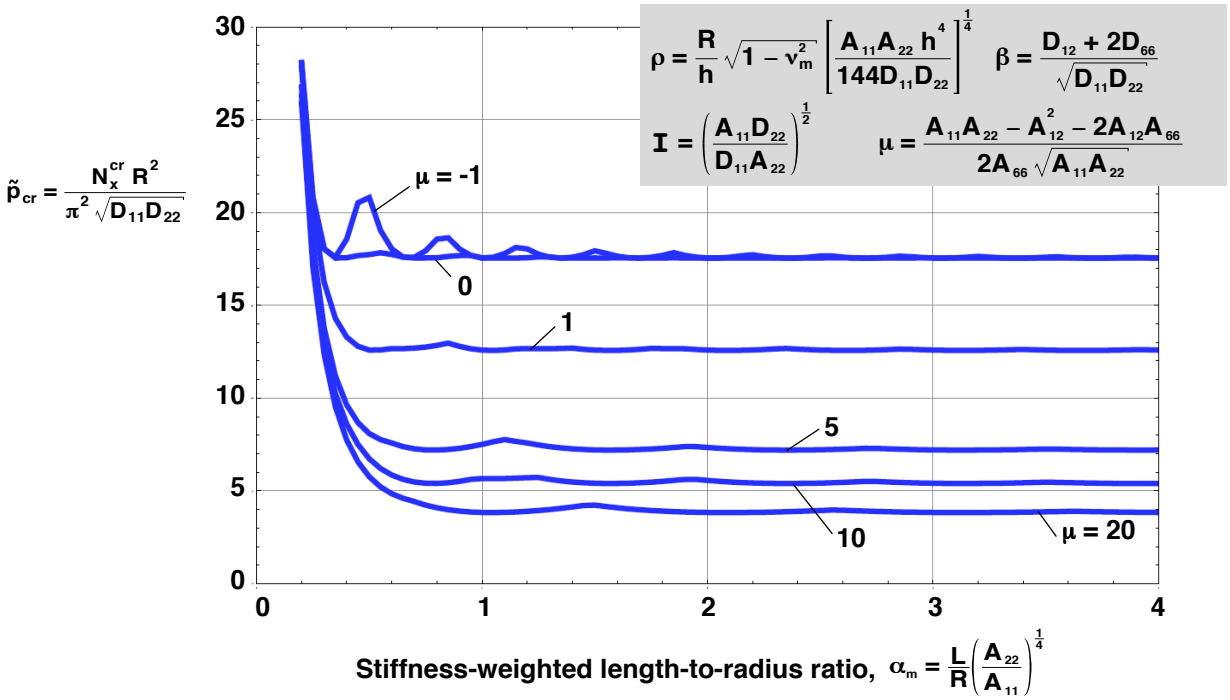

Figure 12. Effects of parameters α_m and μ on nondimensional buckling loads on cylinders with $\beta = 0$, $\mathrm{I} = 1$, and $\rho = 25$.

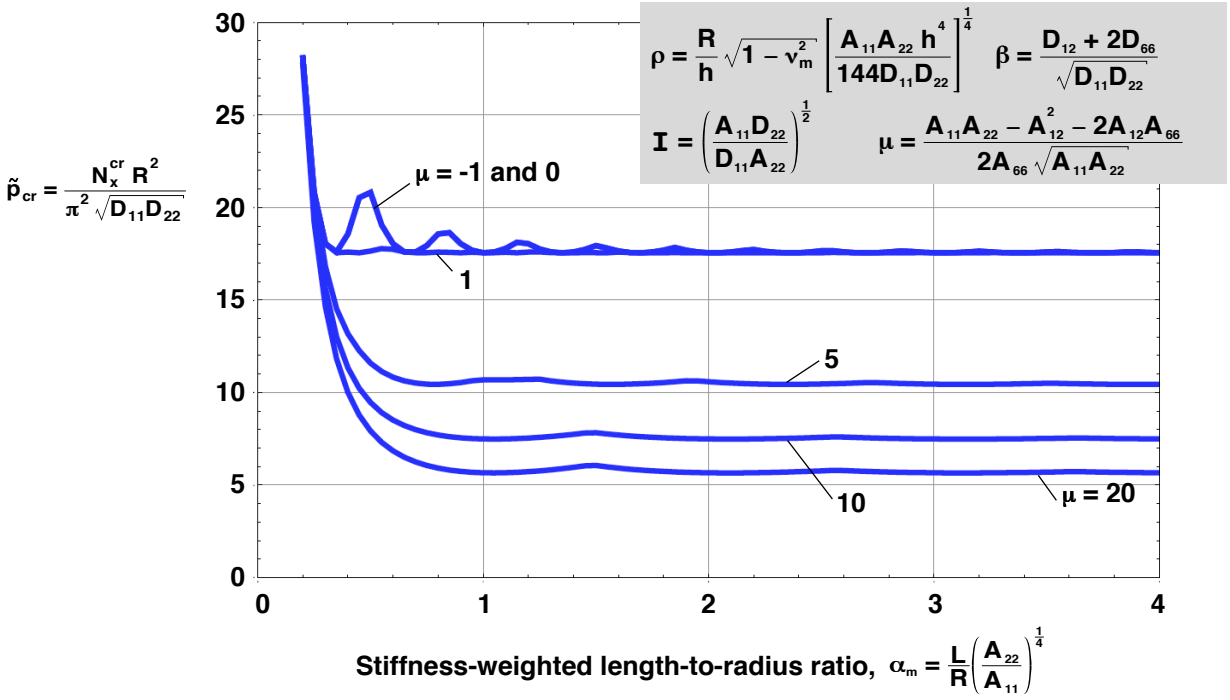

Figure 13. Effects of parameters α_m and μ on nondimensional buckling loads on cylinders with $\beta = 1$, $\mathrm{I} = 1$, and $\rho = 25$.

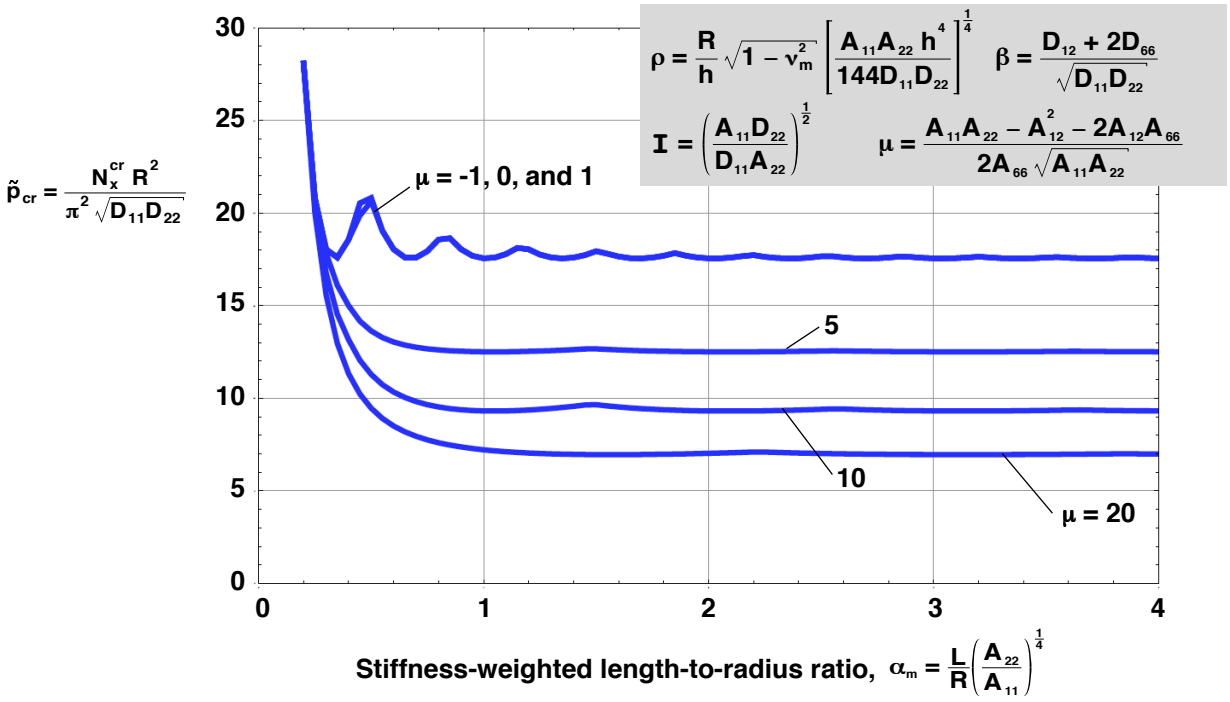

Figure 14. Effects of parameters α_m and μ on nondimensional buckling loads on cylinders with $\beta = 2$, $\gamma = 1$, and $\rho = 25$.

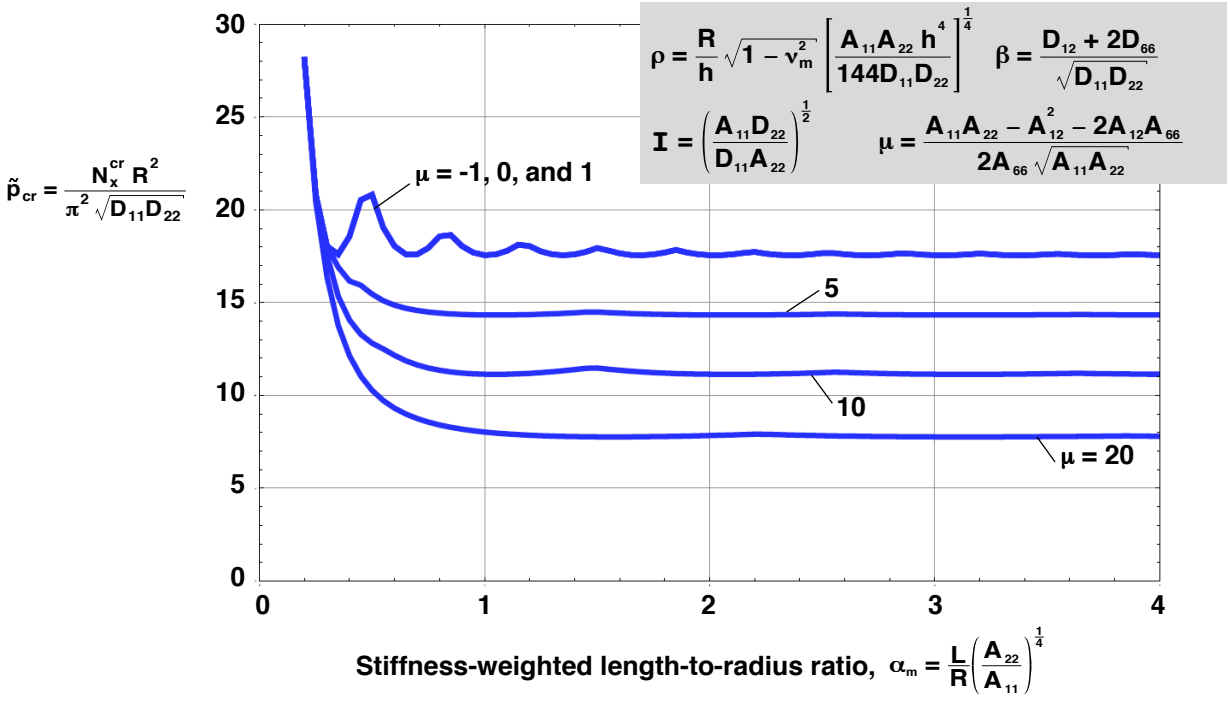

Figure 15. Effects of parameters α_m and μ on nondimensional buckling loads on cylinders with $\beta = 3$, $\gamma = 1$, and $\rho = 25$.

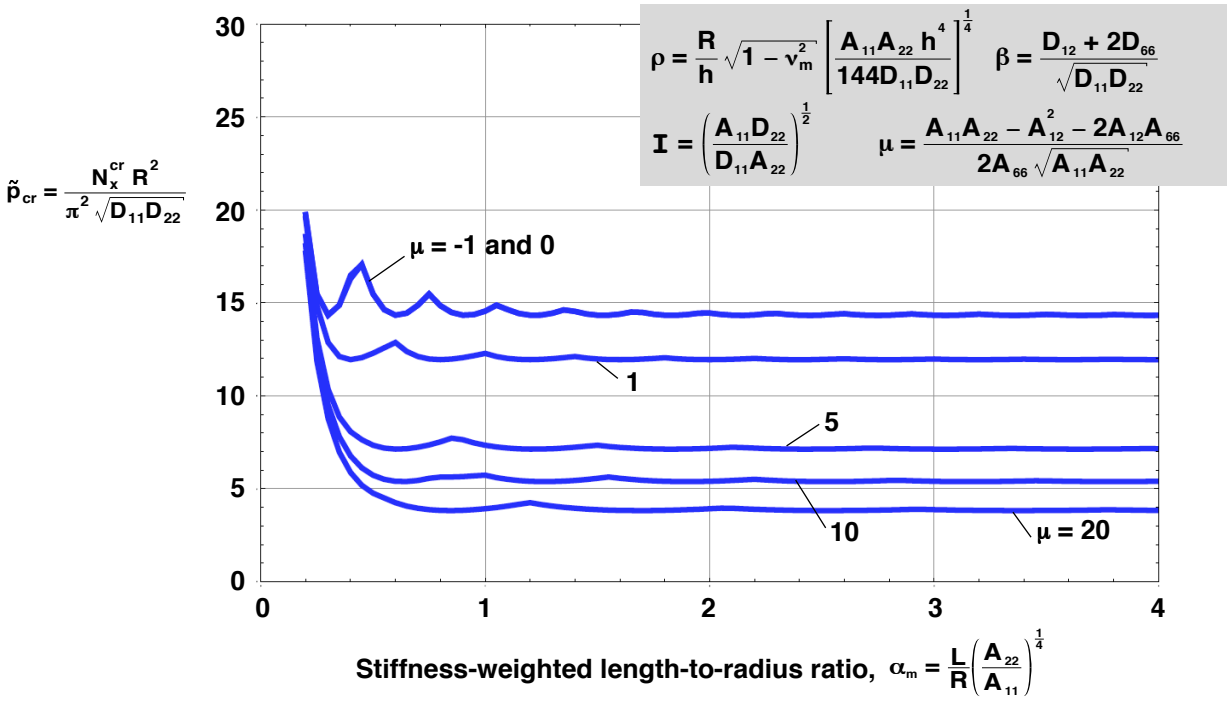

Figure 16. Effects of parameters α_m and μ on nondimensional buckling loads on cylinders with $\beta = 0$, $\gamma = 1.5$, and $\rho = 25$.

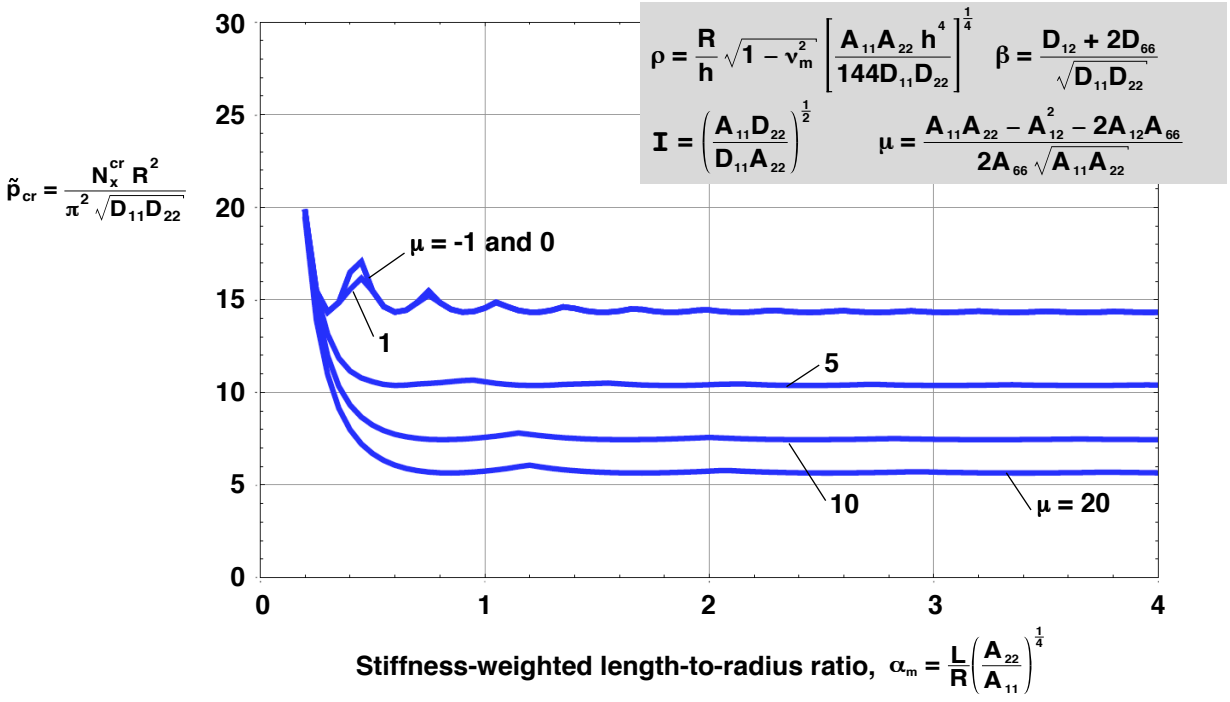

Figure 17. Effects of parameters α_m and μ on nondimensional buckling loads on cylinders with $\beta = 1$, $\gamma = 1.5$, and $\rho = 25$.

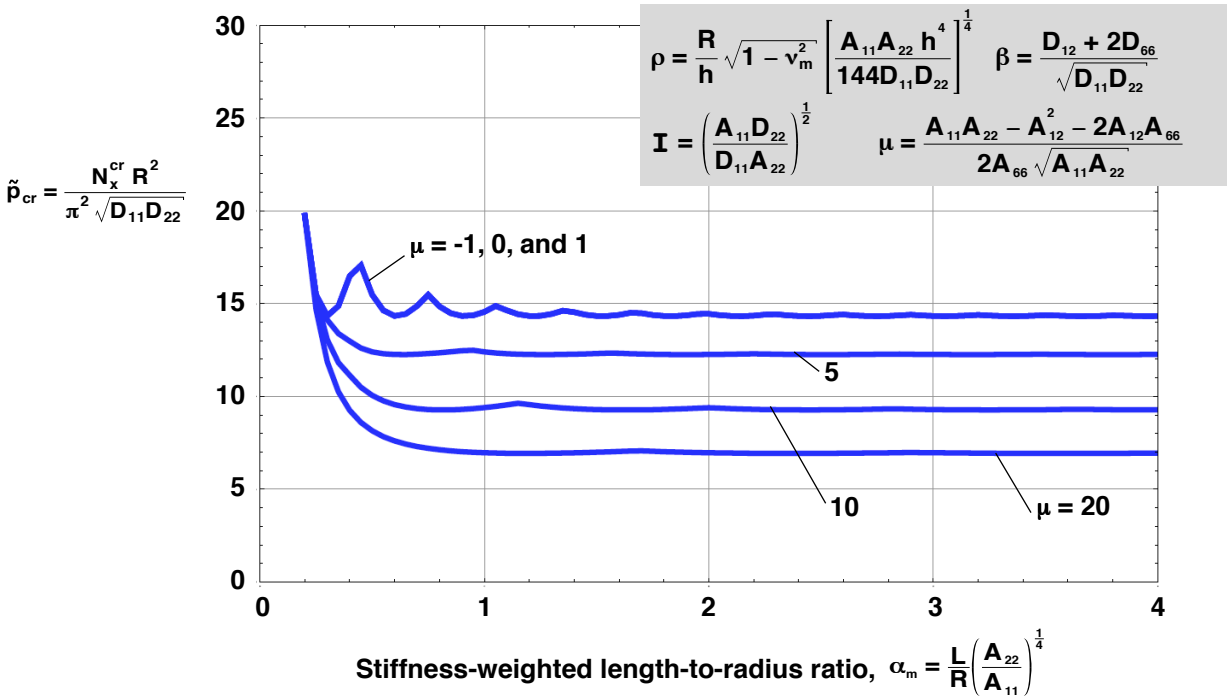

Figure 18. Effects of parameters α_m and μ on nondimensional buckling loads on cylinders with $\beta = 2$, $\gamma = 1.5$, and $\rho = 25$.

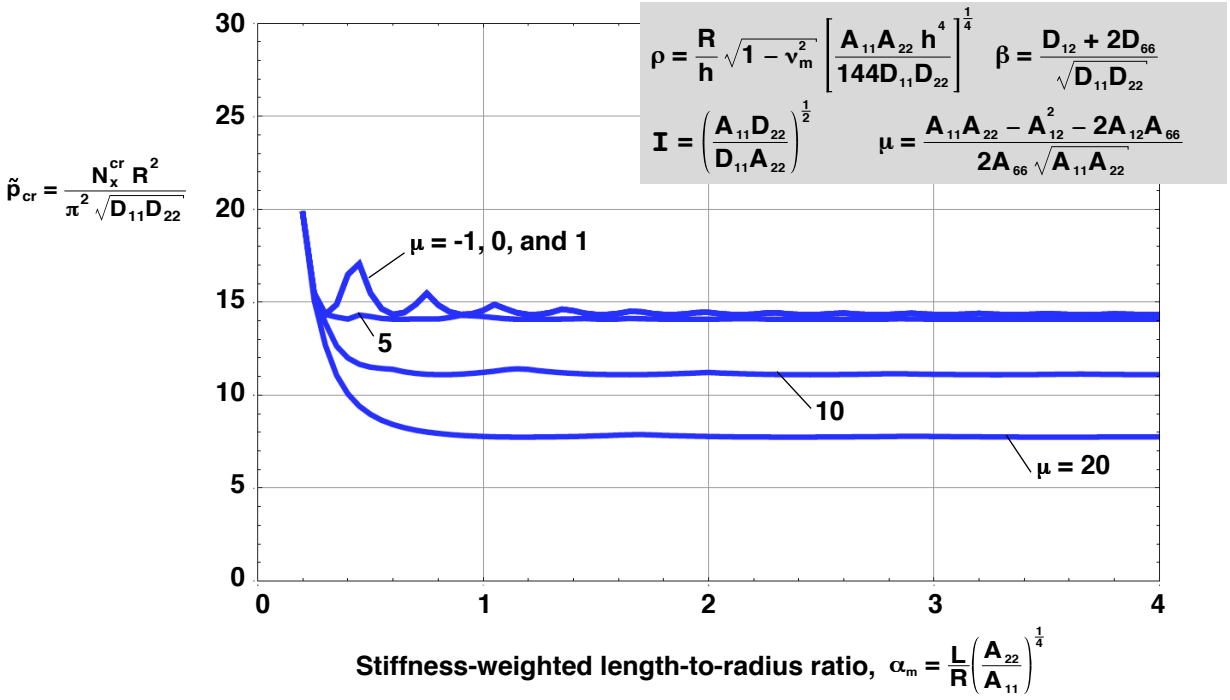

Figure 19. Effects of parameters α_m and μ on nondimensional buckling loads on cylinders with $\beta = 3$, $\gamma = 1.5$, and $\rho = 25$.

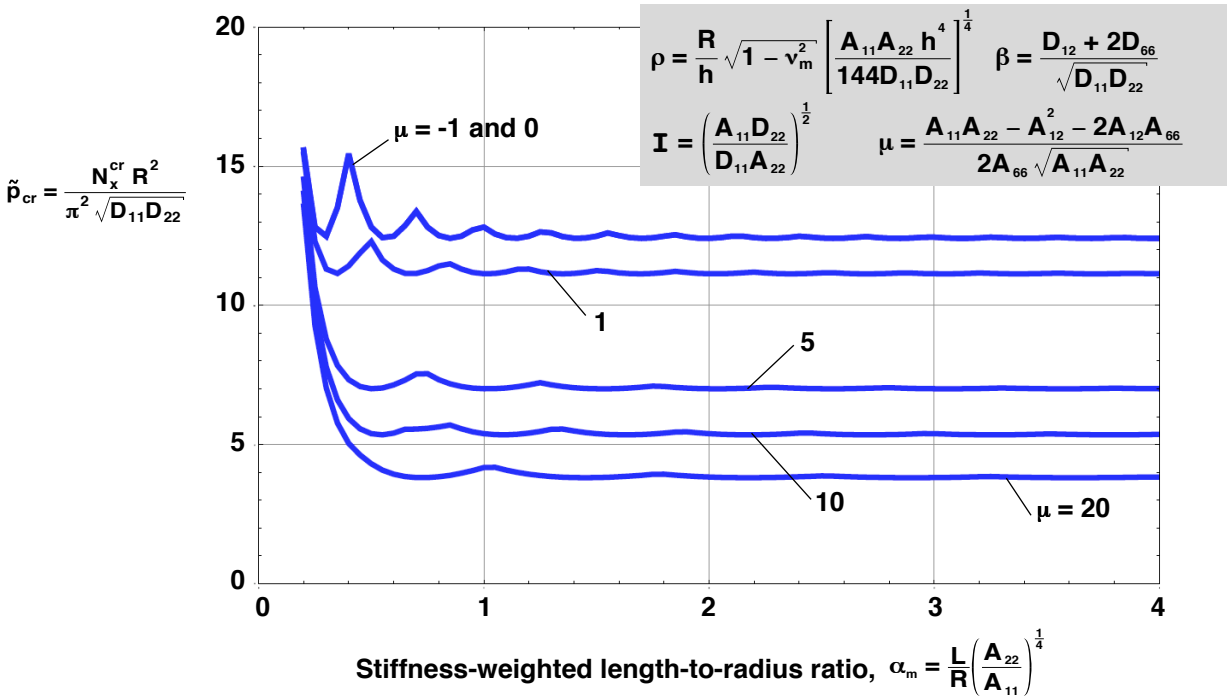

Figure 20. Effects of parameters α_m and μ on nondimensional buckling loads on cylinders with $\beta = 0$, $\mathrm{I} = 2$, and $\rho = 25$.

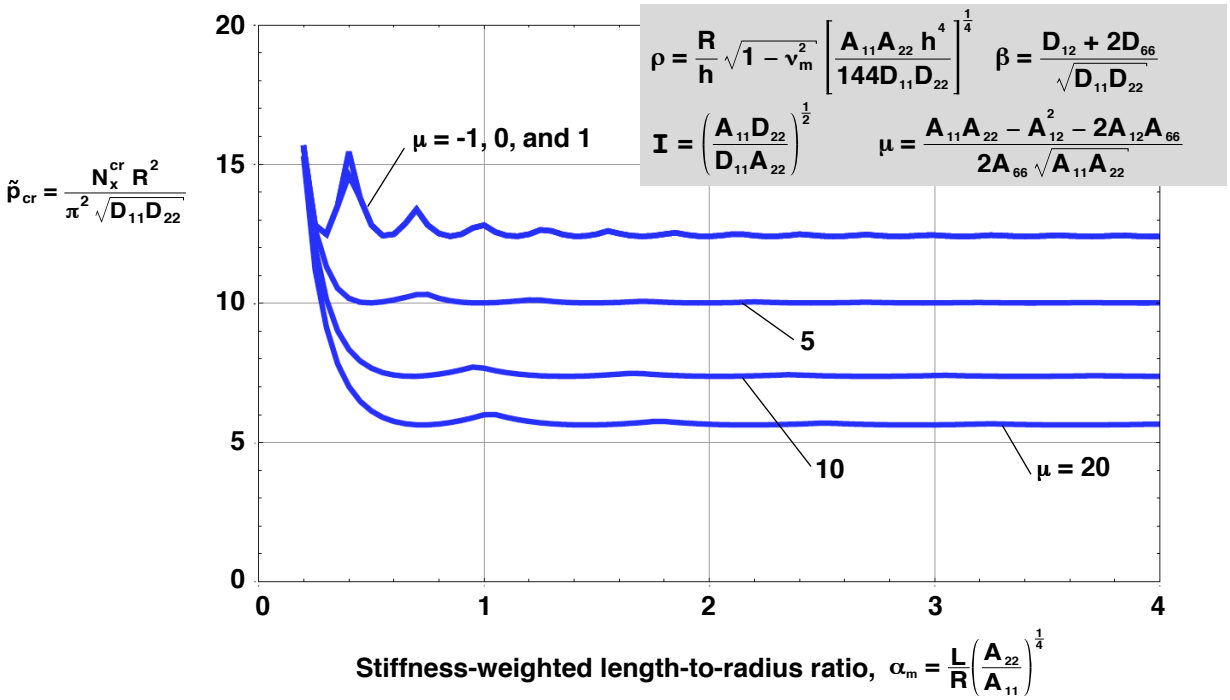

Figure 21. Effects of parameters α_m and μ on nondimensional buckling loads on cylinders with $\beta = 1$, $\mathrm{I} = 2$, and $\rho = 25$.

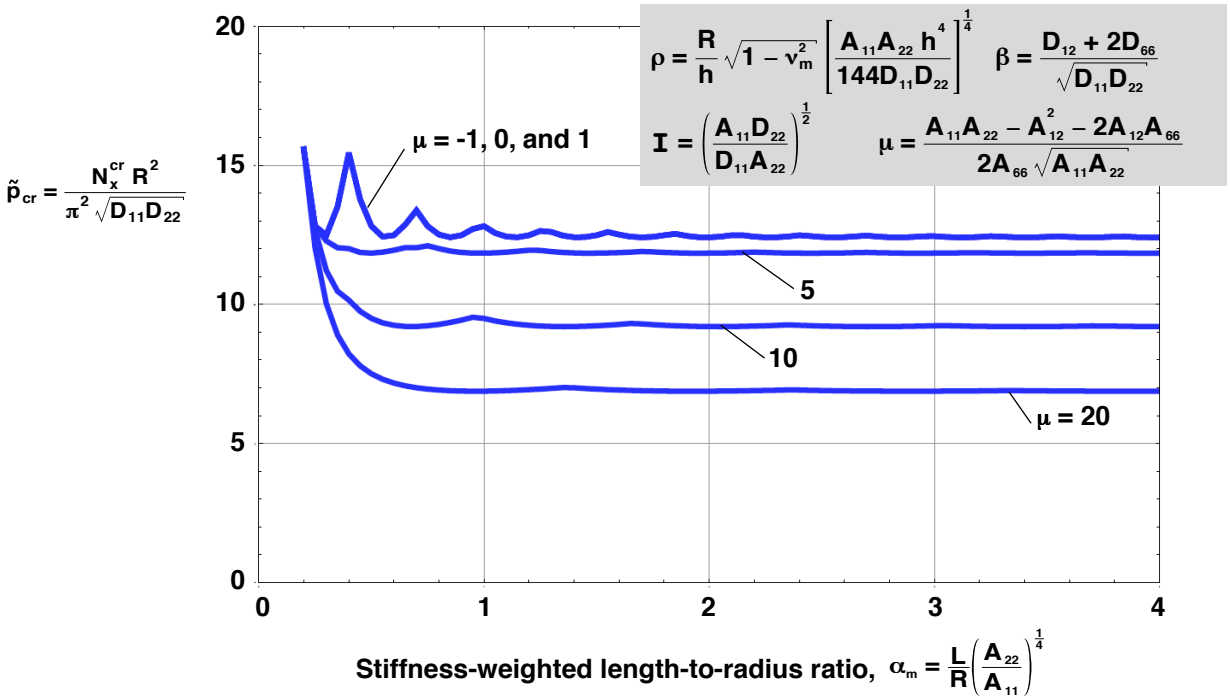

Figure 22. Effects of parameters α_m and μ on nondimensional buckling loads on cylinders with $\beta = 2$, $\gamma = 2$, and $\rho = 25$.

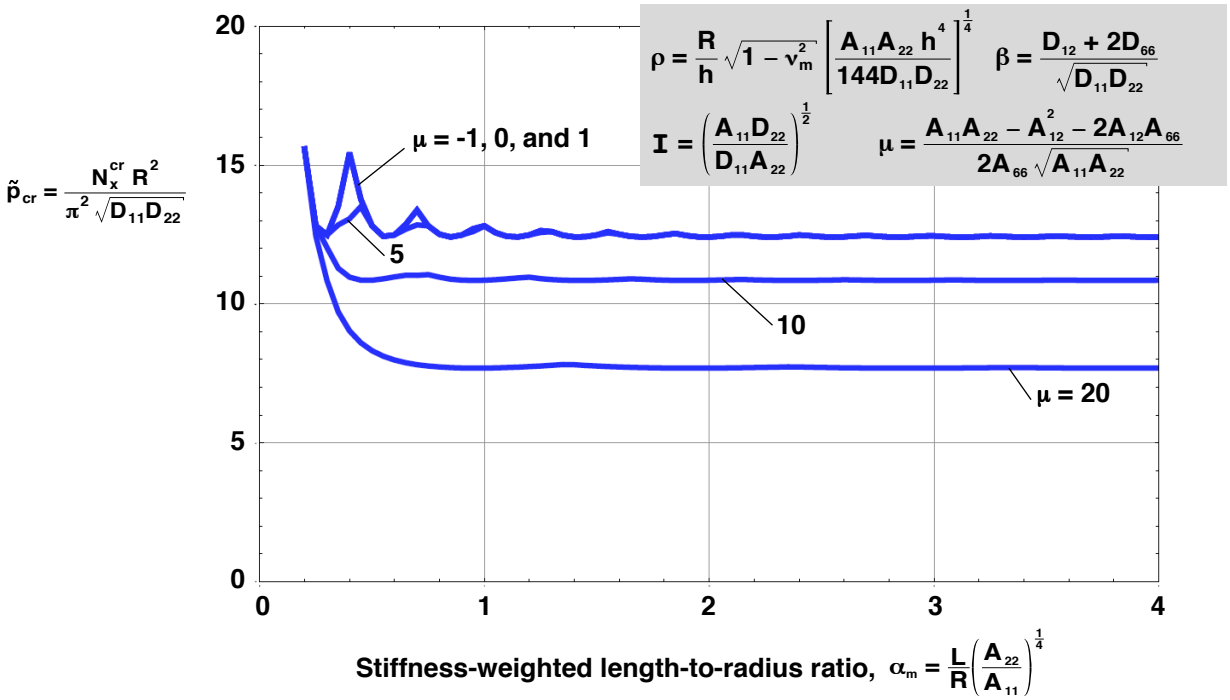

Figure 23. Effects of parameters α_m and μ on nondimensional buckling loads on cylinders with $\beta = 3$, $\gamma = 2$, and $\rho = 25$.

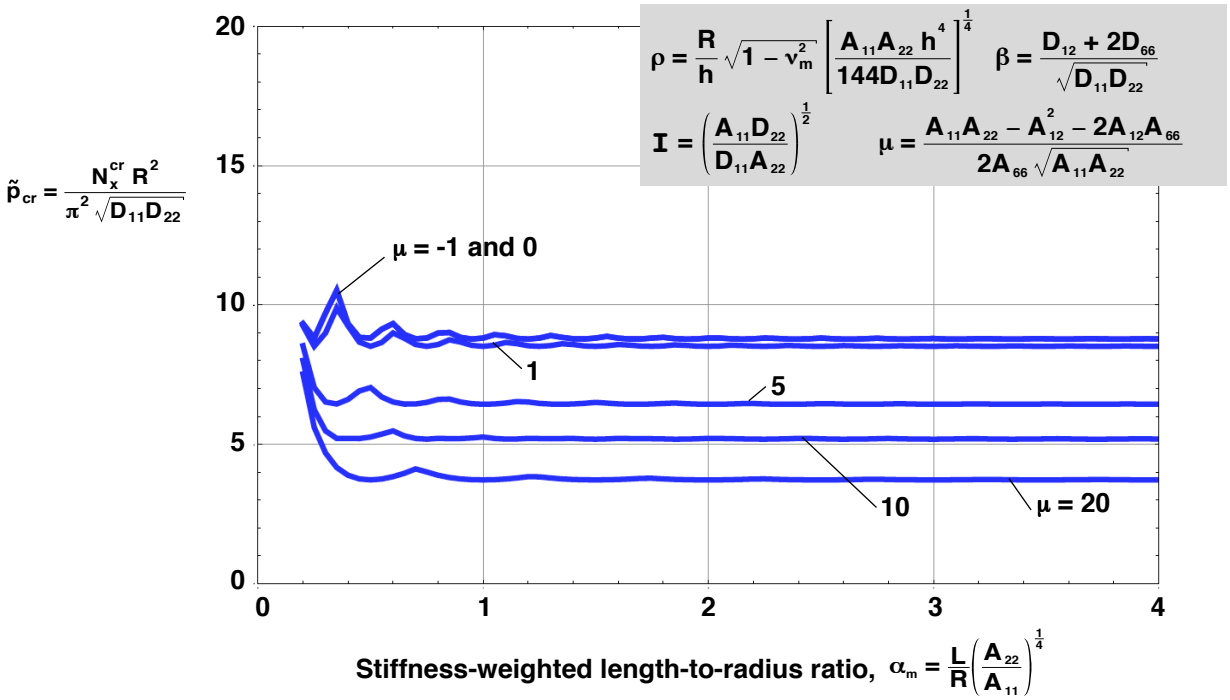

Figure 24. Effects of parameters α_m and μ on nondimensional buckling loads on cylinders with $\beta = 0$, $\gamma = 4$, and $\rho = 25$.

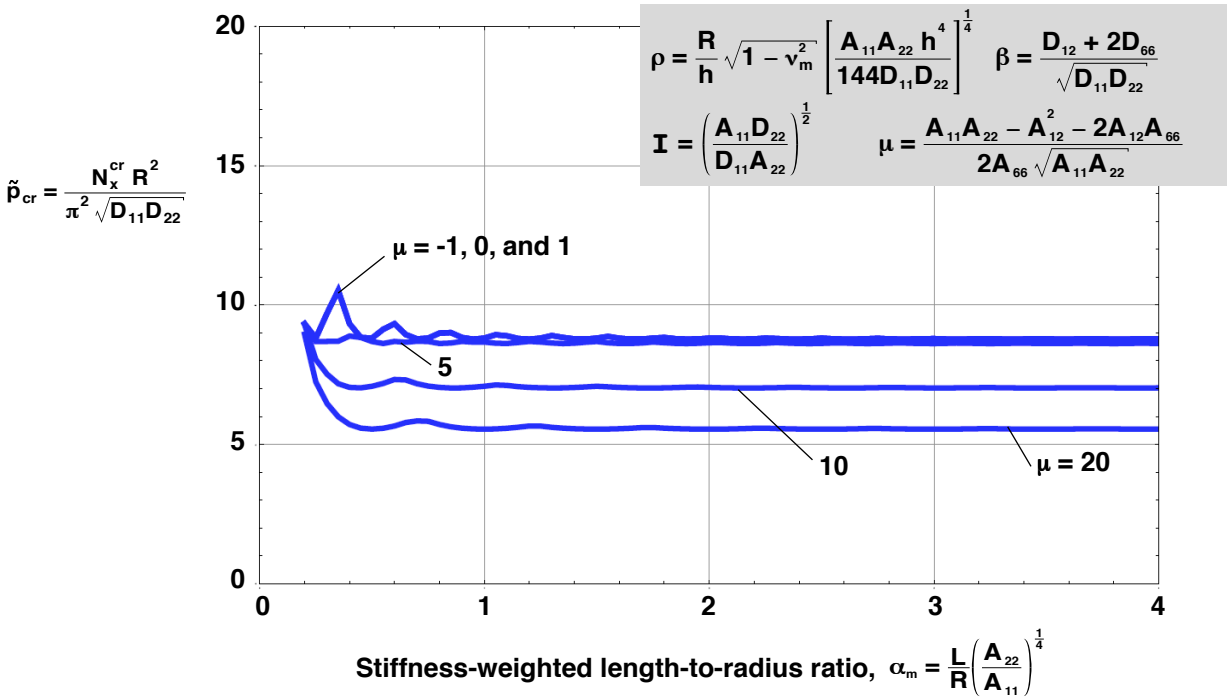

Figure 25. Effects of parameters α_m and μ on nondimensional buckling loads on cylinders with $\beta = 1$, $\gamma = 4$, and $\rho = 25$.

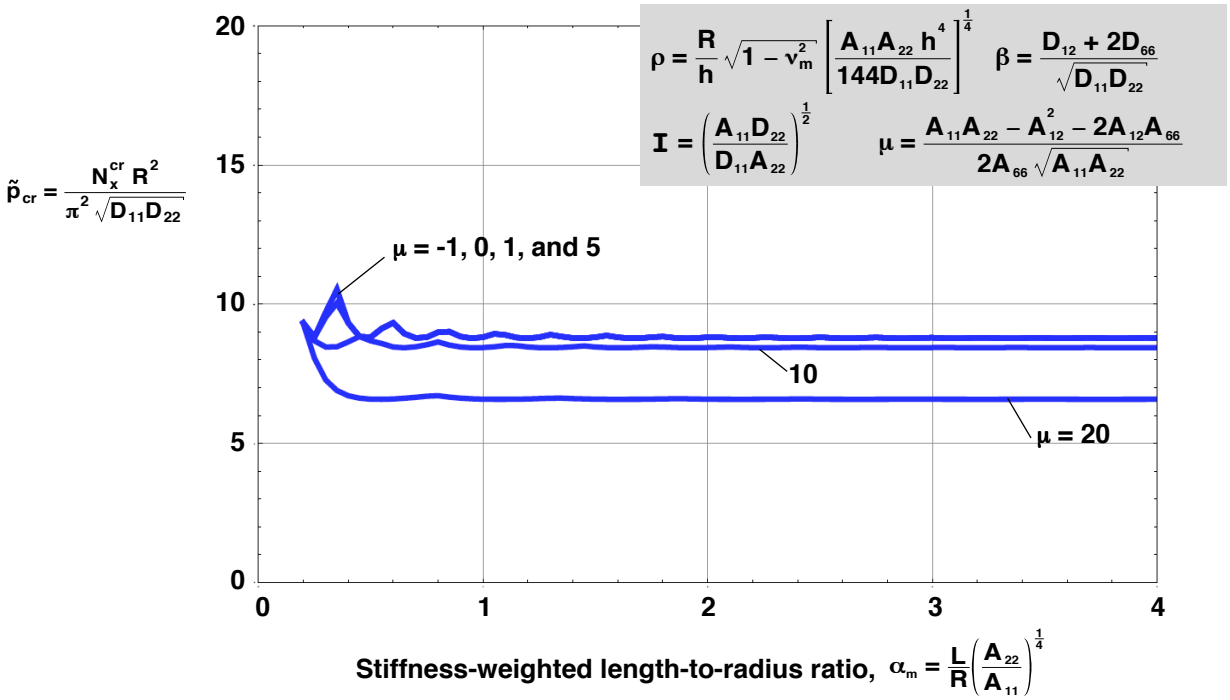

Figure 26. Effects of parameters α_m and μ on nondimensional buckling loads on cylinders with $\beta = 2$, $\gamma = 4$, and $\rho = 25$.

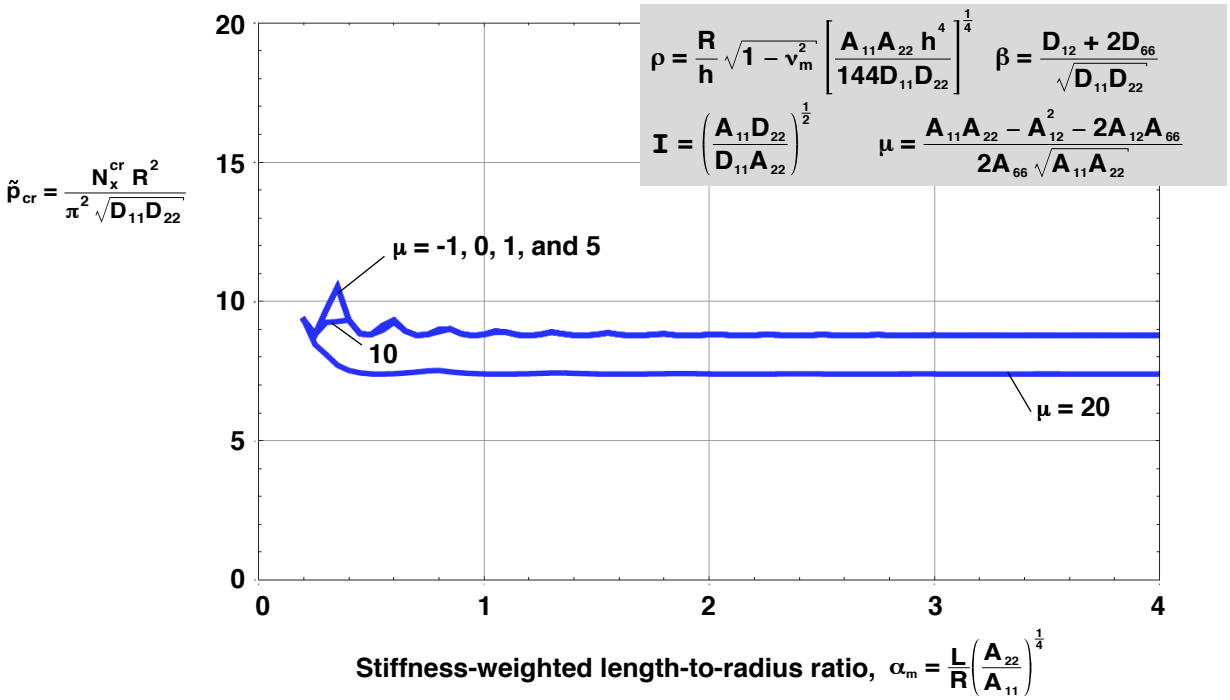

Figure 27. Effects of parameters α_m and μ on nondimensional buckling loads on cylinders with $\beta = 3$, $\gamma = 4$, and $\rho = 25$.

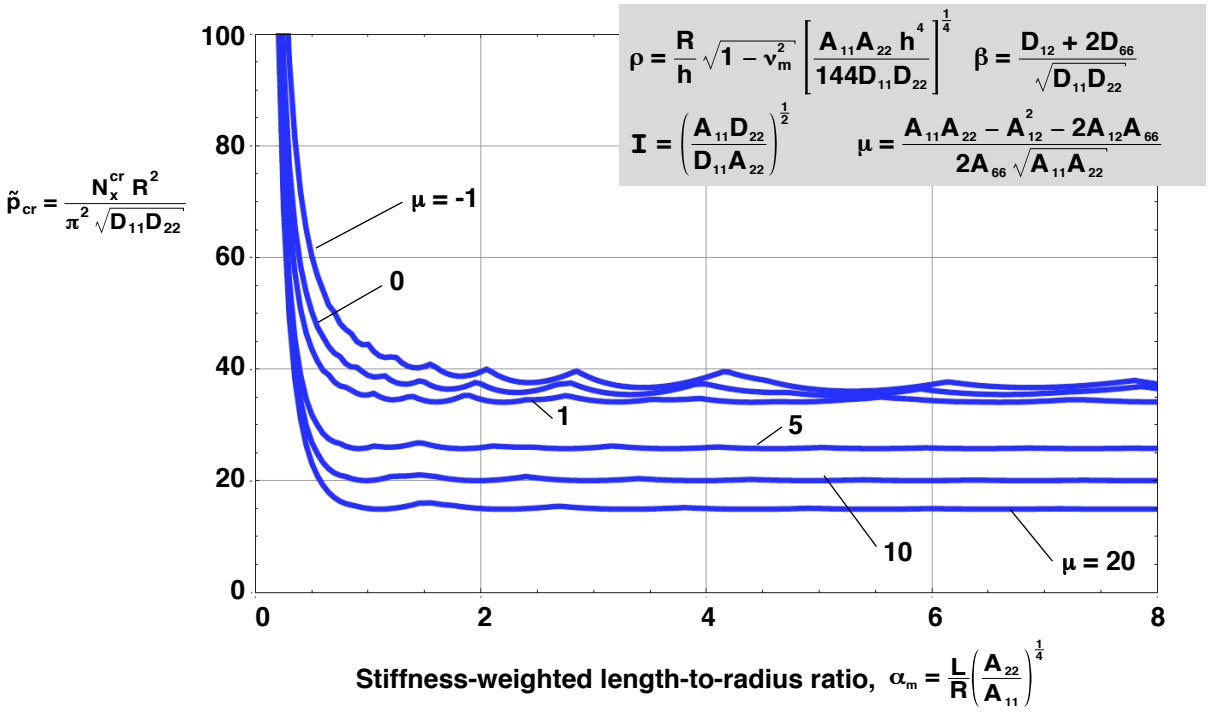

Figure 28. Effects of parameters α_m and μ on nondimensional buckling loads on cylinders with $\beta = 0$, $\mathrm{I} = 0.25$, and $\rho = 100$.

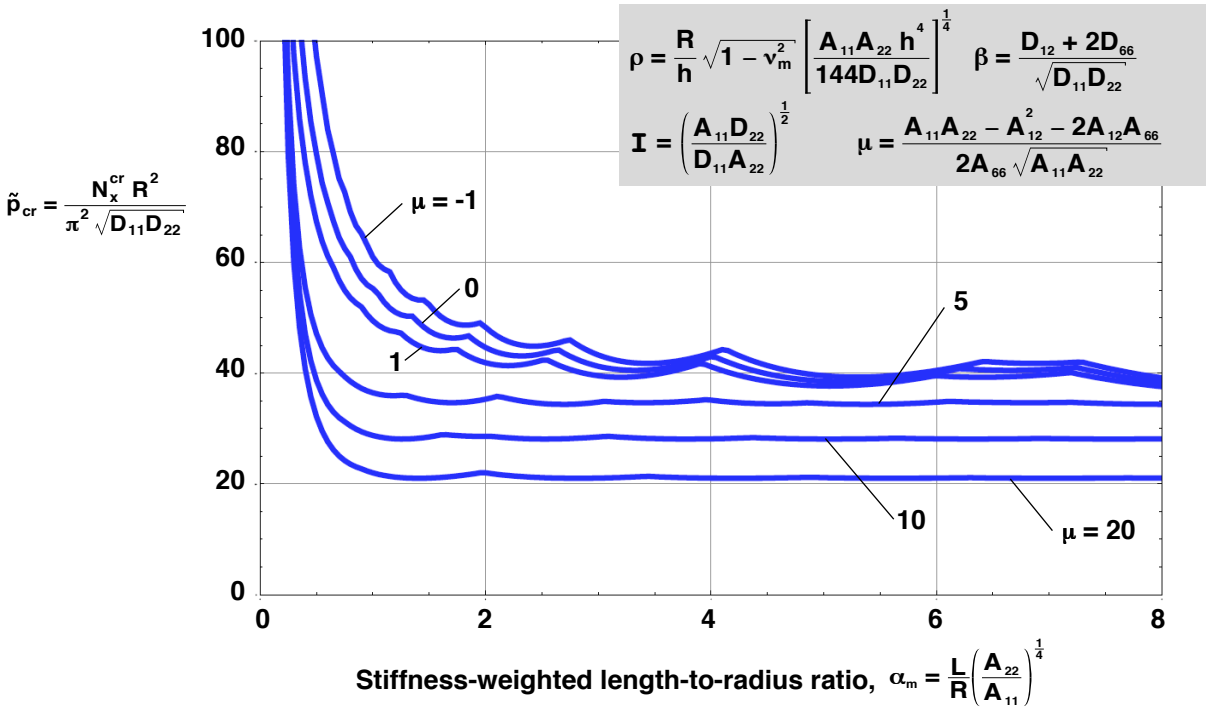

Figure 29. Effects of parameters α_m and μ on nondimensional buckling loads on cylinders with $\beta = 1$, $\mathrm{I} = 0.25$, and $\rho = 100$.

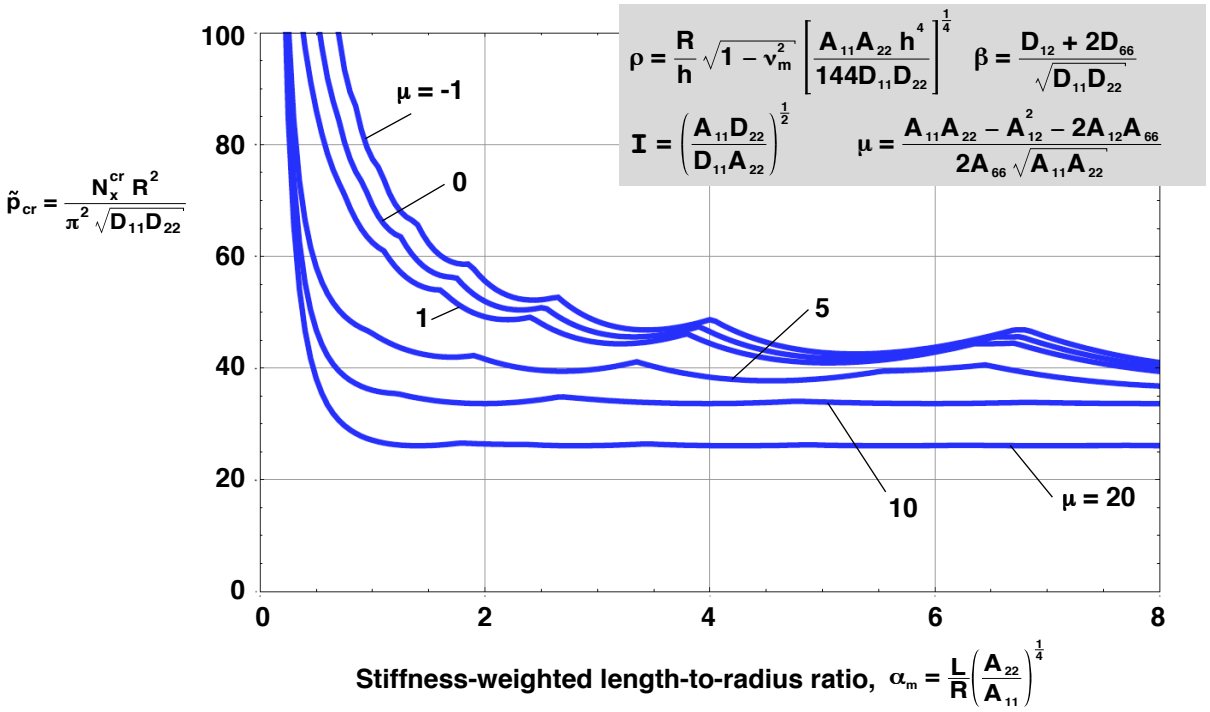

Figure 30. Effects of parameters α_m and μ on nondimensional buckling loads on cylinders with $\beta = 2$, $\gamma = 0.25$, and $\rho = 100$.

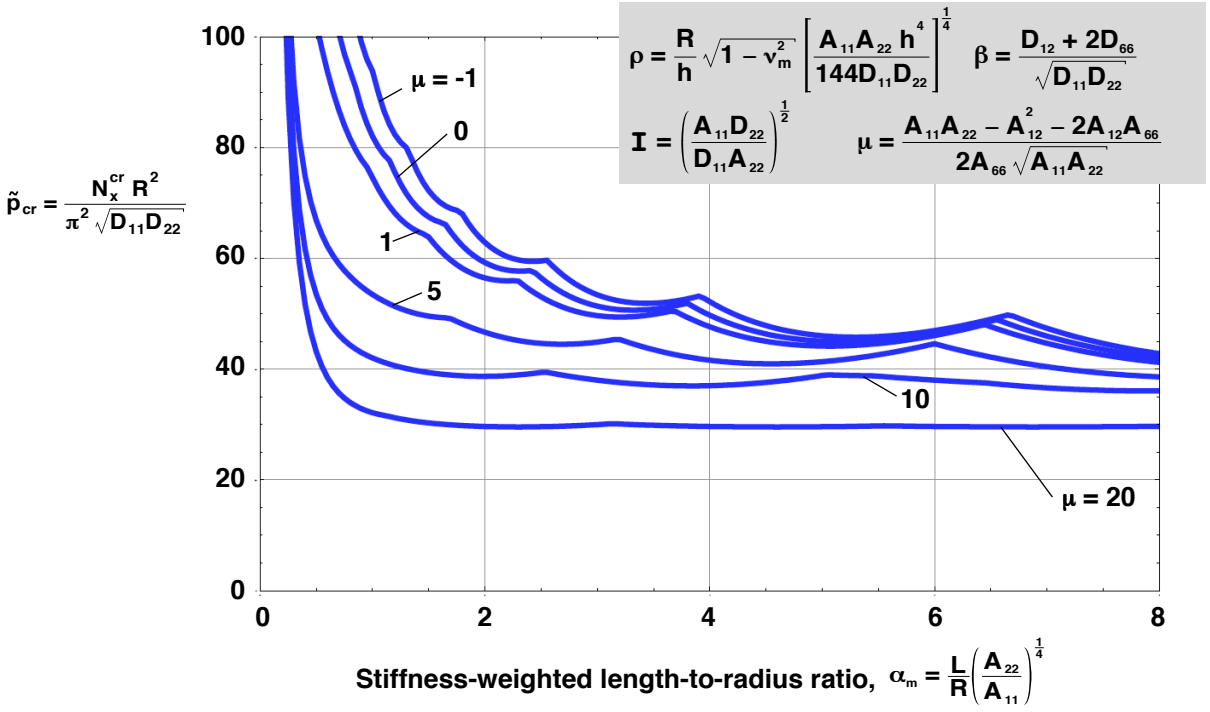

Figure 31. Effects of parameters α_m and μ on nondimensional buckling loads on cylinders with $\beta = 3$, $\gamma = 0.25$, and $\rho = 100$.

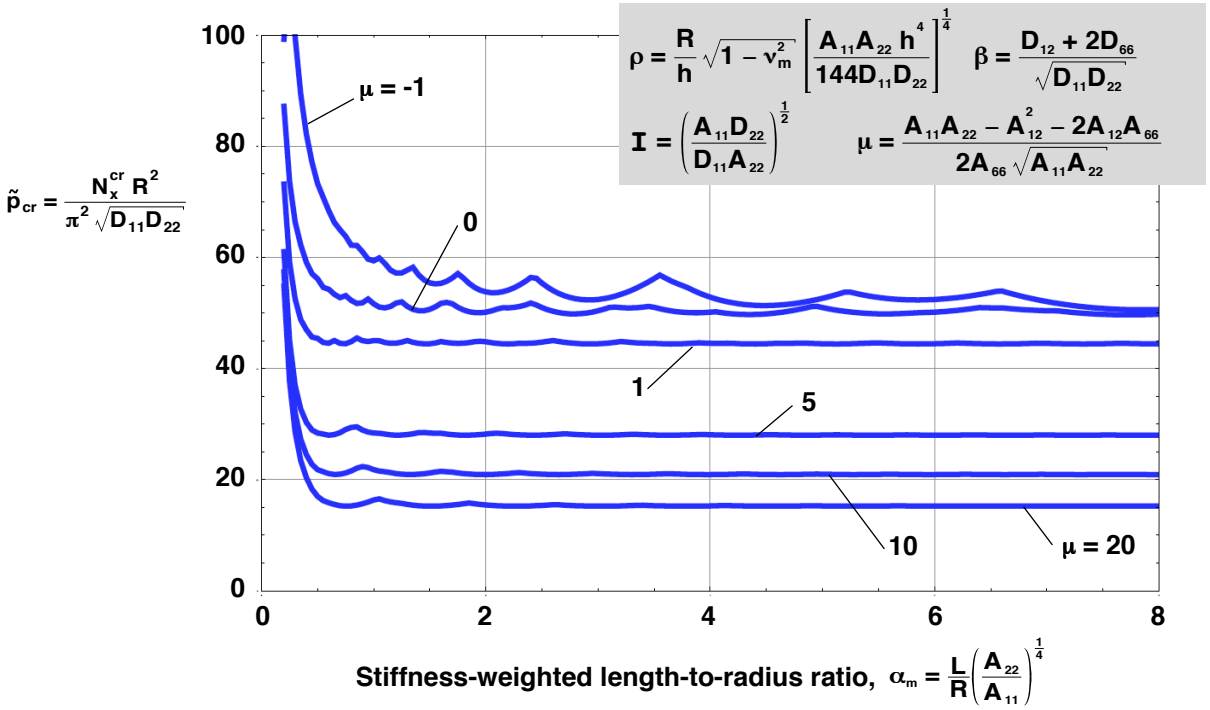

Figure 32. Effects of parameters α_m and μ on nondimensional buckling loads on cylinders with $\beta = 0$, $\mathrm{I} = 0.5$, and $\rho = 100$.

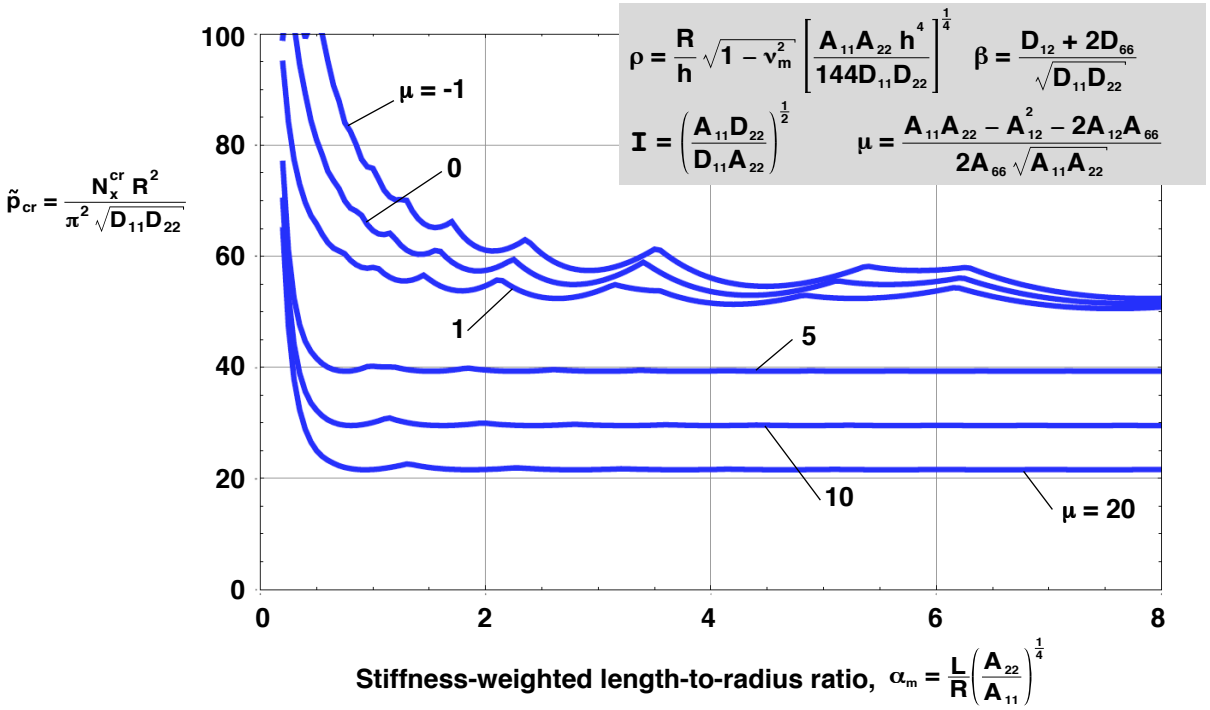

Figure 33. Effects of parameters α_m and μ on nondimensional buckling loads on cylinders with $\beta = 1$, $\mathrm{I} = 0.5$, and $\rho = 100$.

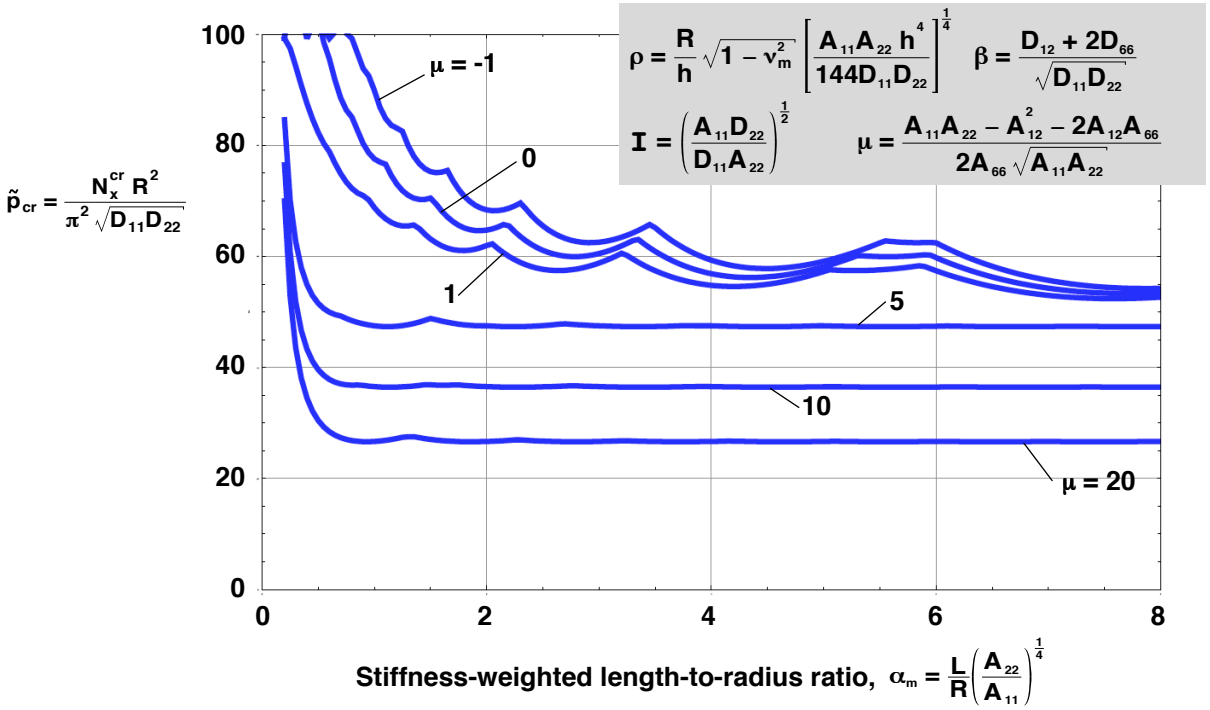

Figure 34. Effects of parameters α_m and μ on nondimensional buckling loads on cylinders with $\beta = 2$, $\mathrm{I} = 0.5$, and $\rho = 100$.

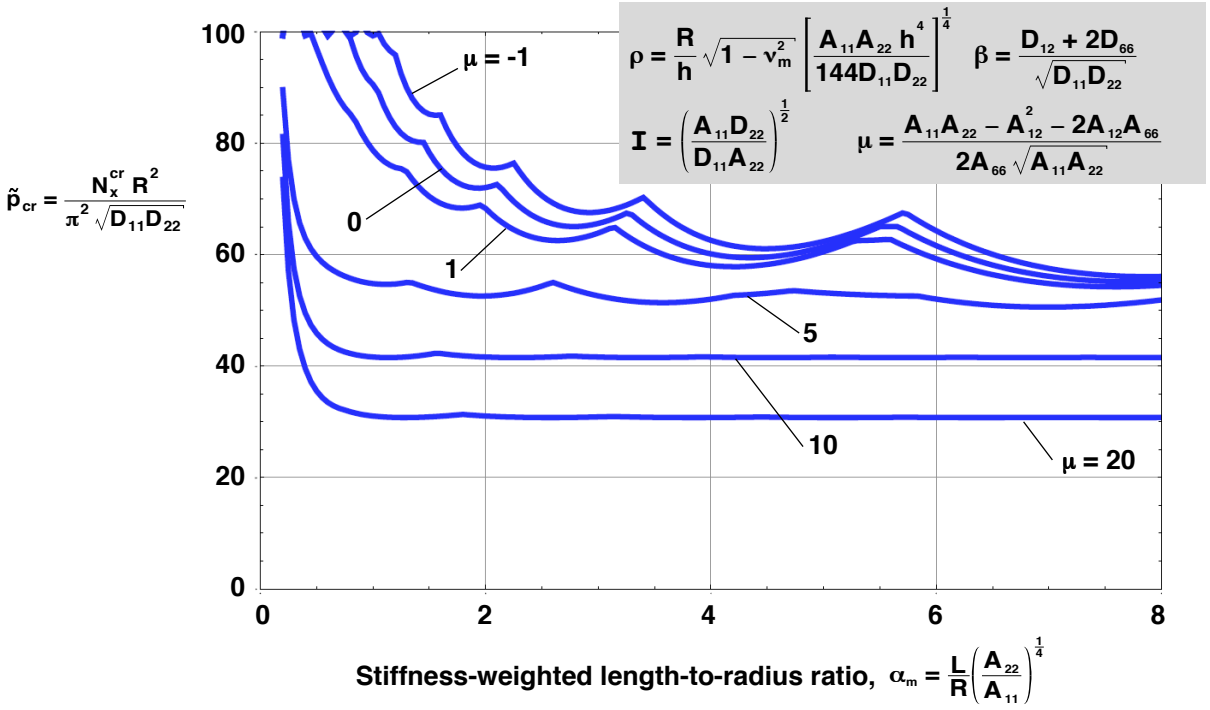

Figure 35. Effects of parameters α_m and μ on nondimensional buckling loads on cylinders with $\beta = 3$, $\mathrm{I} = 0.5$, and $\rho = 100$.

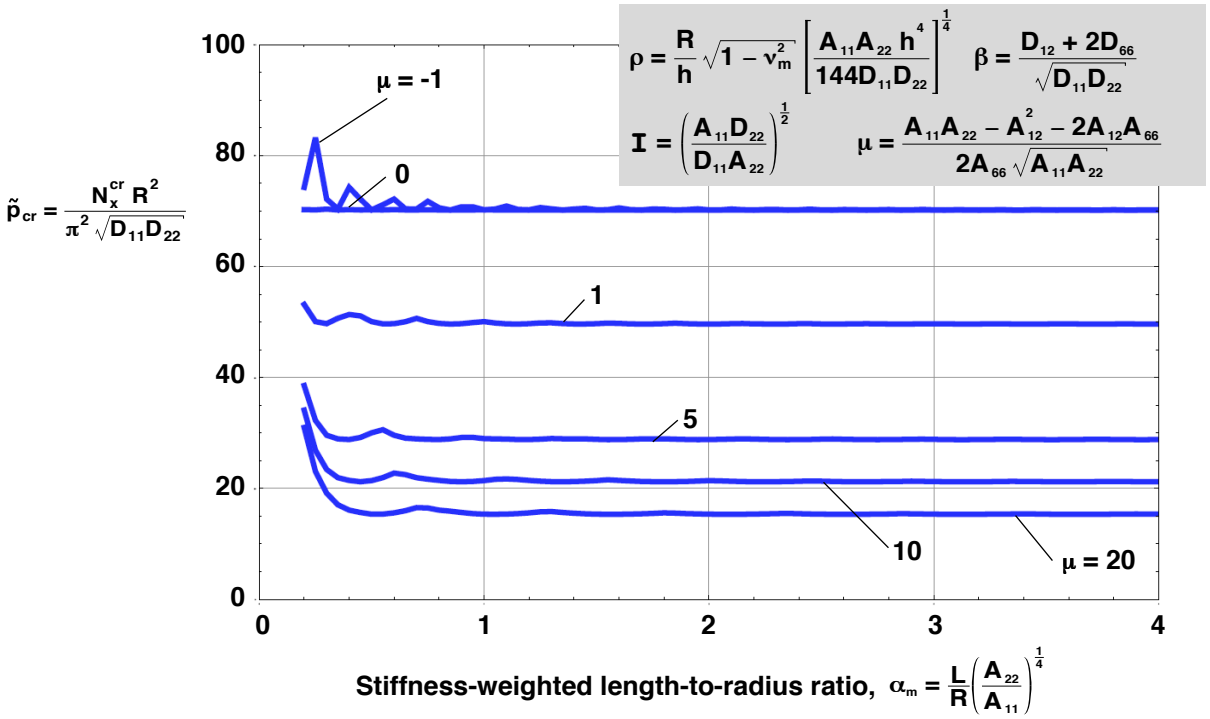

Figure 36. Effects of parameters α_m and μ on nondimensional buckling loads on cylinders with $\beta = 0$, $\mathrm{I} = 1$, and $\rho = 100$.

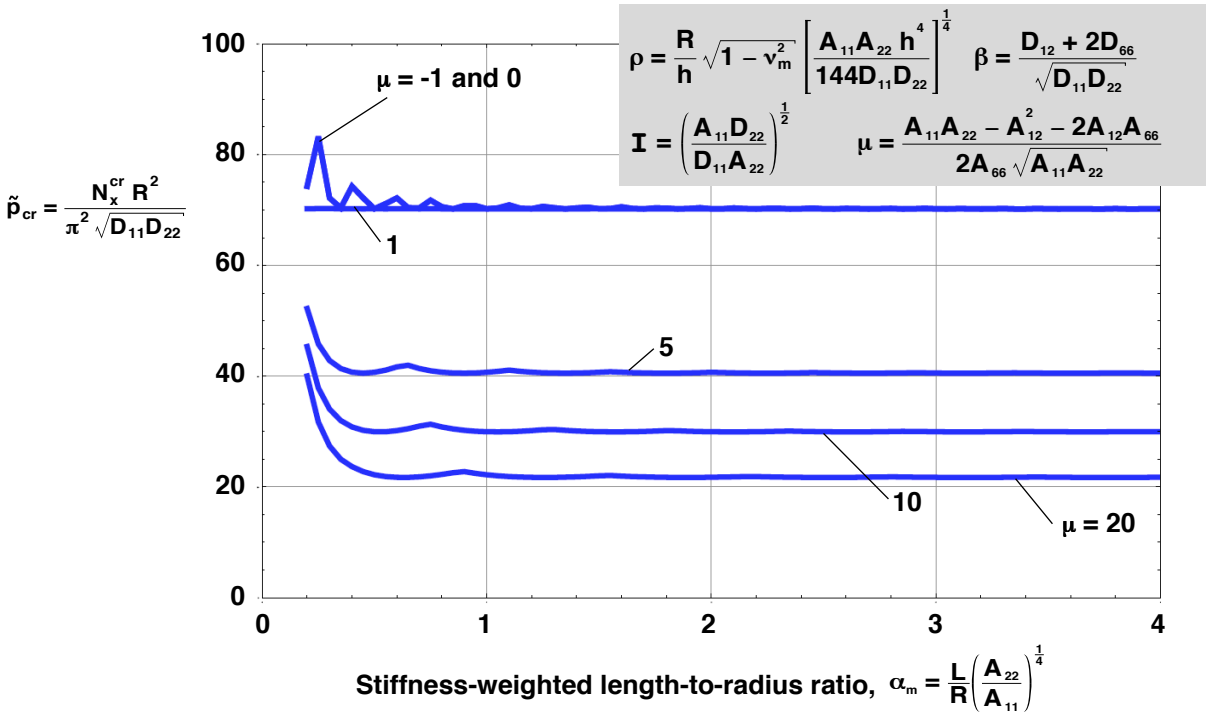

Figure 37. Effects of parameters α_m and μ on nondimensional buckling loads on cylinders with $\beta = 1$, $\mathrm{I} = 1$, and $\rho = 100$.

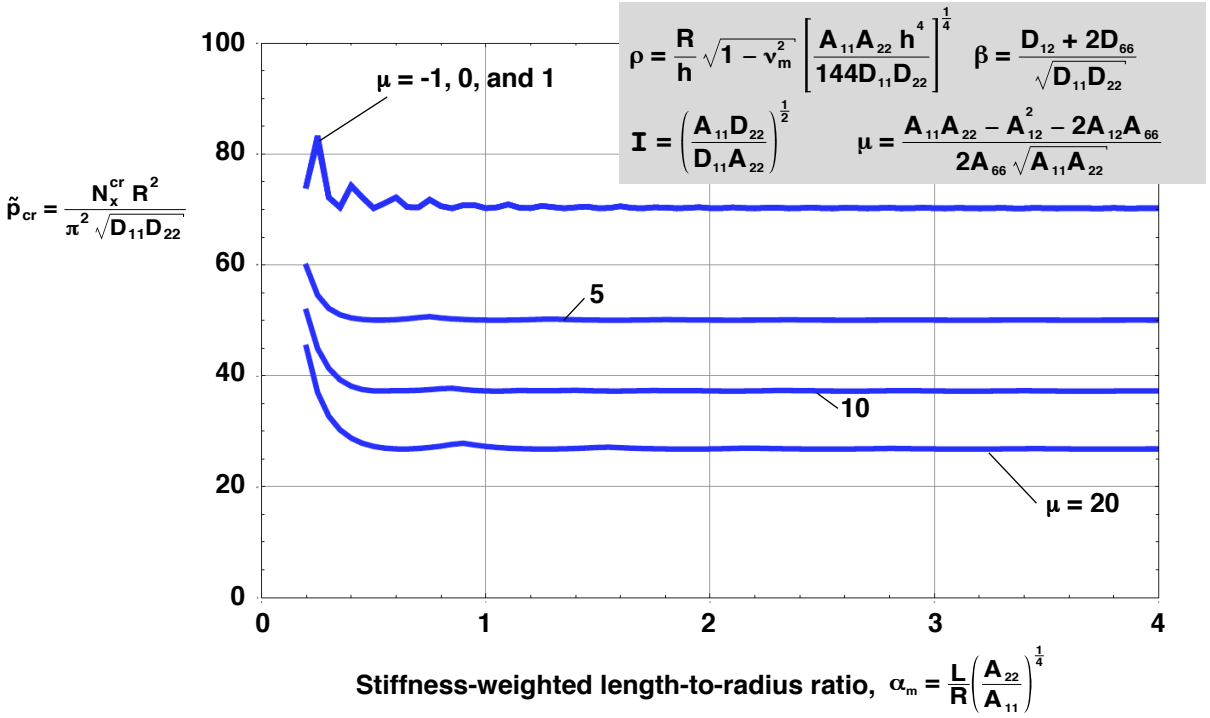

Figure 38. Effects of parameters α_m and μ on nondimensional buckling loads on cylinders with $\beta = 2$, $\mathrm{I} = 1$, and $\rho = 100$.

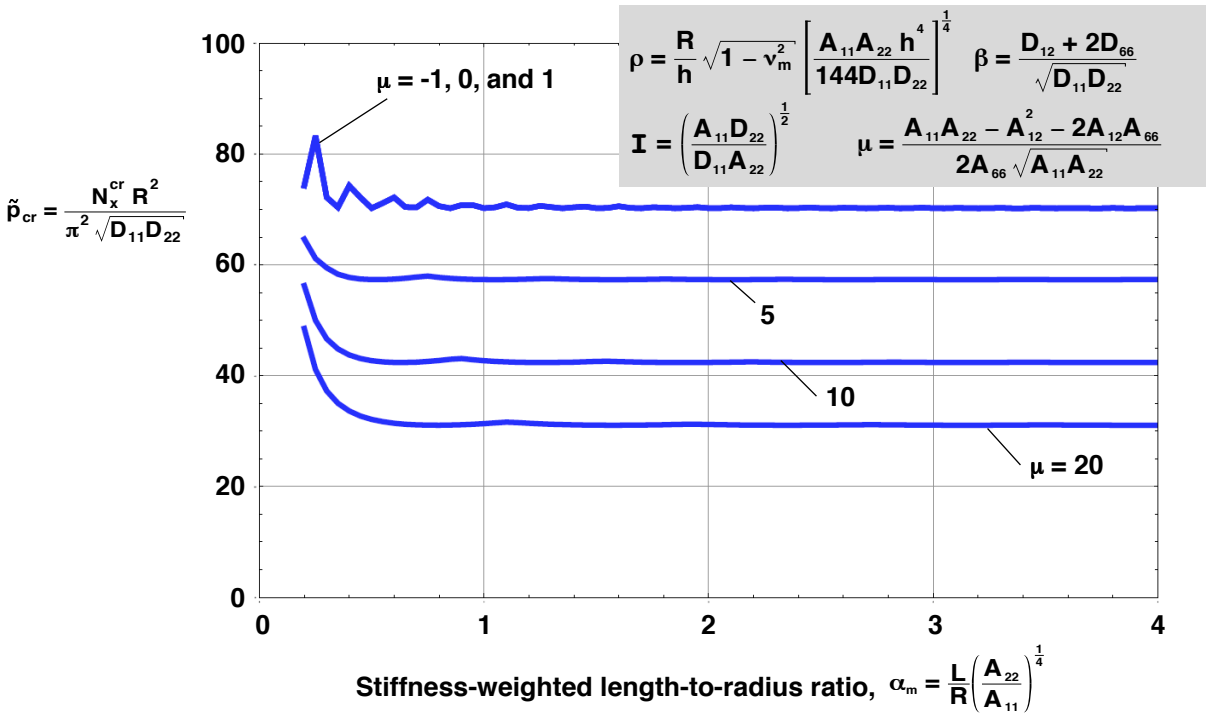

Figure 39. Effects of parameters α_m and μ on nondimensional buckling loads on cylinders with $\beta = 3$, $\mathrm{I} = 1$, and $\rho = 100$.

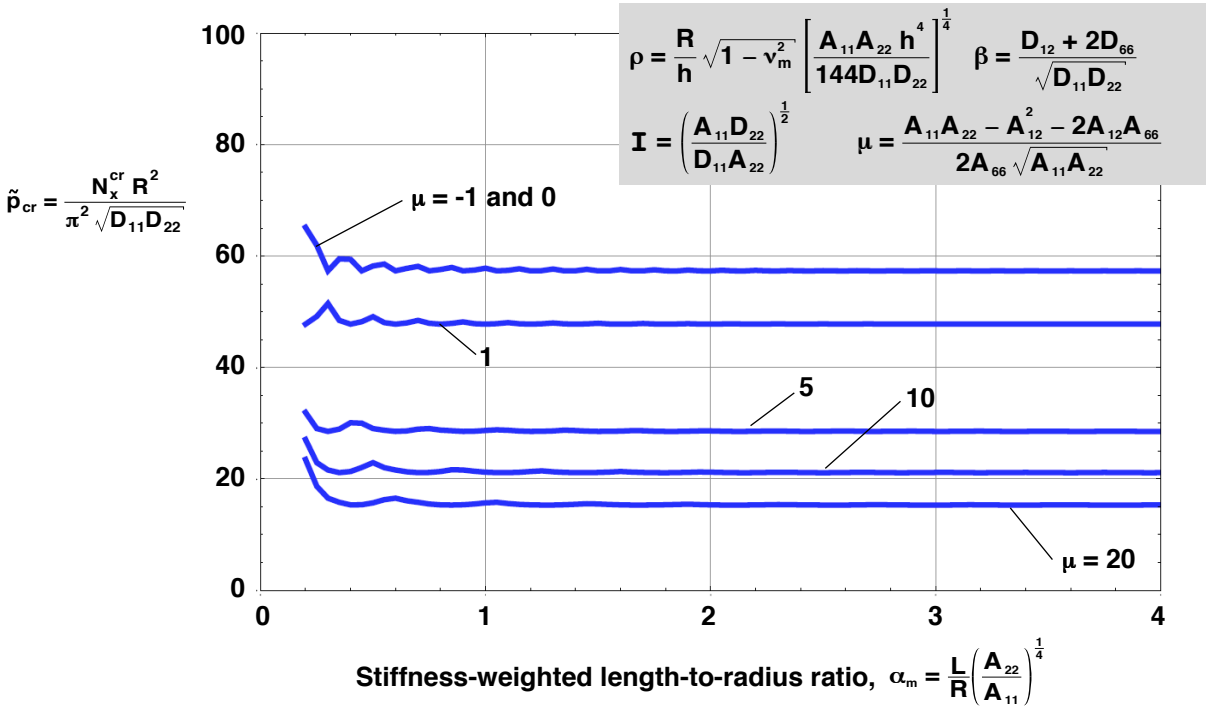

Figure 40. Effects of parameters α_m and μ on nondimensional buckling loads on cylinders with $\beta = 0$, $\mathrm{I} = 1.5$, and $\rho = 100$.

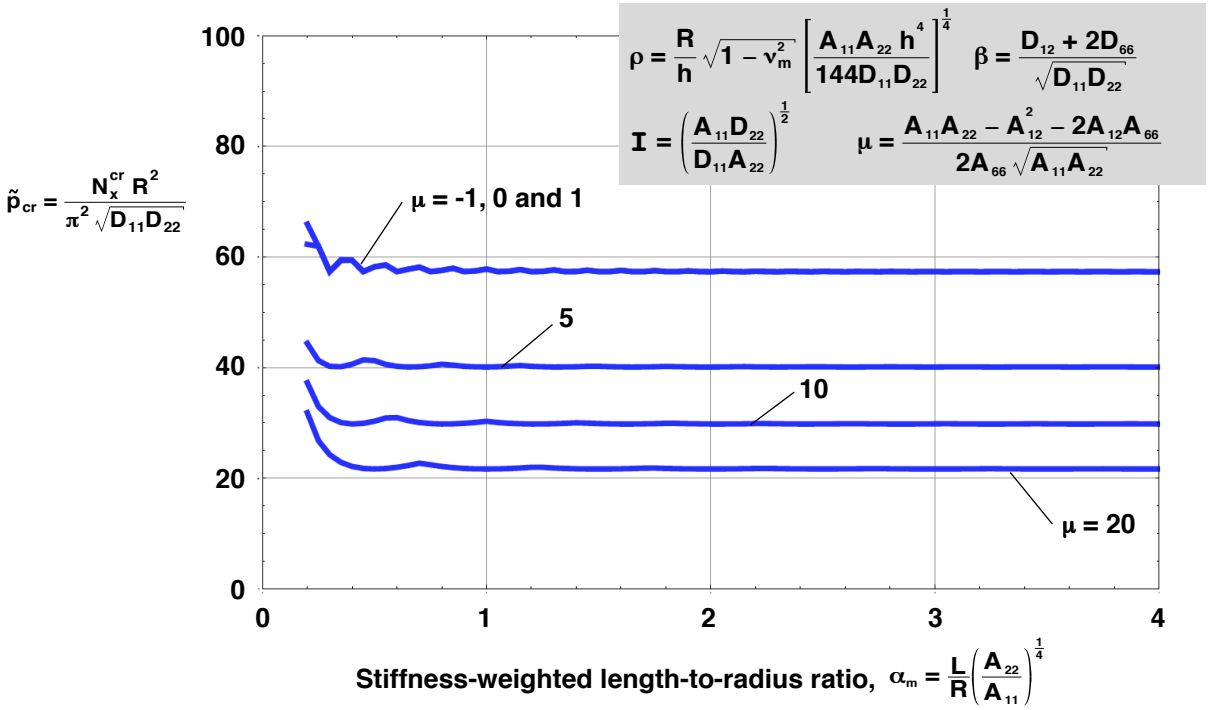

Figure 41. Effects of parameters α_m and μ on nondimensional buckling loads on cylinders with $\beta = 1$, $\mathrm{I} = 1.5$, and $\rho = 100$.

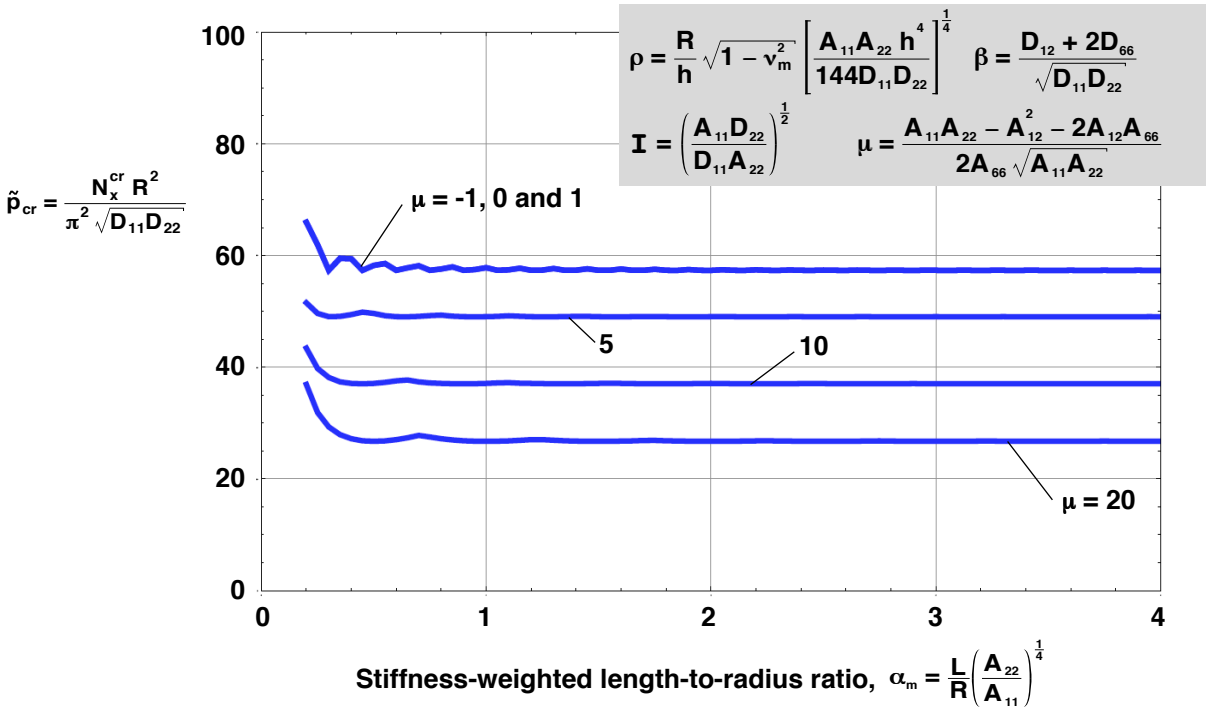

Figure 42. Effects of parameters α_m and μ on nondimensional buckling loads on cylinders with $\beta = 2$, $\mathrm{I} = 1.5$, and $\rho = 100$.

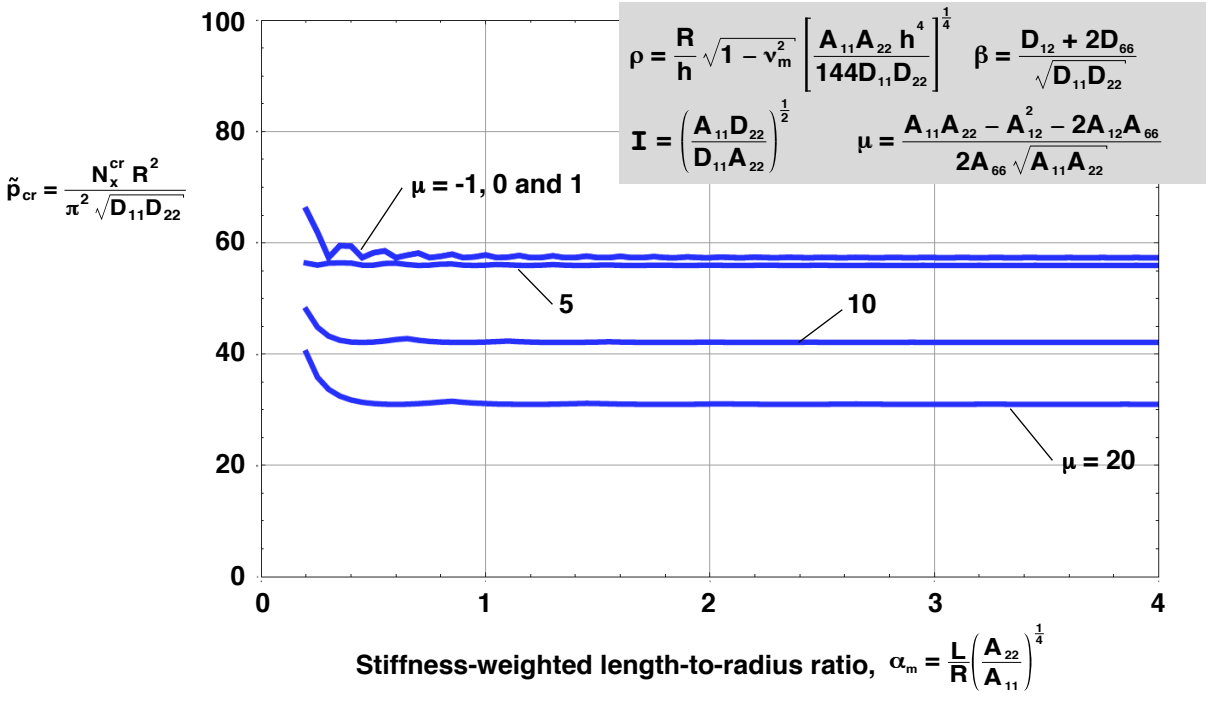

Figure 43. Effects of parameters α_m and μ on nondimensional buckling loads on cylinders with $\beta = 3$, $\mathrm{I} = 1.5$, and $\rho = 100$.

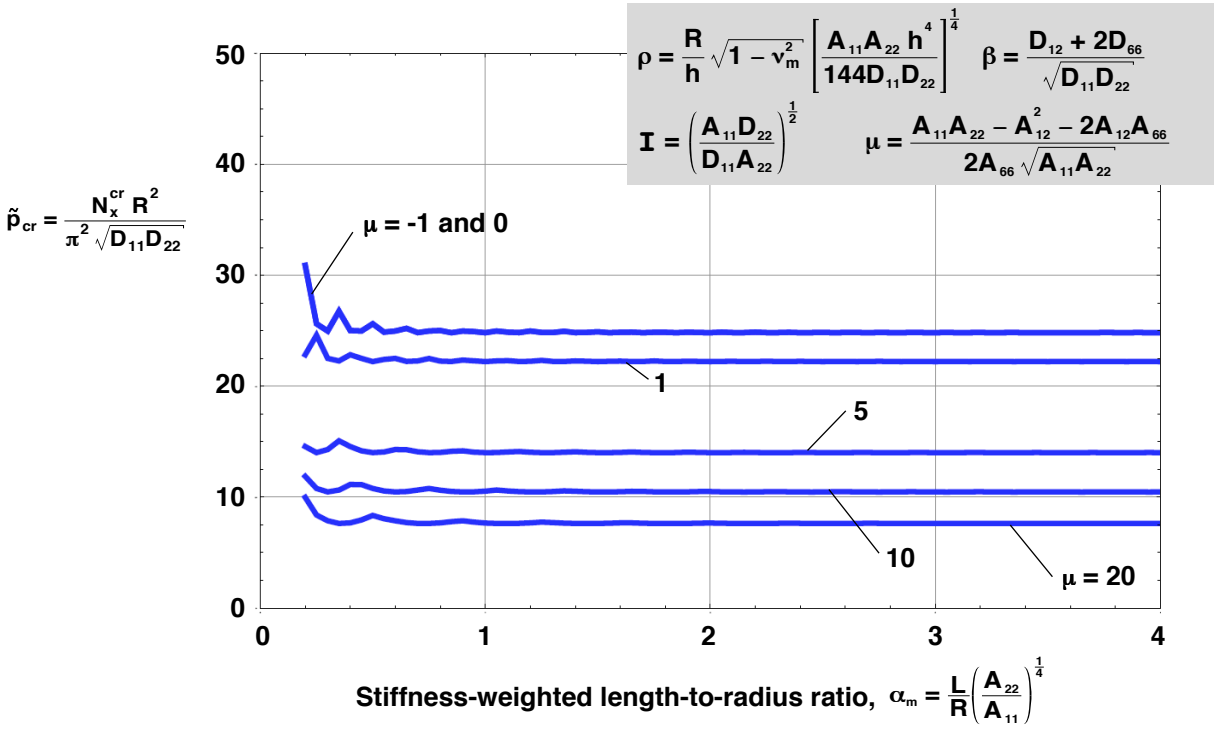

Figure 44. Effects of parameters α_m and μ on nondimensional buckling loads on cylinders with $\beta = 0$, $I = 2$, and $\rho = 100$.

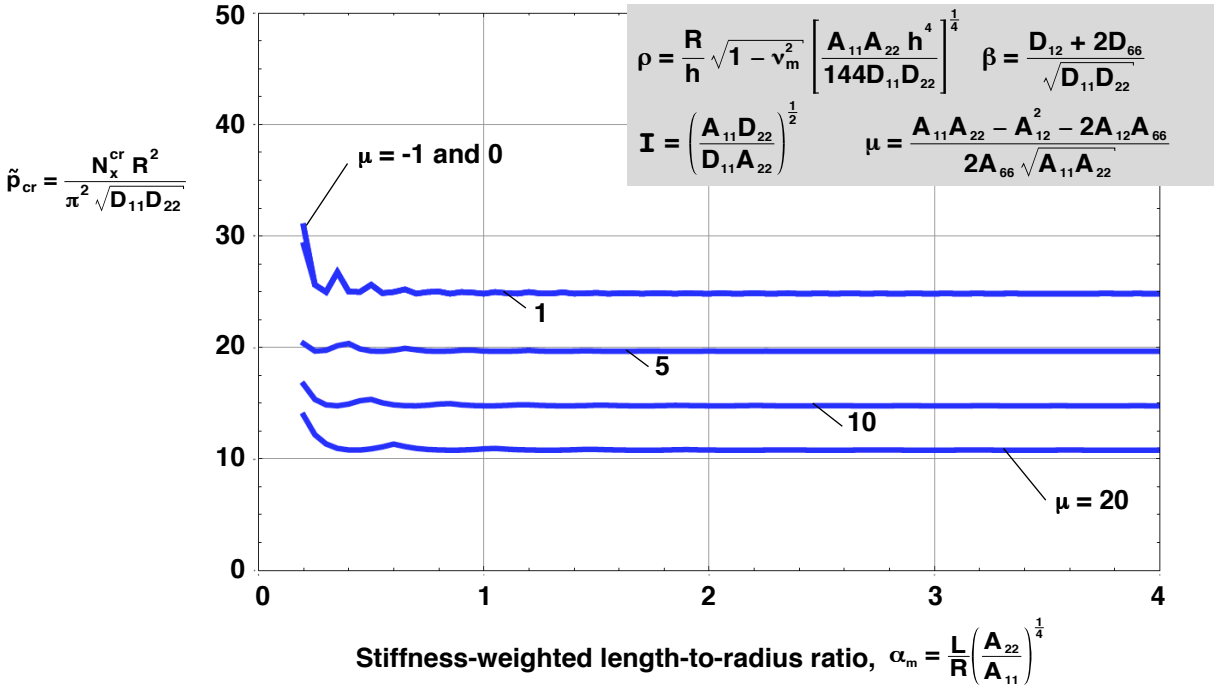

Figure 45. Effects of parameters α_m and μ on nondimensional buckling loads on cylinders with $\beta = 1$, $I = 2$, and $\rho = 100$.

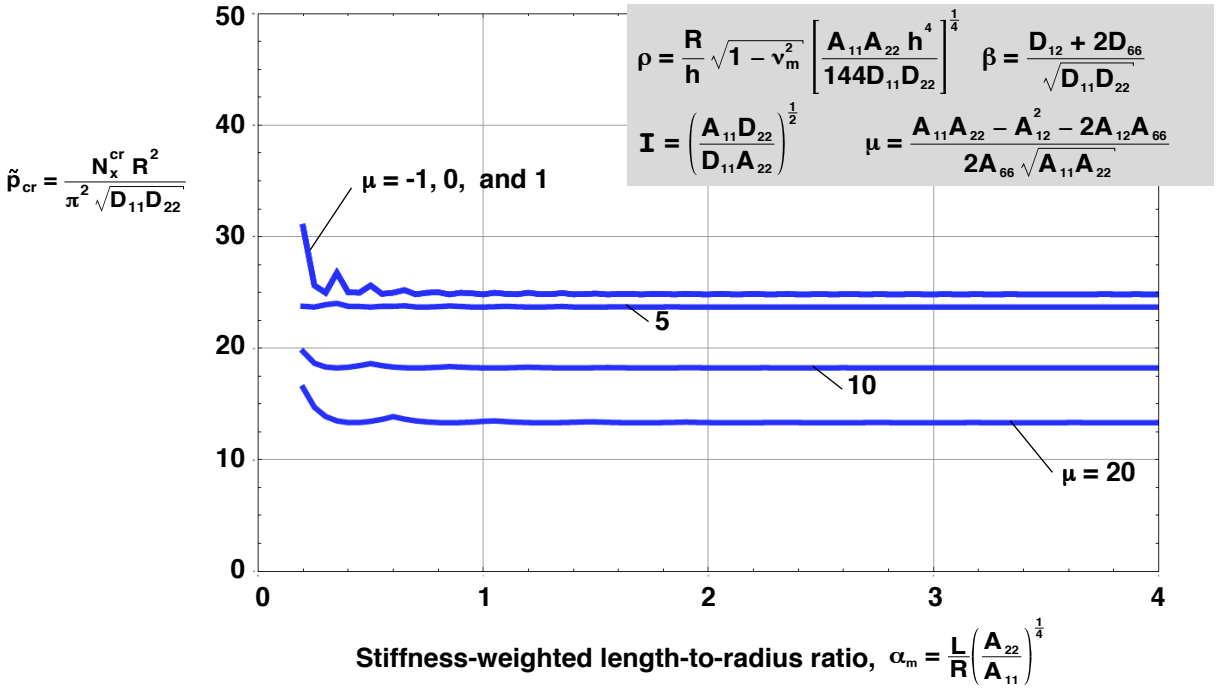

Figure 46. Effects of parameters α_m and μ on nondimensional buckling loads on cylinders with $\beta = 2$, $\gamma = 2$, and $\rho = 100$.

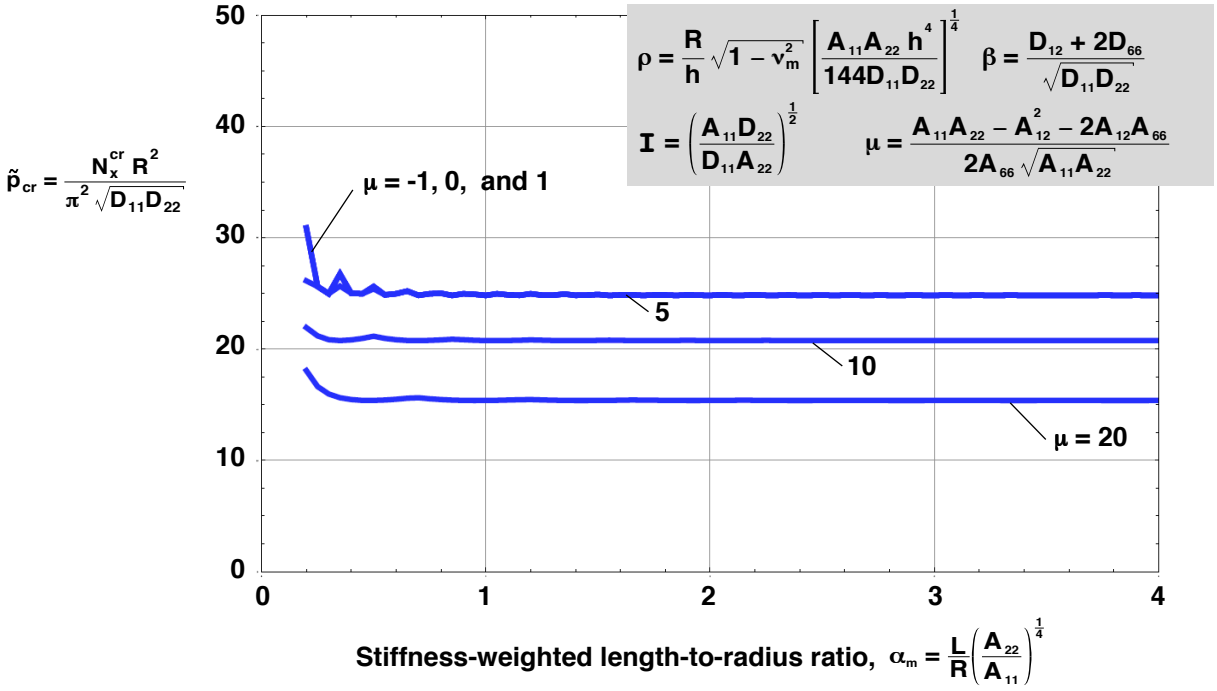

Figure 47. Effects of parameters α_m and μ on nondimensional buckling loads on cylinders with $\beta = 3$, $\gamma = 2$, and $\rho = 100$.

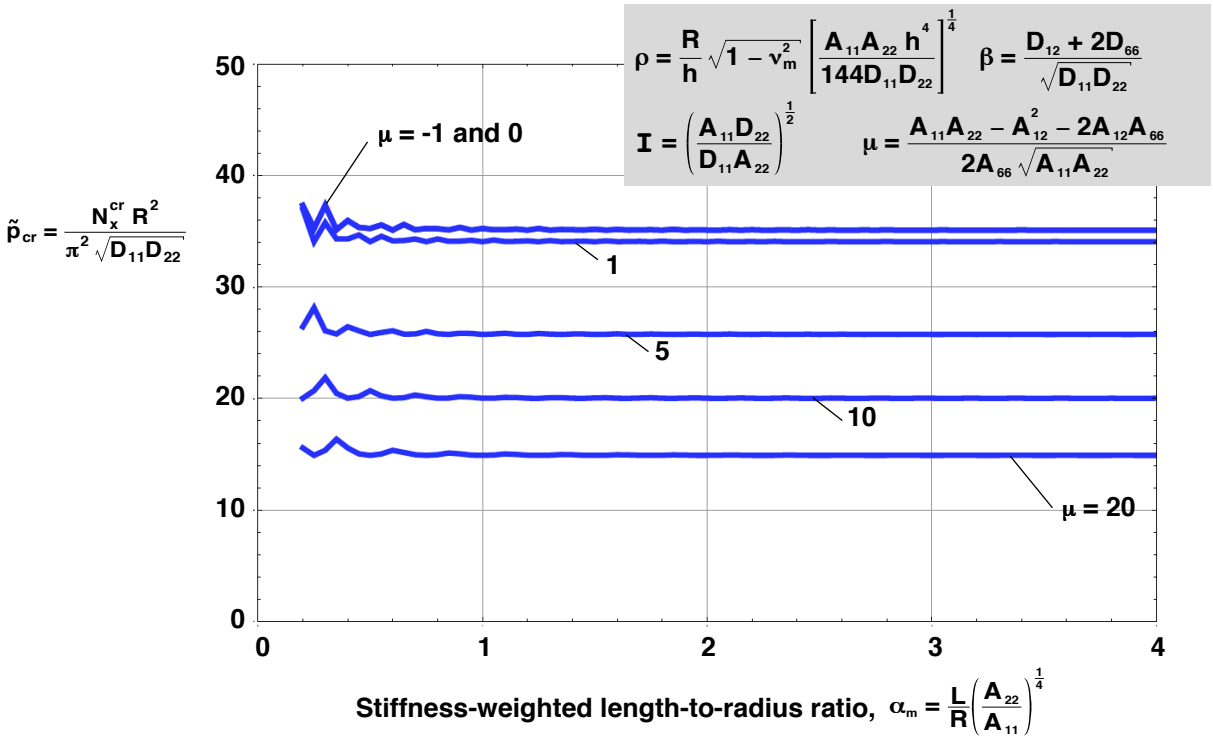

Figure 48. Effects of parameters α_m and μ on nondimensional buckling loads on cylinders with $\beta = 0$, $I = 4$, and $\rho = 100$.

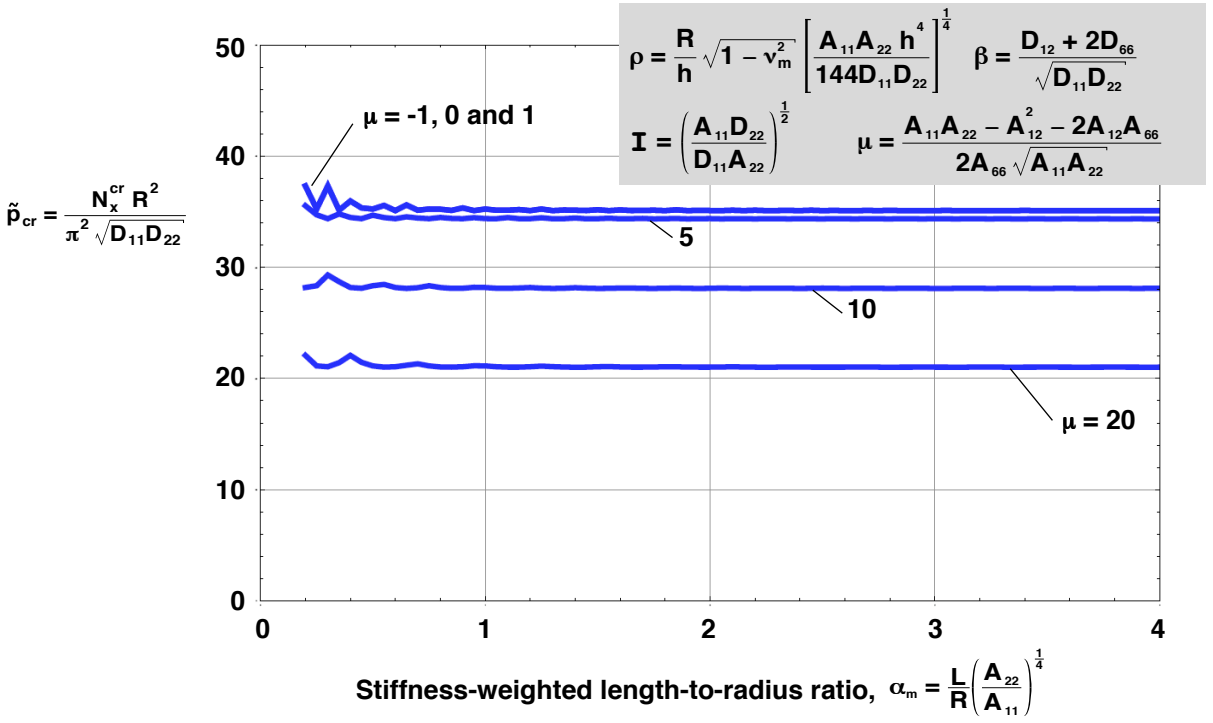

Figure 49. Effects of parameters α_m and μ on nondimensional buckling loads on cylinders with $\beta = 1$, $I = 4$, and $\rho = 100$.

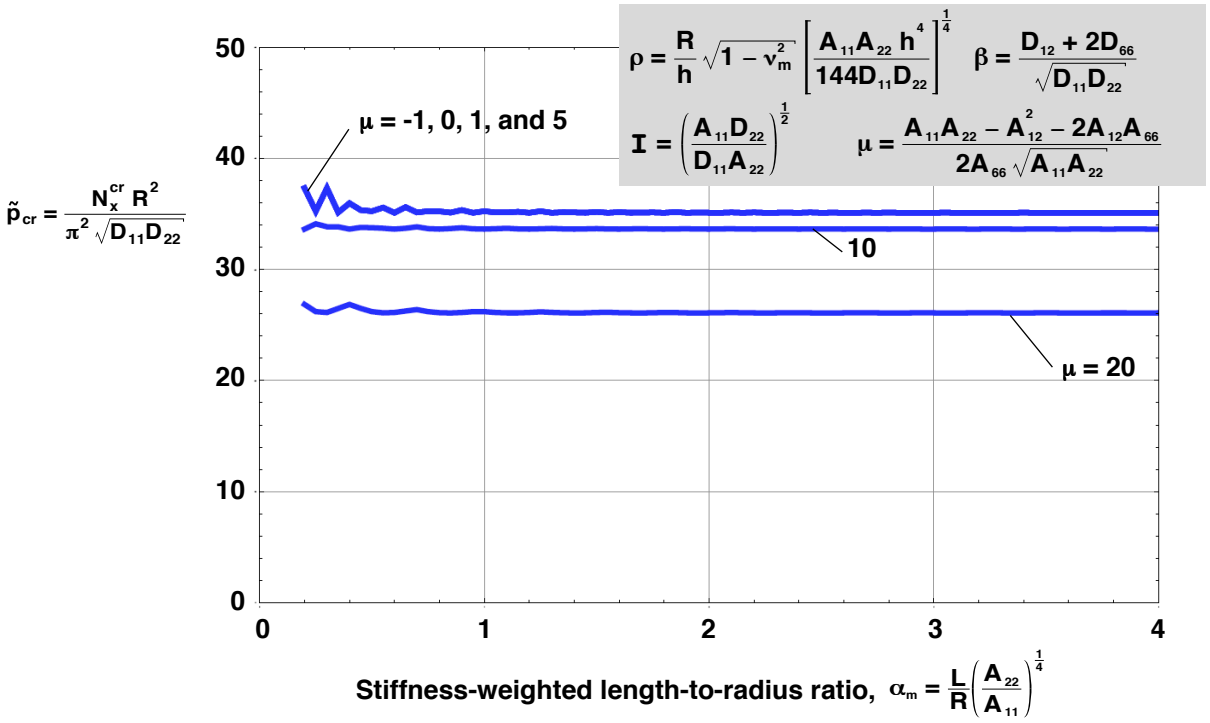

Figure 50. Effects of parameters α_m and μ on nondimensional buckling loads on cylinders with $\beta = 2$, $\mathrm{I} = 4$, and $\rho = 100$.

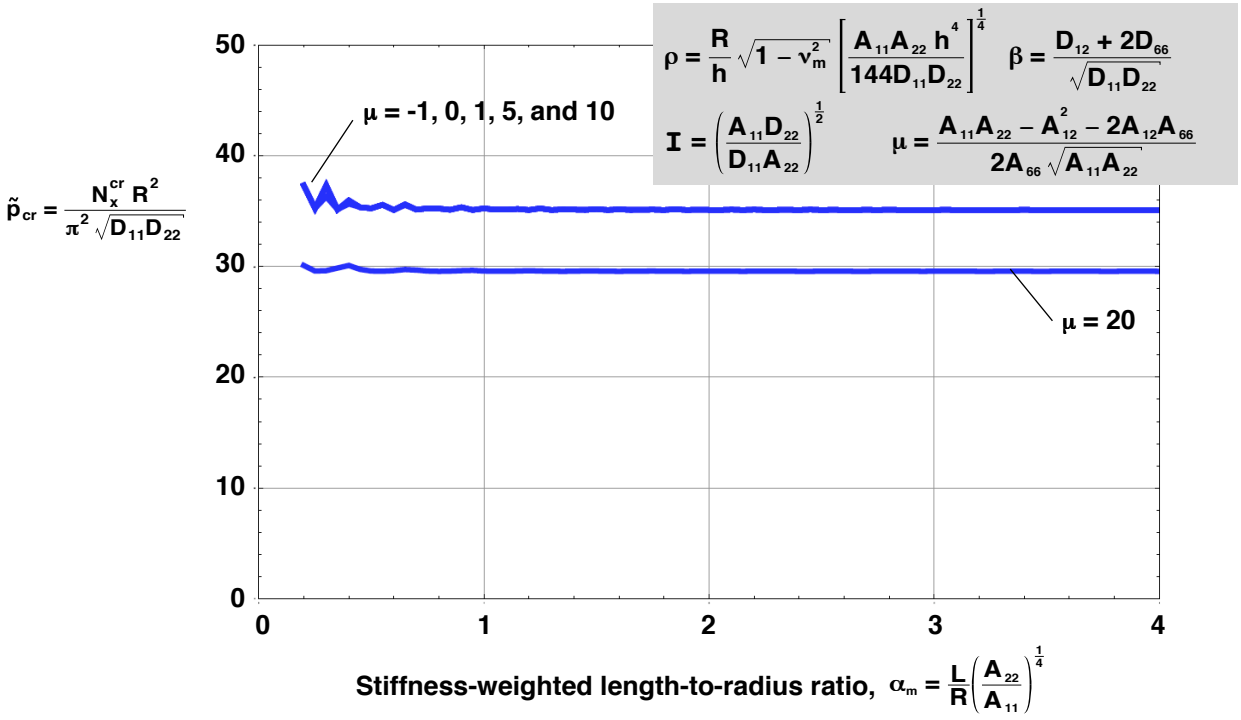

Figure 51. Effects of parameters α_m and μ on nondimensional buckling loads on cylinders with $\beta = 3$, $\mathrm{I} = 4$, and $\rho = 100$.

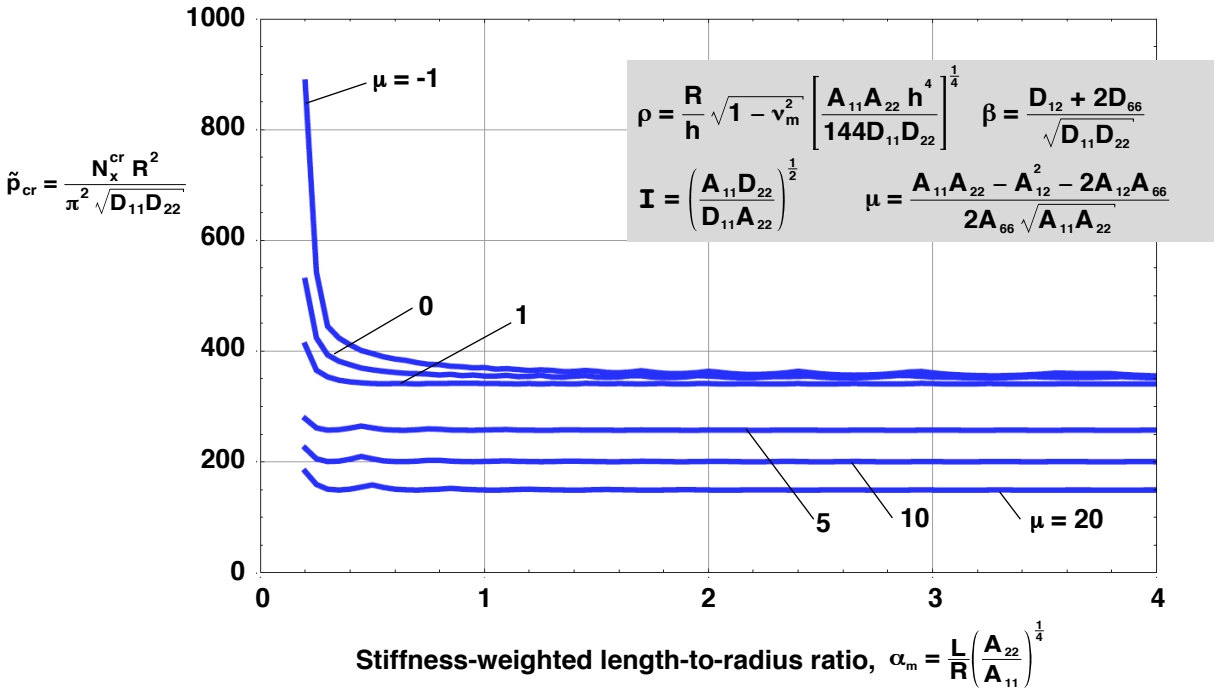

Figure 52. Effects of parameters α_m and μ on nondimensional buckling loads on cylinders with $\beta = 0$, $\mathrm{I} = .25$, and $\rho = 1000$.

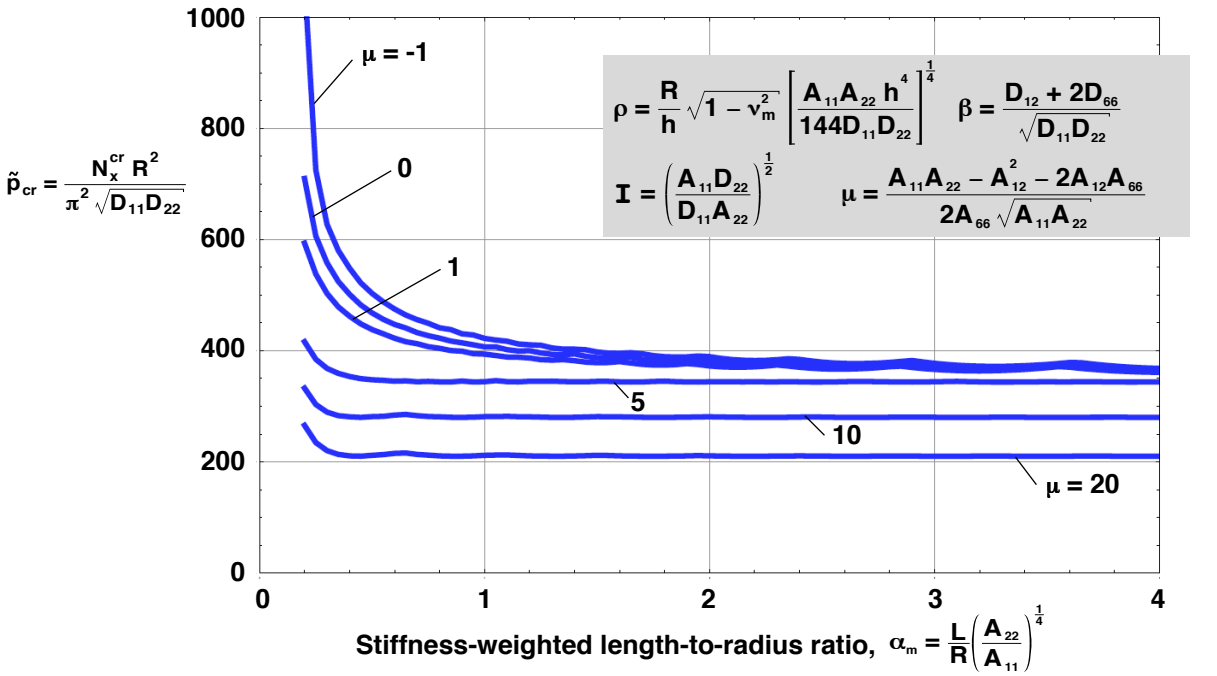

Figure 53. Effects of parameters α_m and μ on nondimensional buckling loads on cylinders with $\beta = 1$, $\mathrm{I} = .25$, and $\rho = 1000$.

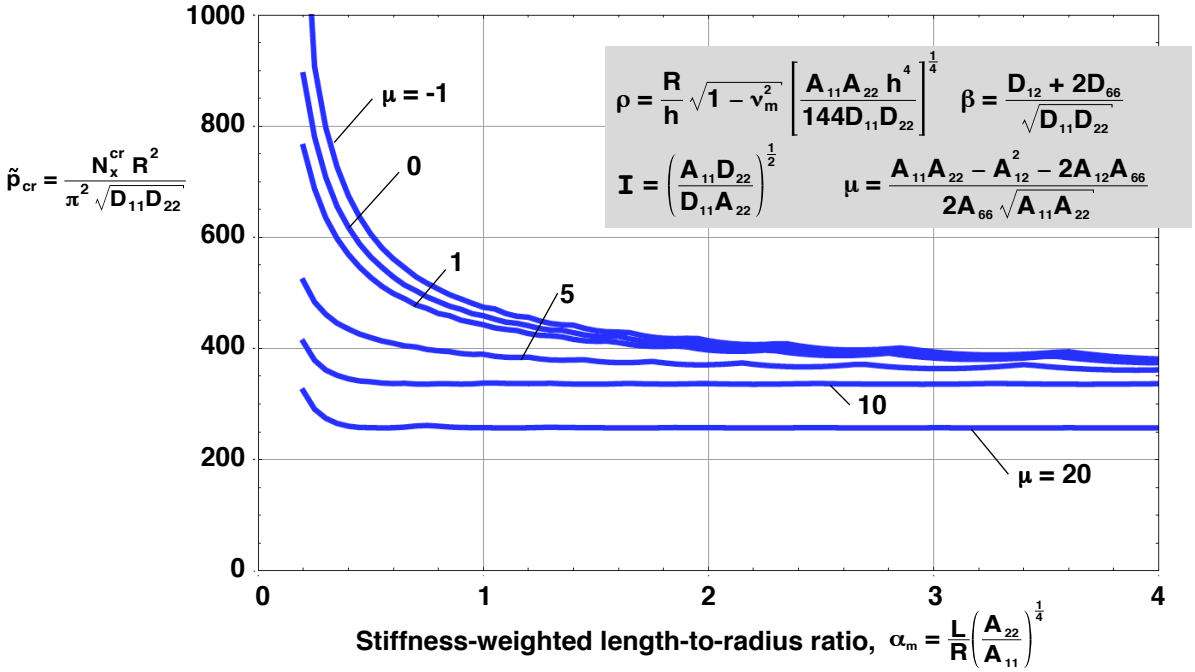

Figure 54. Effects of parameters α_m and μ on nondimensional buckling loads on cylinders with $\beta = 2$, $\mathrm{I} = .25$, and $\rho = 1000$.

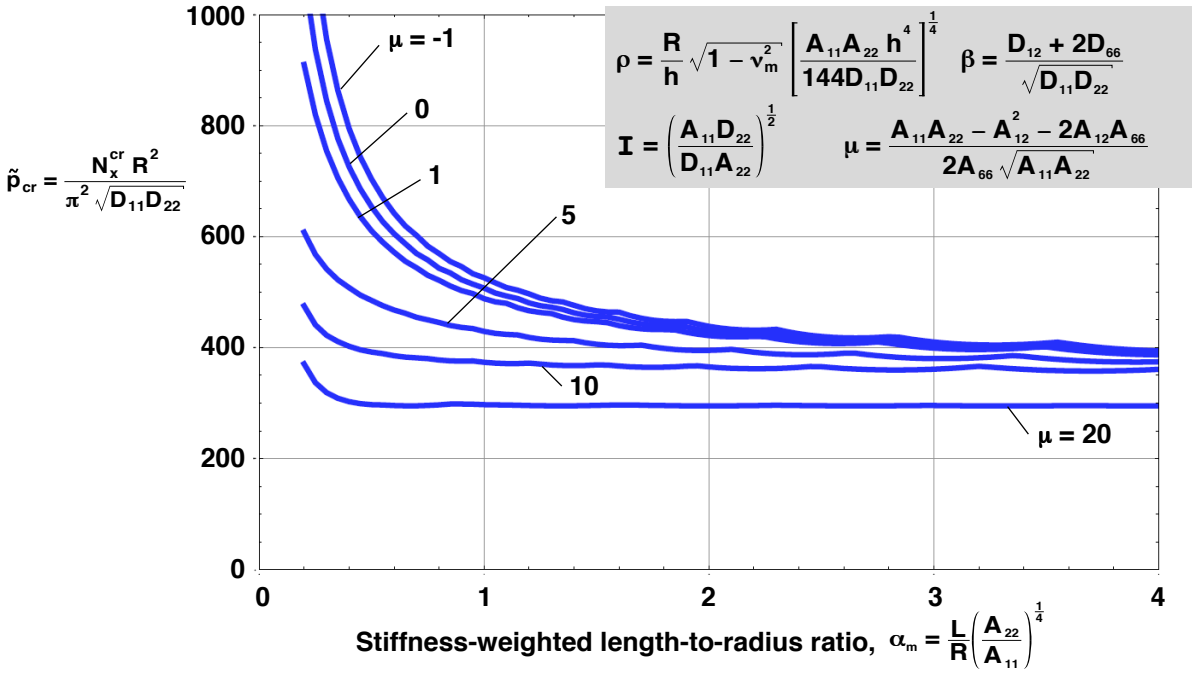

Figure 55. Effects of parameters α_m and μ on nondimensional buckling loads on cylinders with $\beta = 3$, $\mathrm{I} = .25$, and $\rho = 1000$.

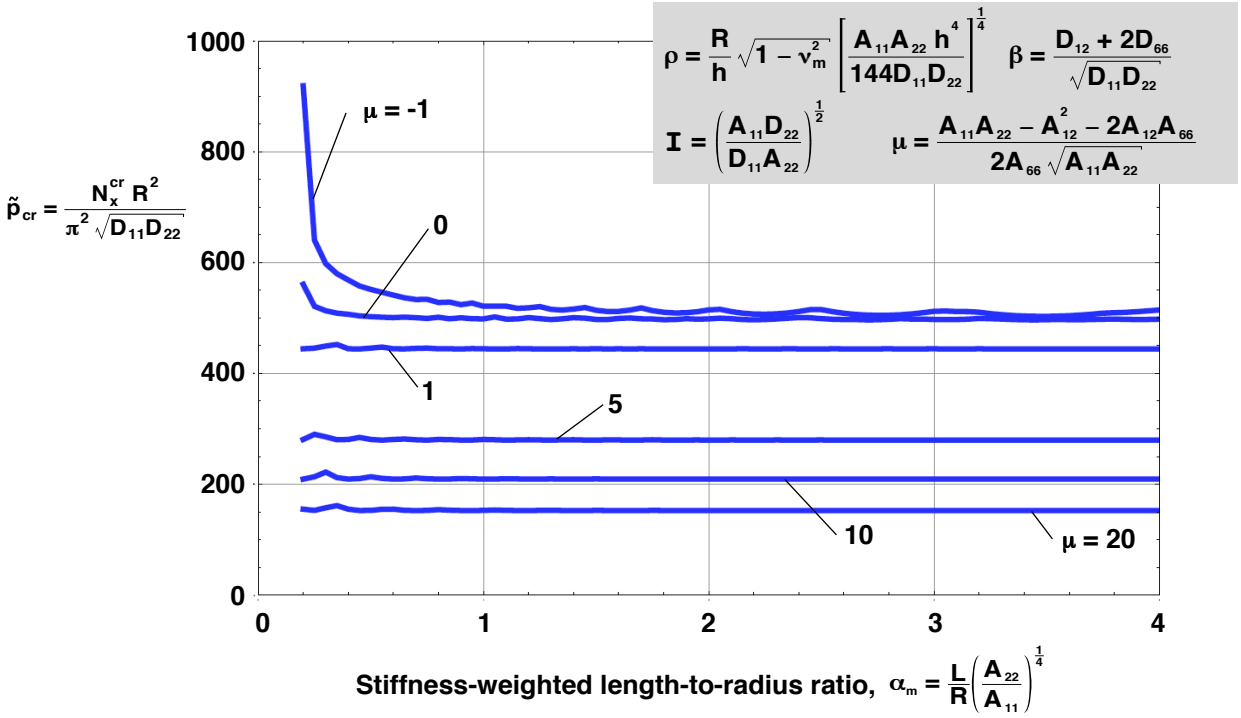

Figure 56. Effects of parameters α_m and μ on nondimensional buckling loads on cylinders with $\beta = 0$, $\mathrm{I} = 0.5$, and $\rho = 1000$.

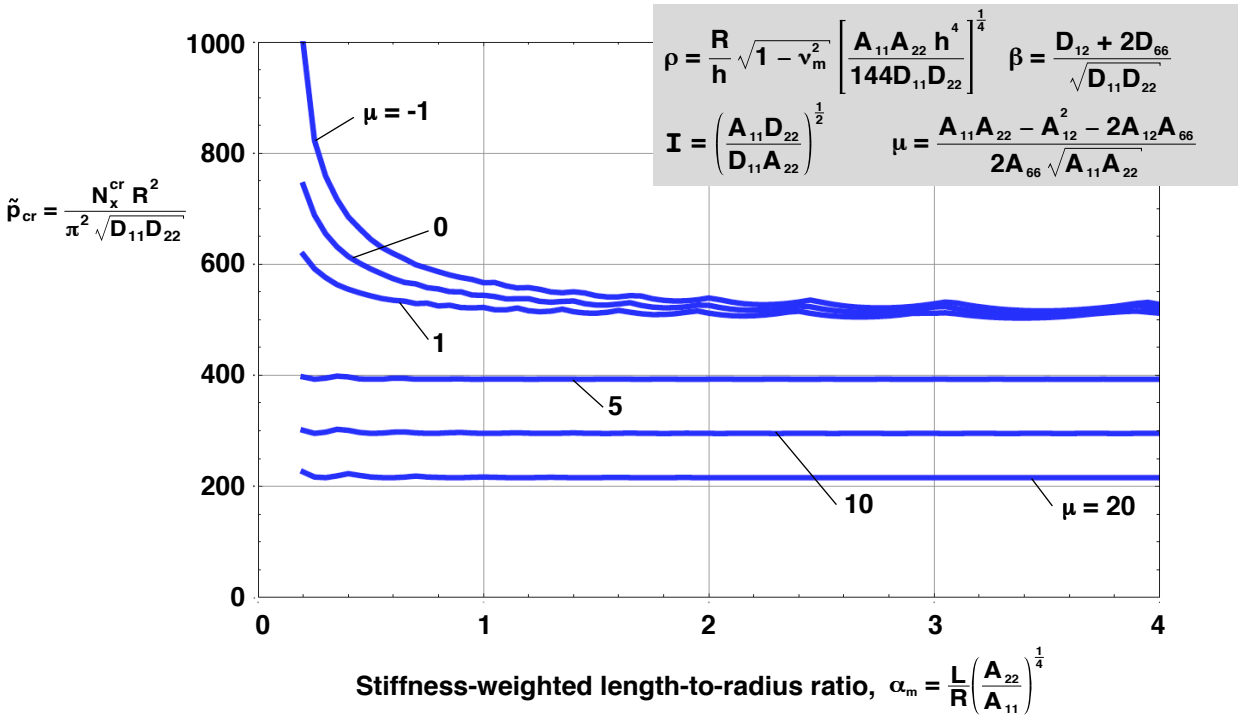

Figure 57. Effects of parameters α_m and μ on nondimensional buckling loads on cylinders with $\beta = 1$, $\mathrm{I} = 0.5$, and $\rho = 1000$.

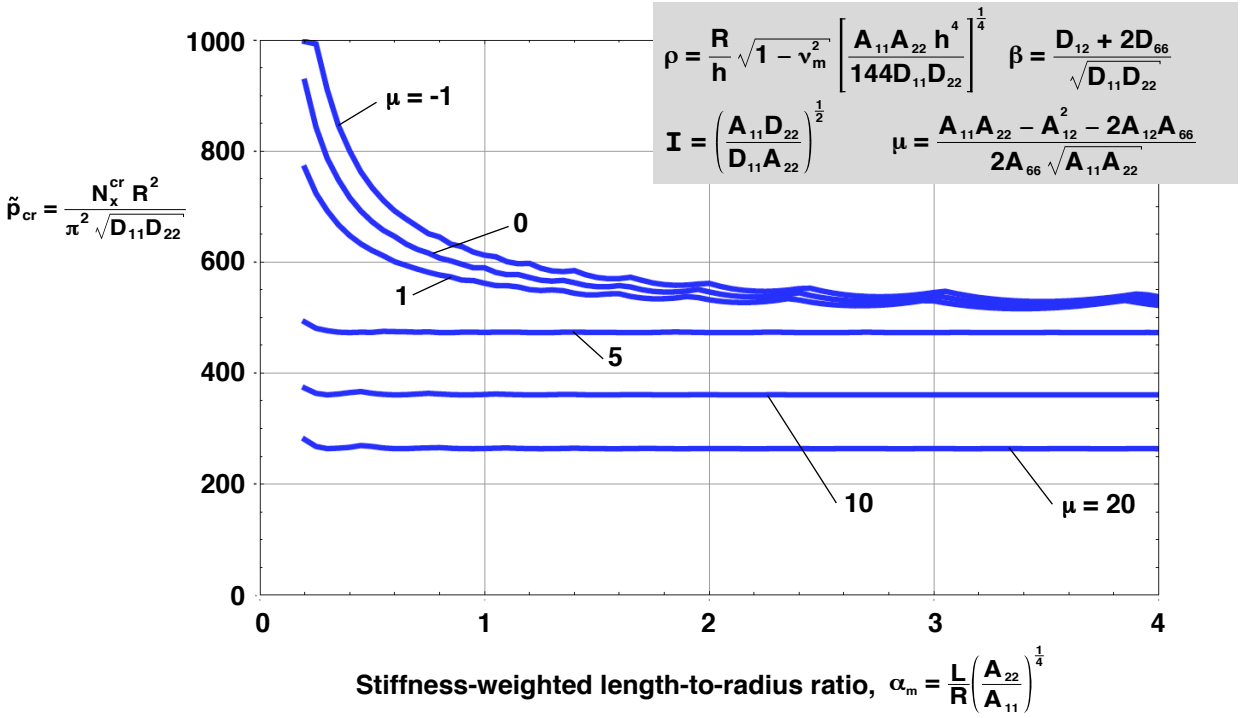

Figure 58. Effects of parameters α_m and μ on nondimensional buckling loads on cylinders with $\beta = 2$, $\mathrm{I} = 0.5$, and $\rho = 1000$.

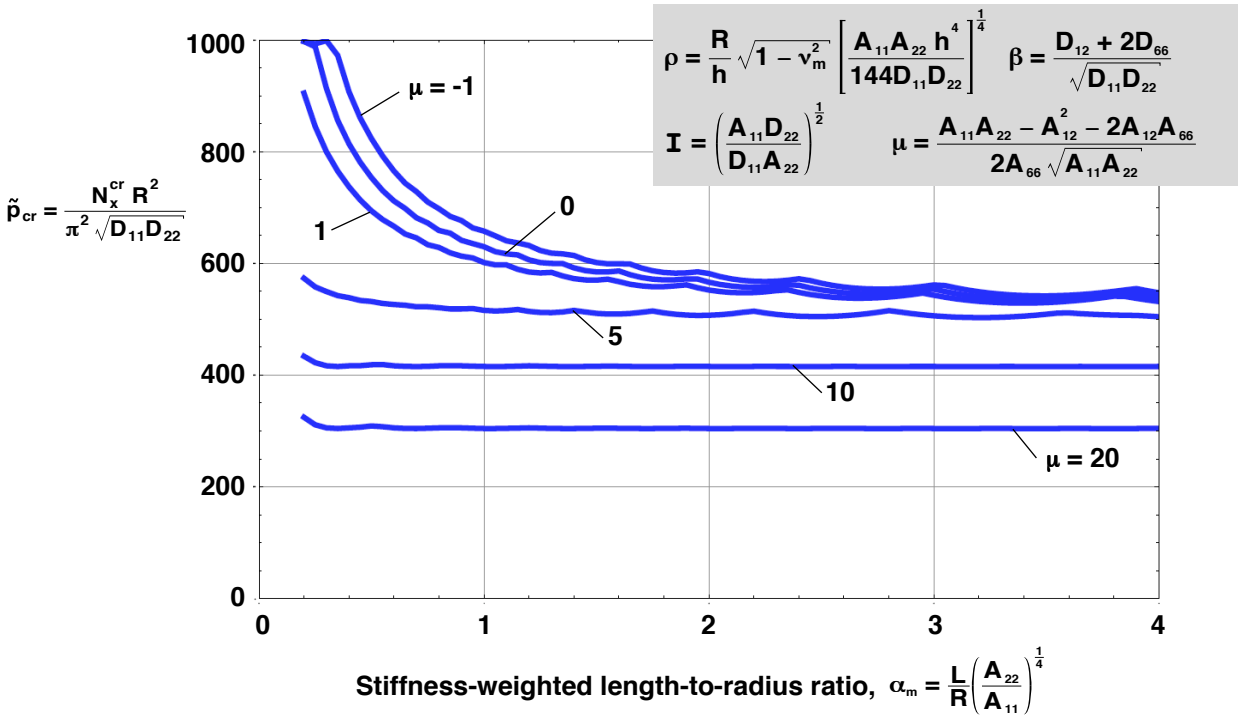

Figure 59. Effects of parameters α_m and μ on nondimensional buckling loads on cylinders with $\beta = 3$, $\mathrm{I} = 0.5$, and $\rho = 1000$.

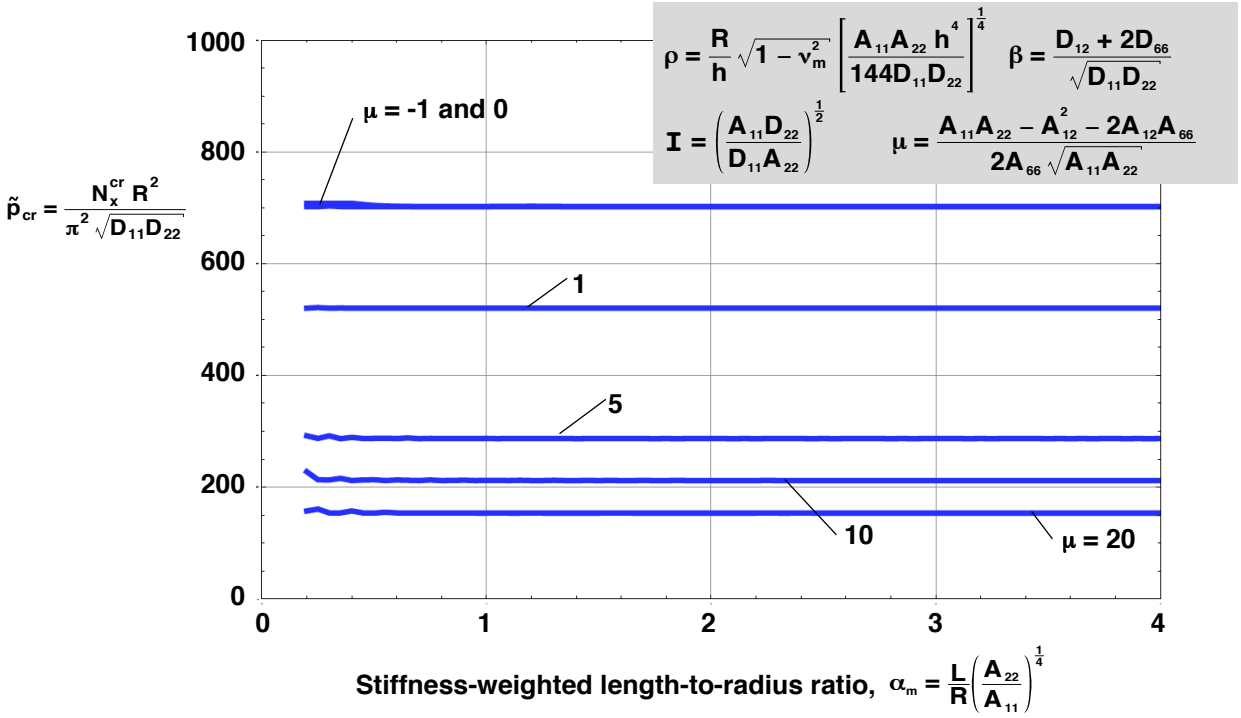

Figure 60. Effects of parameters α_m and μ on nondimensional buckling loads on cylinders with $\beta = 0$, $\mathrm{I} = 1$, and $\rho = 1000$.

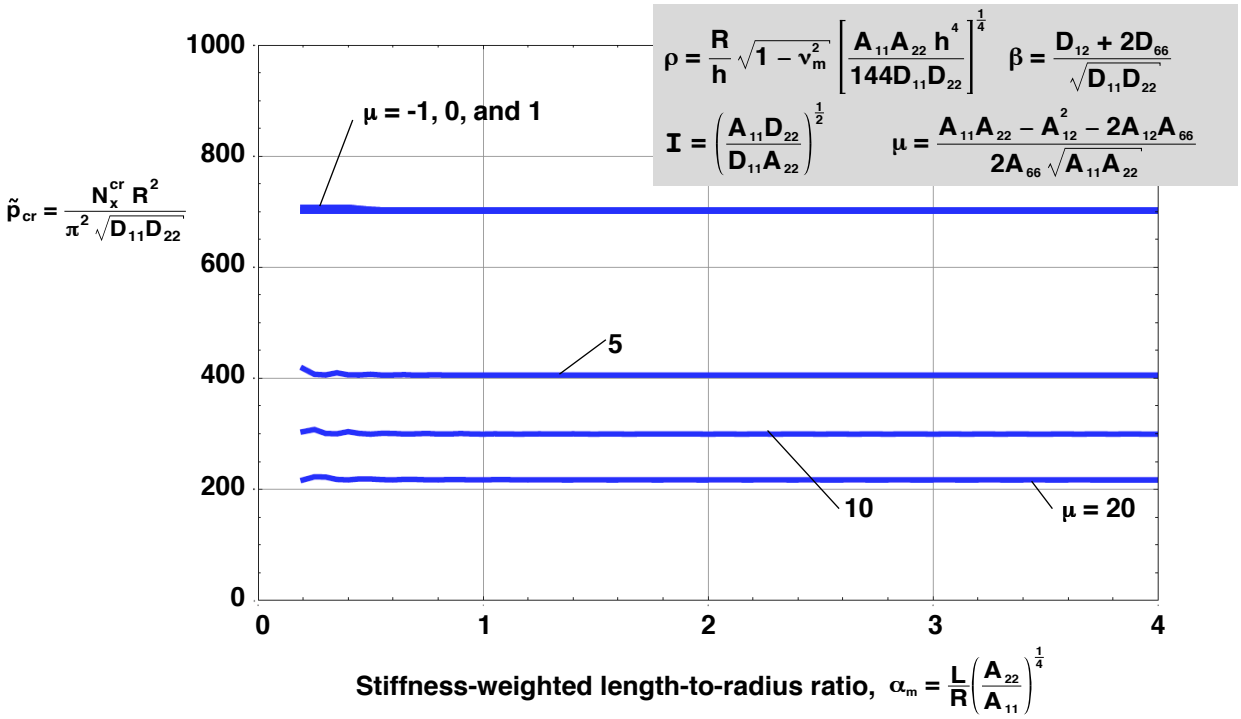

Figure 61. Effects of parameters α_m and μ on nondimensional buckling loads on cylinders with $\beta = 1$, $\mathrm{I} = 1$, and $\rho = 1000$.

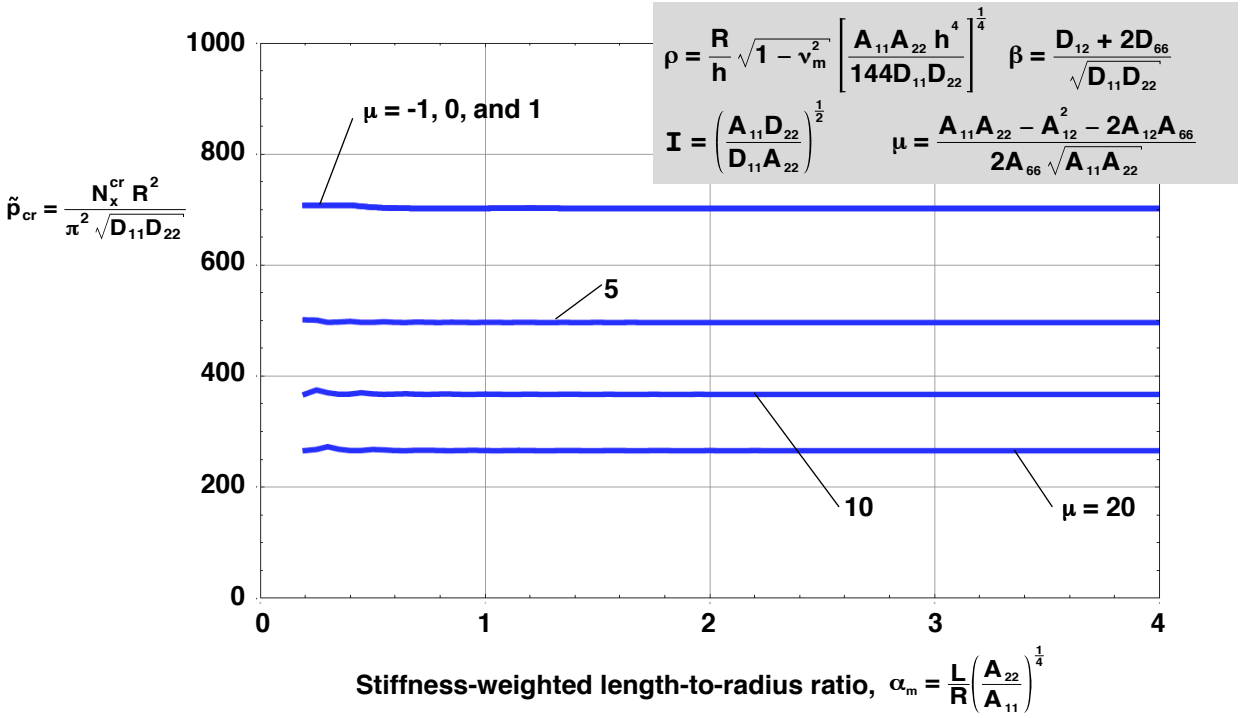

Figure 62. Effects of parameters α_m and μ on nondimensional buckling loads on cylinders with $\beta = 2$, $\mathrm{I} = 1$, and $\rho = 1000$.

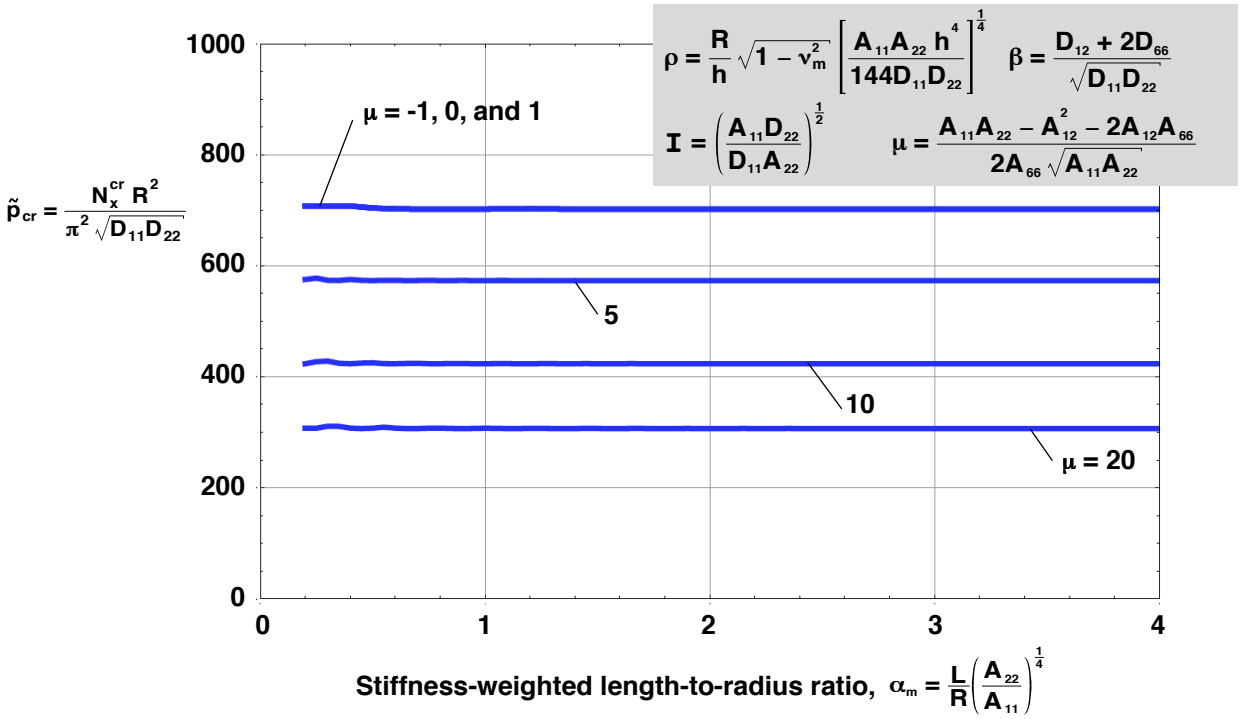

Figure 63. Effects of parameters α_m and μ on nondimensional buckling loads on cylinders with $\beta = 3$, $\mathrm{I} = 1$, and $\rho = 1000$.

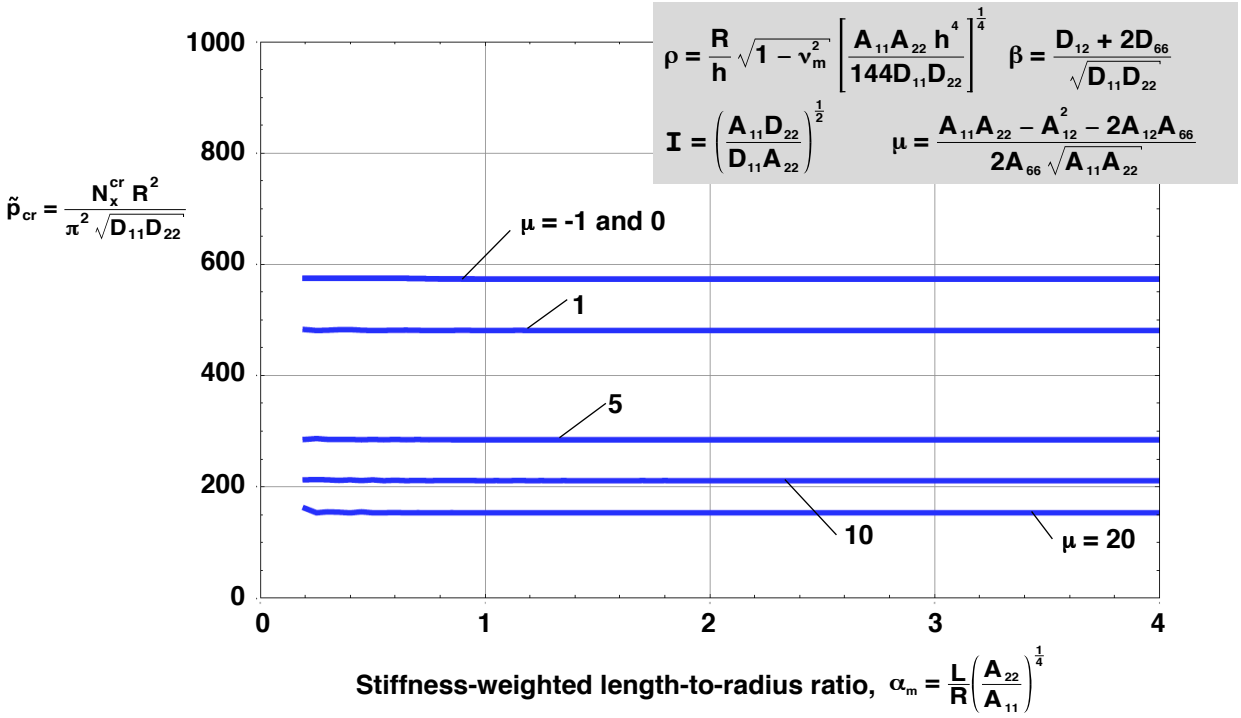

Figure 64. Effects of parameters α_m and μ on nondimensional buckling loads on cylinders with $\beta = 0$, $\mathrm{I} = 1.5$, and $\rho = 1000$.

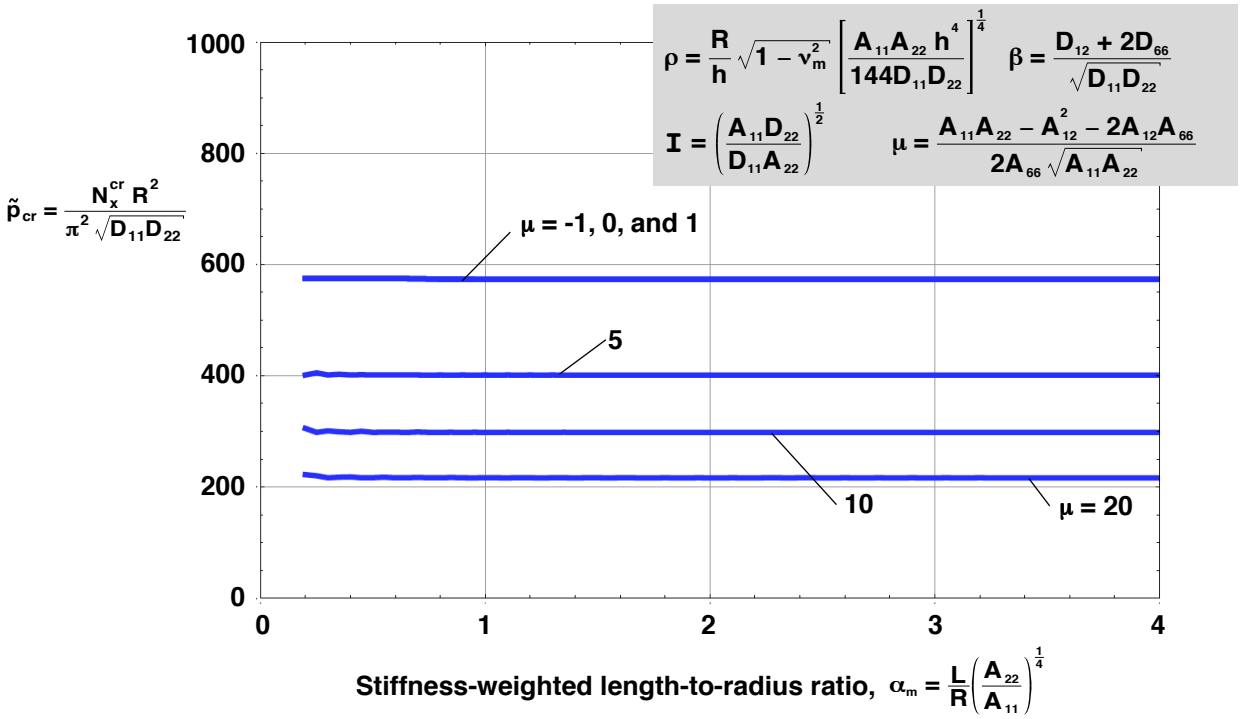

Figure 65. Effects of parameters α_m and μ on nondimensional buckling loads on cylinders with $\beta = 1$, $\mathrm{I} = 1.5$, and $\rho = 1000$.

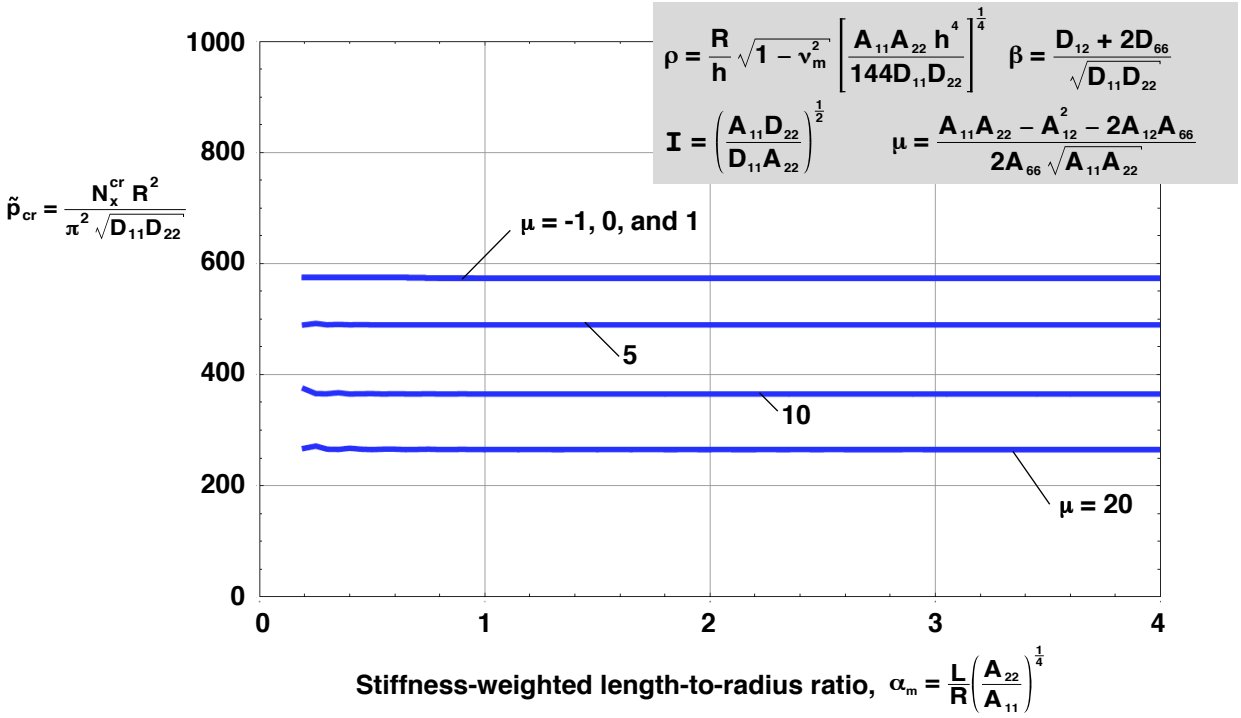

Figure 66. Effects of parameters α_m and μ on nondimensional buckling loads on cylinders with $\beta = 2$, $\mathrm{I} = 1.5$, and $\rho = 1000$.

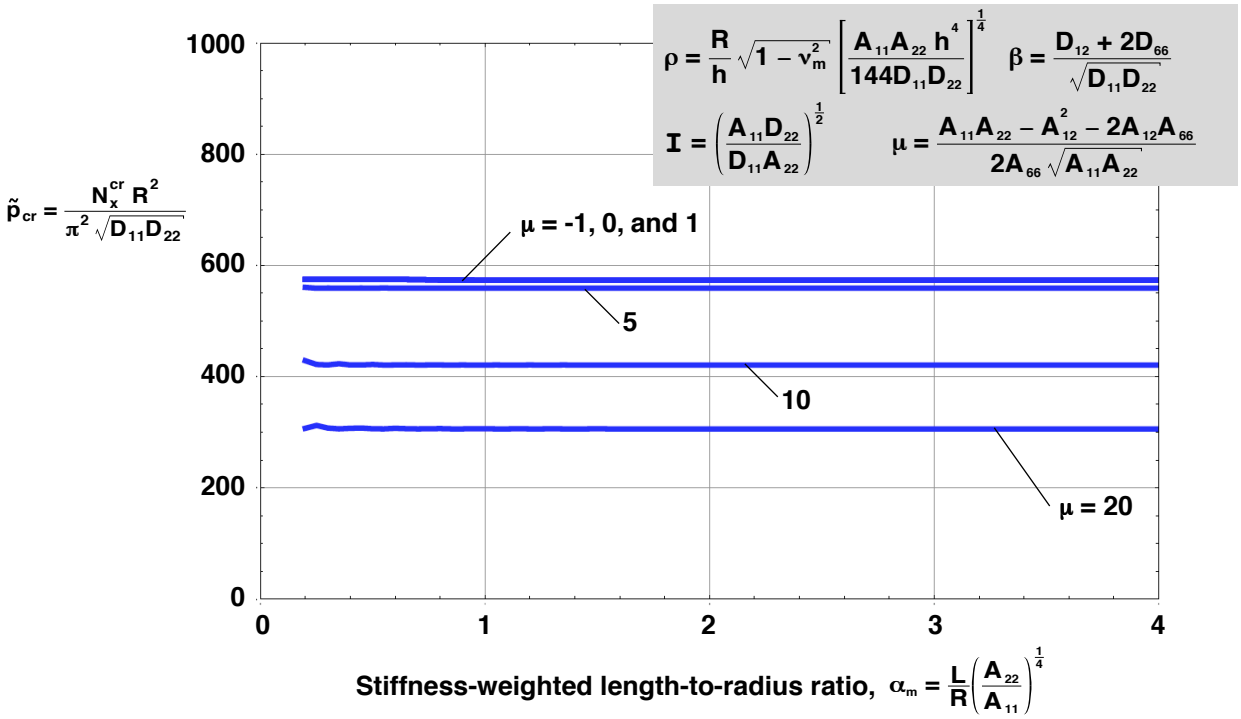

Figure 67. Effects of parameters α_m and μ on nondimensional buckling loads on cylinders with $\beta = 3$, $\mathrm{I} = 1.5$, and $\rho = 1000$.

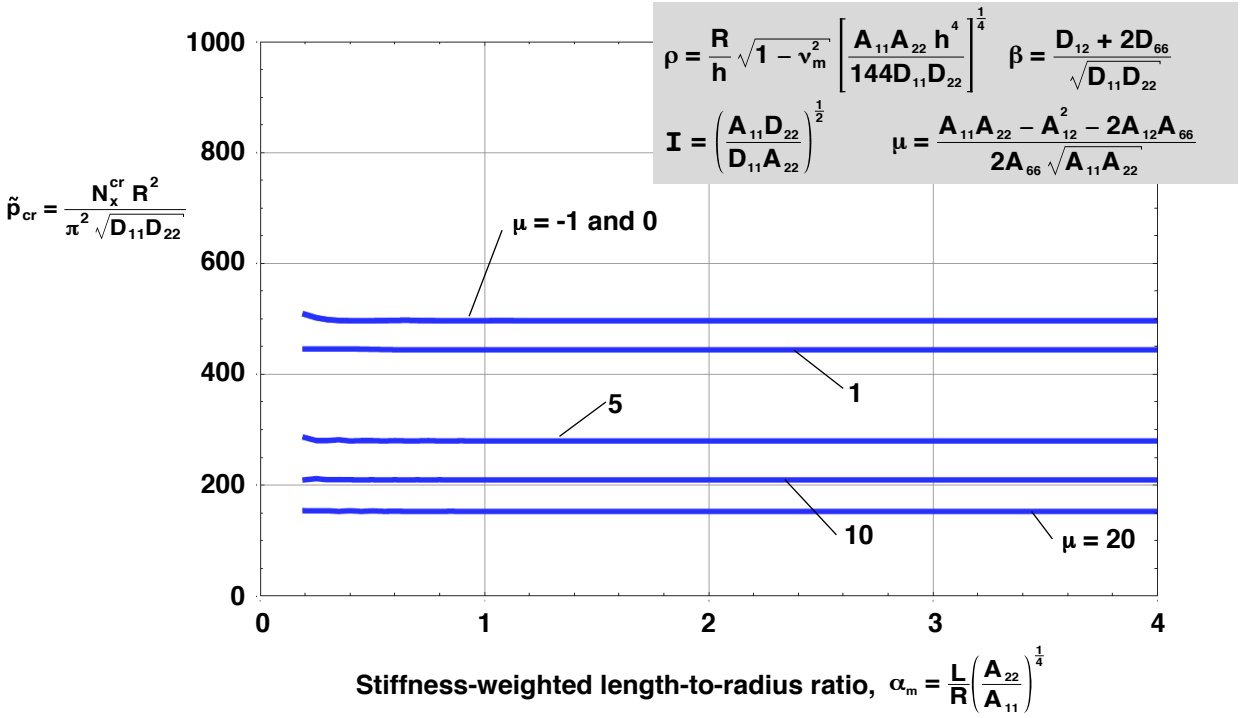

Figure 68. Effects of parameters α_m and μ on nondimensional buckling loads on cylinders with $\beta = 0$, $\mathrm{I} = 2$, and $\rho = 1000$.

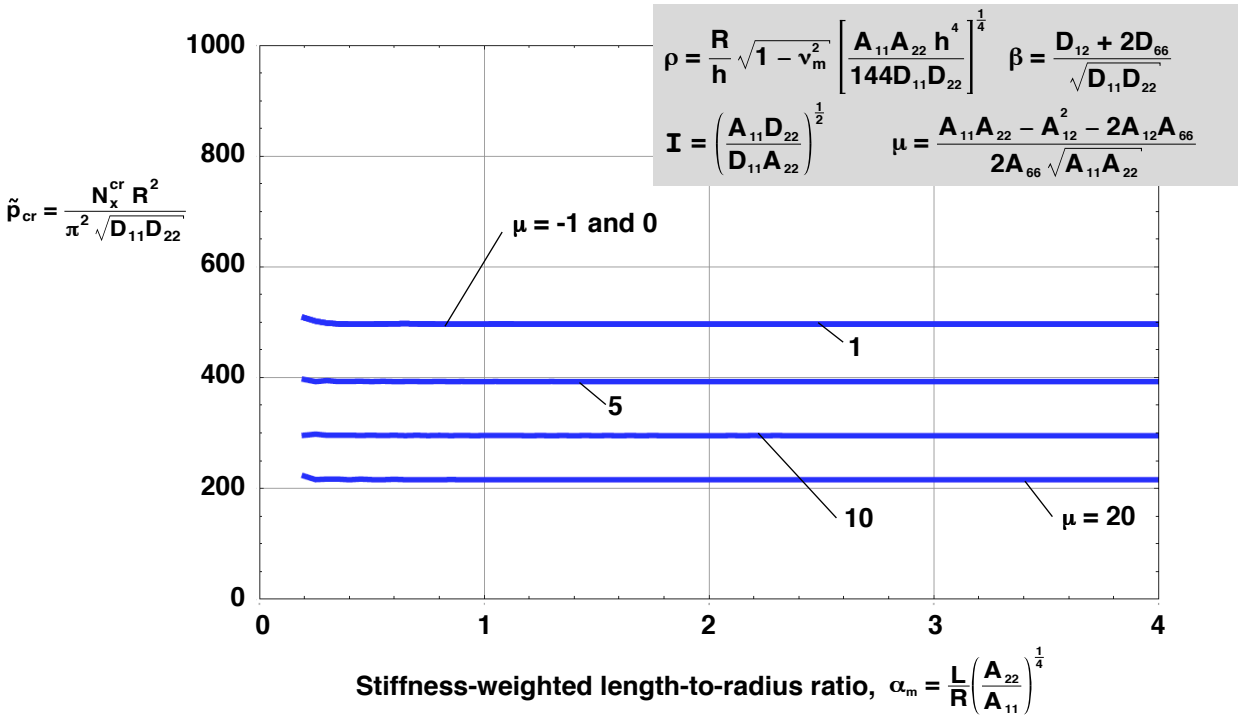

Figure 69. Effects of parameters α_m and μ on nondimensional buckling loads on cylinders with $\beta = 1$, $\mathrm{I} = 2$, and $\rho = 1000$.

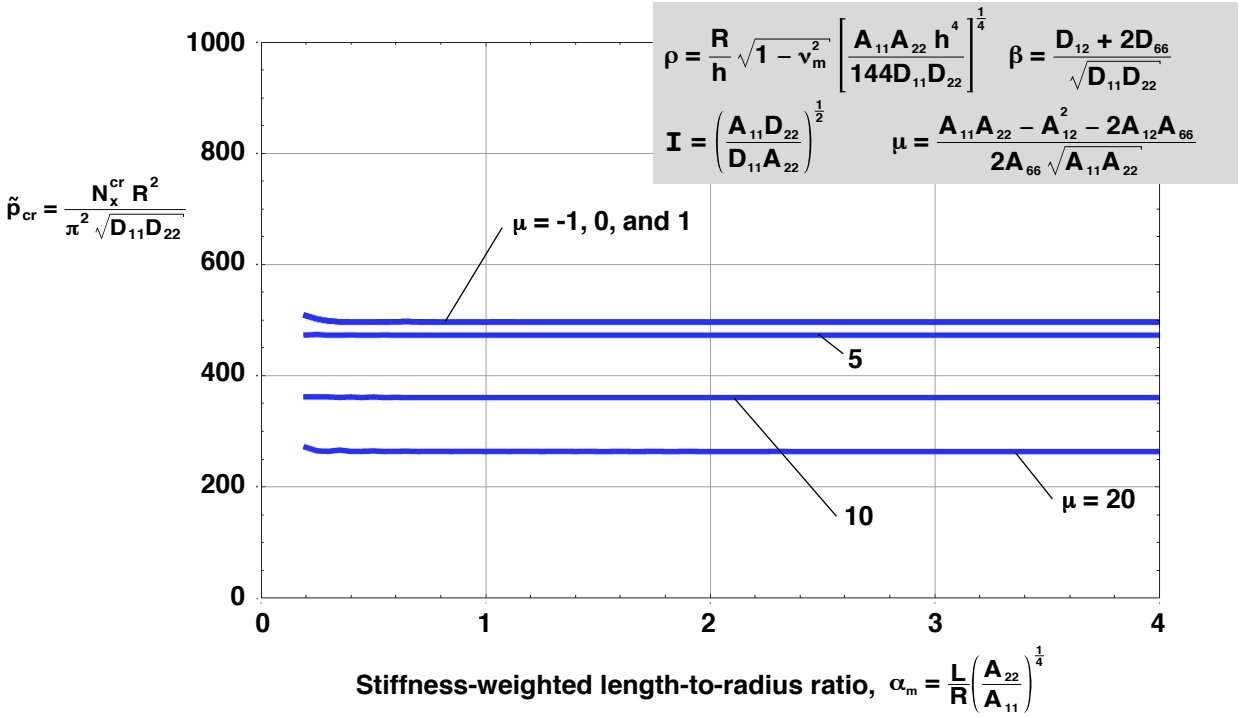

Figure 70. Effects of parameters α_m and μ on nondimensional buckling loads on cylinders with $\beta = 2$, $\mathrm{I} = 2$, and $\rho = 1000$.

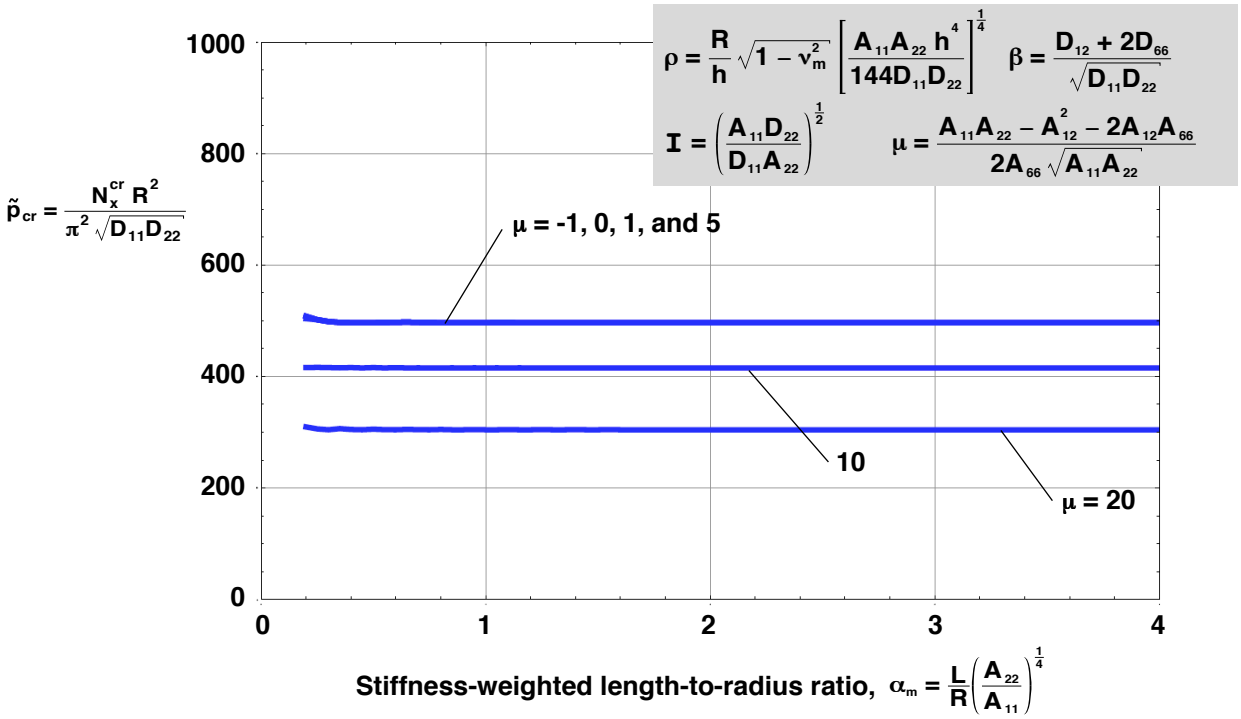

Figure 71. Effects of parameters α_m and μ on nondimensional buckling loads on cylinders with $\beta = 3$, $\mathrm{I} = 2$, and $\rho = 1000$.

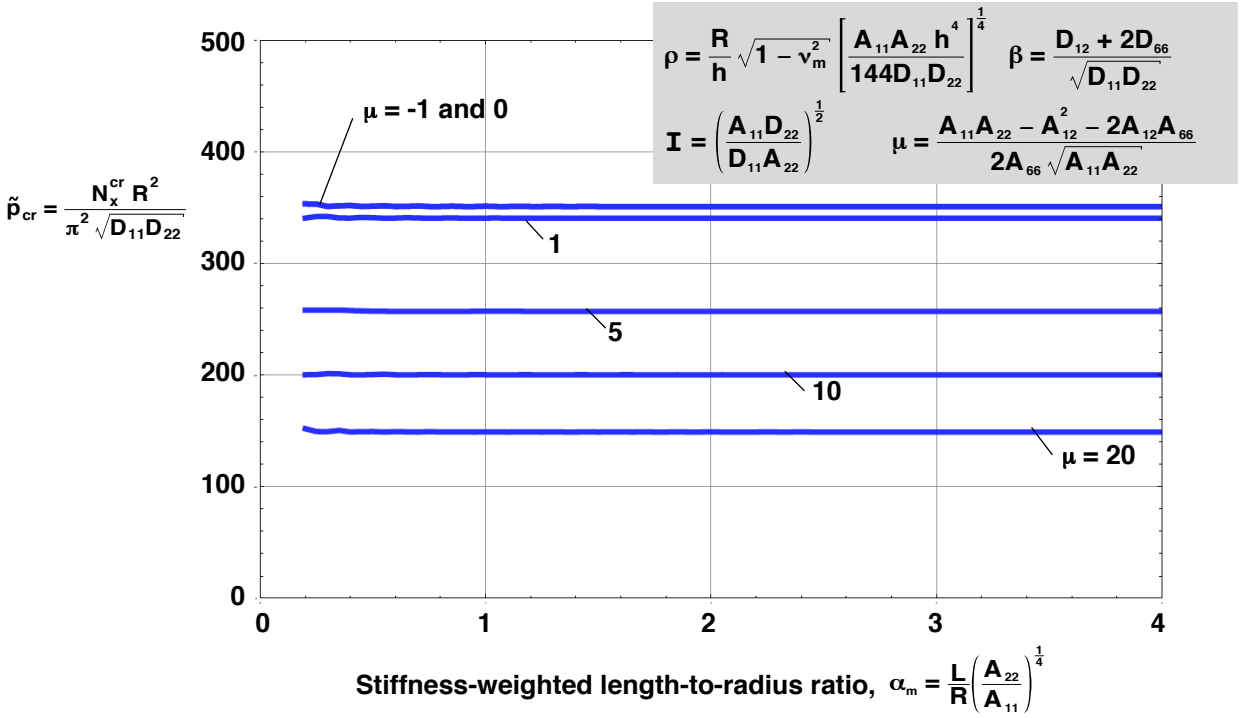

Figure 72. Effects of parameters α_m and μ on nondimensional buckling loads on cylinders with $\beta = 0$, $\mathrm{I} = 4$, and $\rho = 1000$.

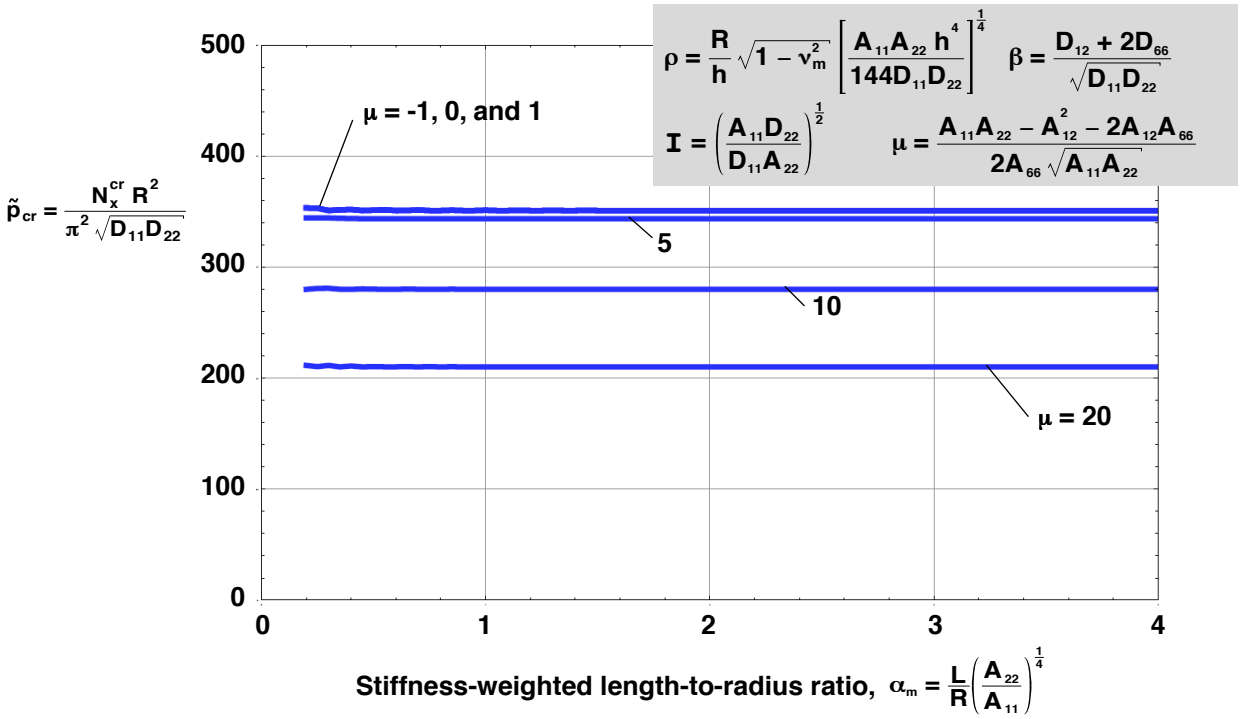

Figure 73. Effects of parameters α_m and μ on nondimensional buckling loads on cylinders with $\beta = 1$, $\mathrm{I} = 4$, and $\rho = 1000$.

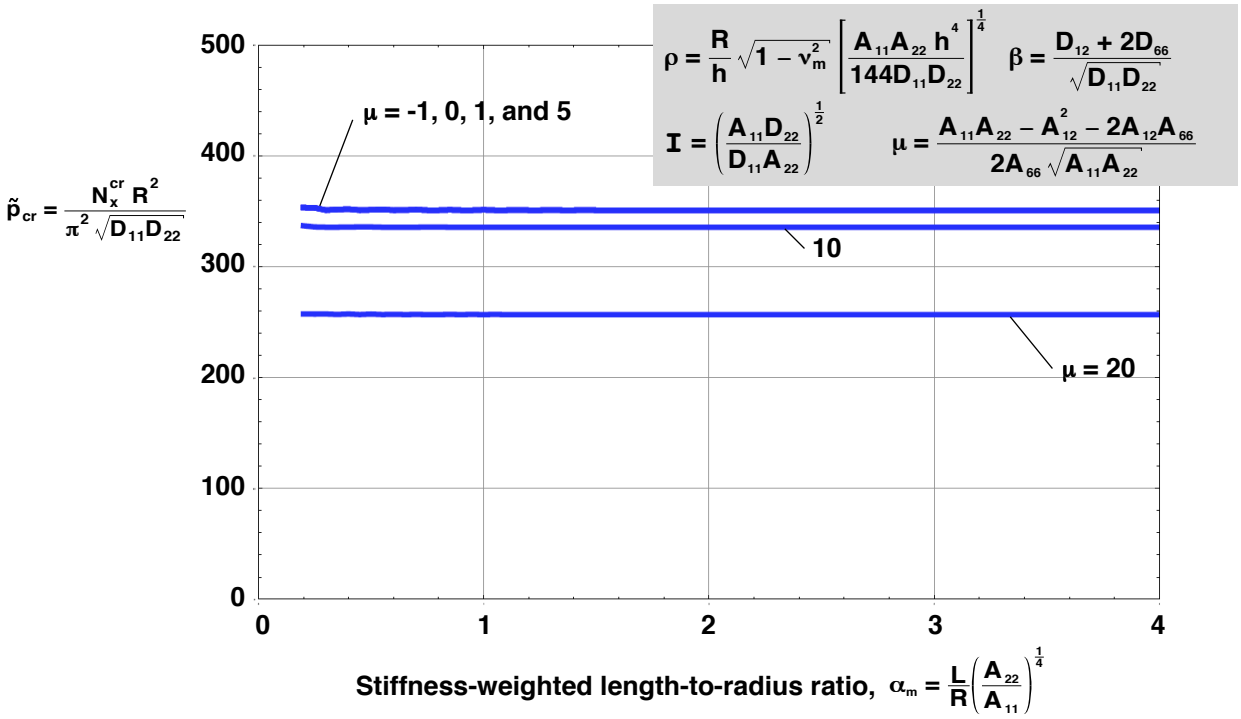

Figure 74. Effects of parameters α_m and μ on nondimensional buckling loads on cylinders with $\beta = 2$, $\mathrm{I} = 4$, and $\rho = 1000$.

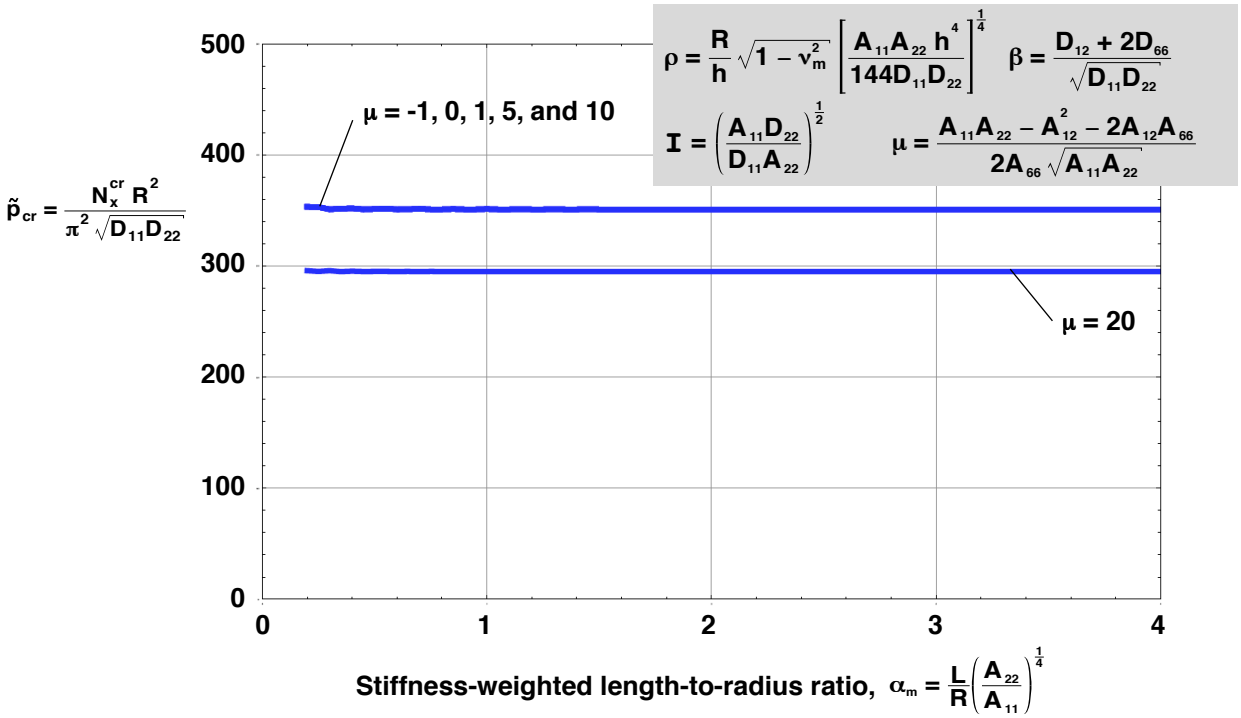

Figure 75. Effects of parameters α_m and μ on nondimensional buckling loads on cylinders with $\beta = 3$, $\mathrm{I} = 4$, and $\rho = 1000$.

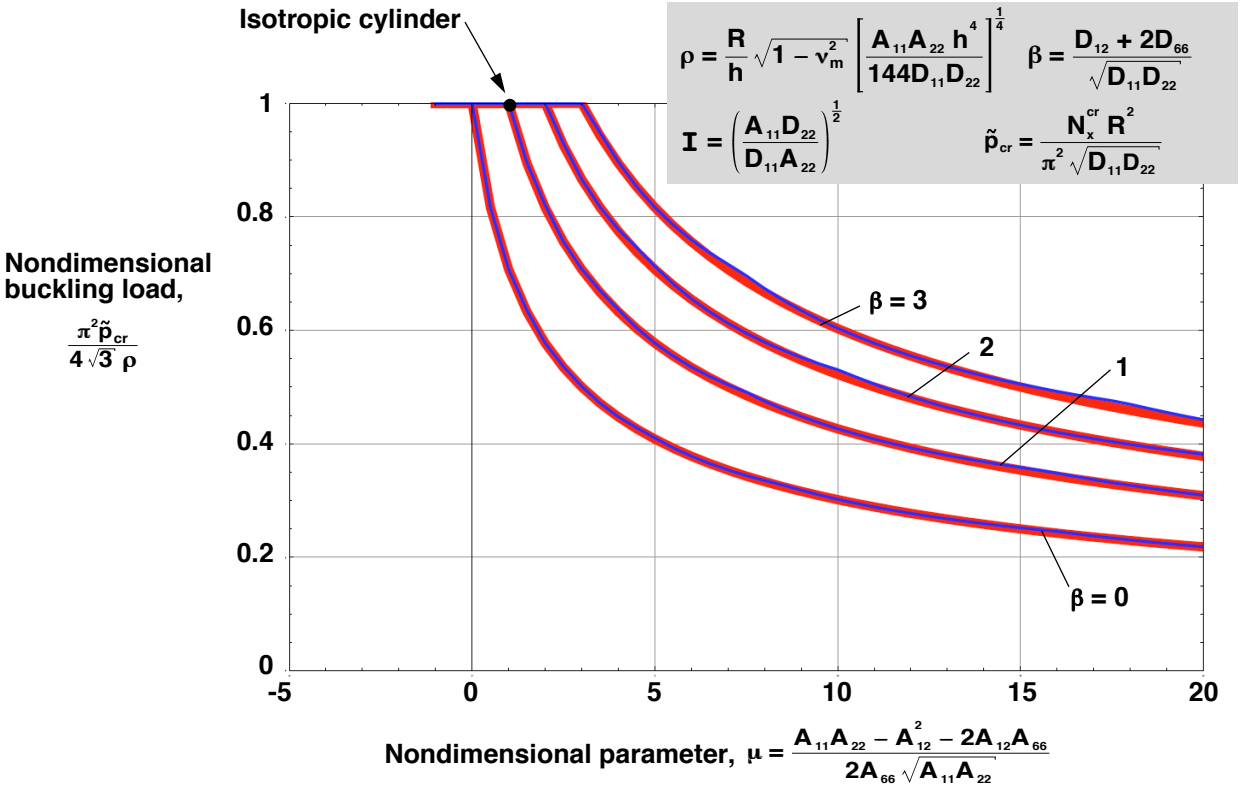

Figure 76. Nondimensional buckling loads of infinitely long cylinders with $I = 1$.

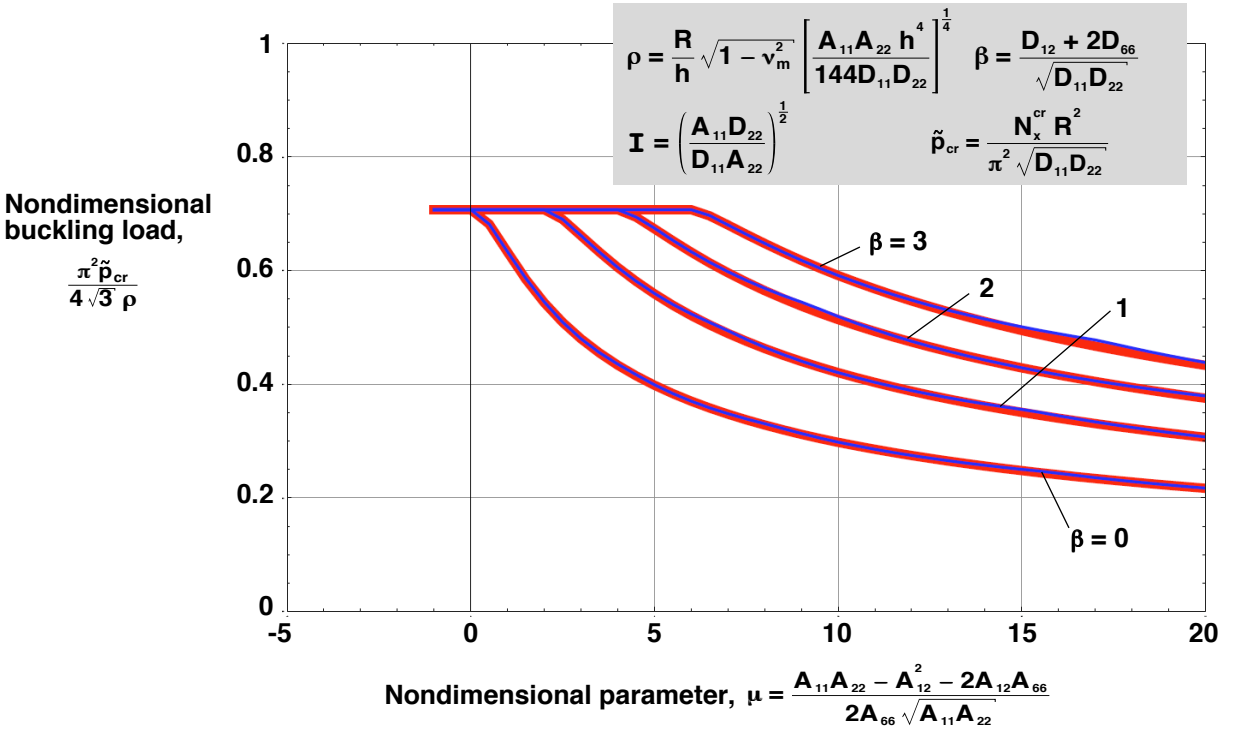

Figure 77. Nondimensional buckling loads of infinitely long cylinders with $I = 0.5$ and $I = 2$.

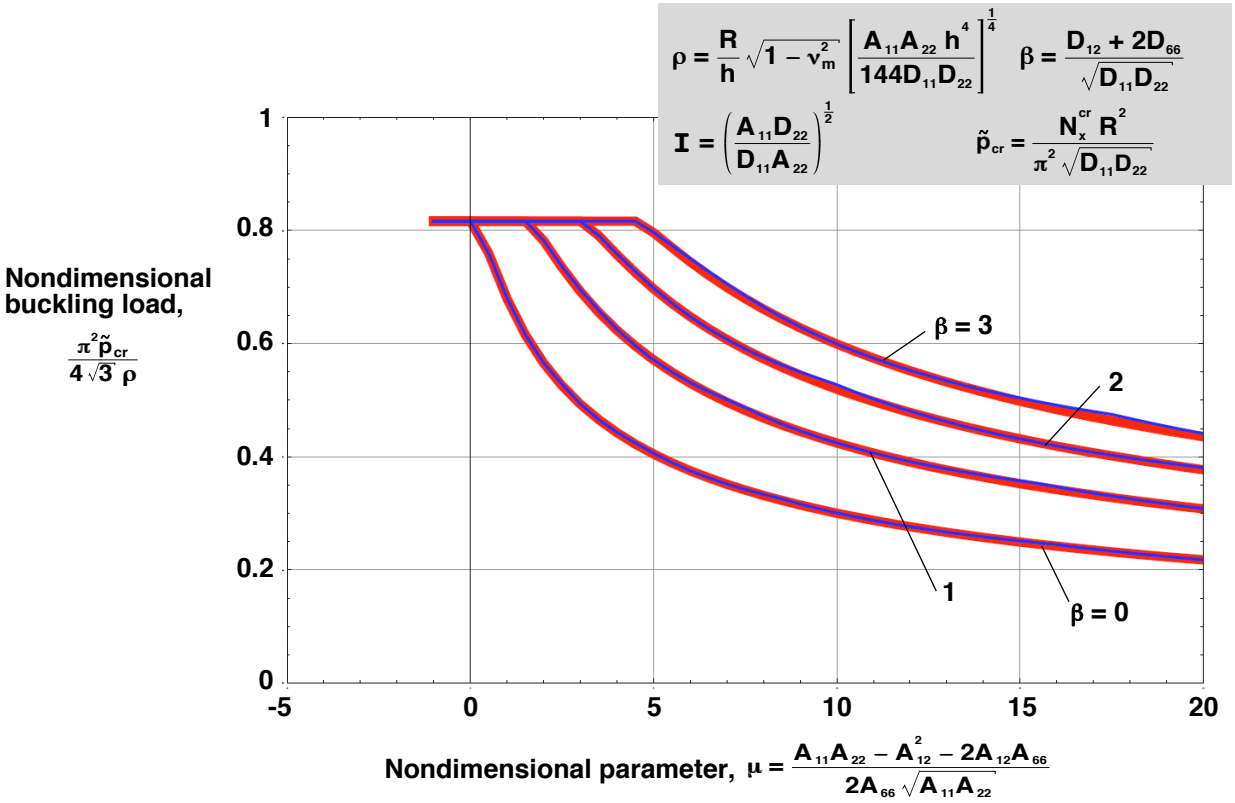

Figure 78. Nondimensional buckling loads of infinitely long cylinders with $I = 0.67$ and $I = 1.5$.

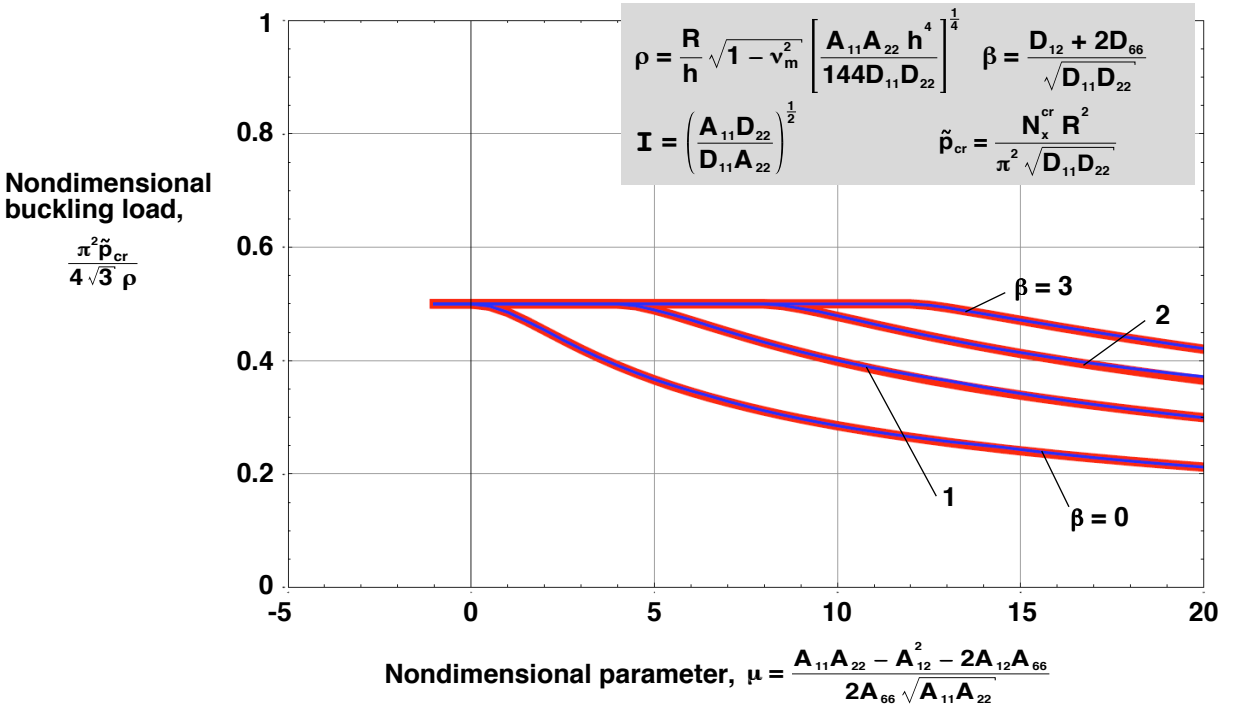

Figure 79. Nondimensional buckling loads of infinitely long cylinders with $I = 0.25$ and $I = 4$.

REPORT DOCUMENTATION PAGE

Form Approved
OMB No. 0704-0188

1. REPORT DATE *(DD-MM-YYYY)*	2. REPORT TYPE	3. DATES COVERED *(From - To)*
01- 05 - 2013	Technical Memorandum	

4. TITLE AND SUBTITLE

An Approximate Solution and Master Curves for Buckling of Symmetrically Laminated Composite Cylinders

5a. CONTRACT NUMBER

5b. GRANT NUMBER

5c. PROGRAM ELEMENT NUMBER

6. AUTHOR(S)

Nemeth, Michael P.

5d. PROJECT NUMBER

5e. TASK NUMBER

5f. WORK UNIT NUMBER

869021.04.07.01.13

7. PERFORMING ORGANIZATION NAME(S) AND ADDRESS(ES)

NASA Langley Research Center
Hampton, VA 23681-2199

8. PERFORMING ORGANIZATION REPORT NUMBER

L-20250

9. SPONSORING/MONITORING AGENCY NAME(S) AND ADDRESS(ES)

National Aeronautics and Space Administration
Washington, DC 20546-0001

10. SPONSOR/MONITOR'S ACRONYM(S)

NASA

11. SPONSOR/MONITOR'S REPORT NUMBER(S)

NASA/TM-2013-217999

12. DISTRIBUTION/AVAILABILITY STATEMENT

Unclassified - Unlimited
Subject Category 39
Availability: NASA CASI (443) 757-5802

13. SUPPLEMENTARY NOTES

14. ABSTRACT

Nondimensional buckling equations for symmetrically laminated cylinders with negligible shell-wall anisotropies and subjected to uniform axial compression are presented. These equations are solved exactly for the practical case of simply supported ends and nondimensional quantities are used to characterize the buckling behavior. Numerous generic plots of nondimensional buckling load versus a stiffness-weighted length-to-radius ratio are presented for various combinations of other parameters. These plots show how the parameter values affect the distribution and size of the festoons forming each response curve and how they affect the attenuation of each response curve to the corresponding solution for an infinitely long cylinder. Approximate formulas for the nondimensional buckling load are also derived that give the buckling response of an infinitely long cylinder in terms of the nondimensional parameters. A relatively small number of "master curves" are presented that give a nondimensional measure of the buckling load of an infinitely long cylinder as a function of the orthotropy and wall inhomogeneity parameters.

15. SUBJECT TERMS

Buckling; Laminated composites; Shells

16. SECURITY CLASSIFICATION OF:			17. LIMITATION OF ABSTRACT	18. NUMBER OF PAGES	19a. NAME OF RESPONSIBLE PERSON
a. REPORT	b. ABSTRACT	c. THIS PAGE			STI Help Desk (email: help@sti.nasa.gov)
					19b. TELEPHONE NUMBER *(Include area code)*
U	U	U	UU	65	(443) 757-5802